

Signature Page

A Synthetic Investigation of Substituted Cyclopentadienyl Complexes of Bismuth and  
Germanium

By  
Deana Lillian Gladys Symes

A Thesis Submitted to  
Saint Mary's University, Halifax, Nova Scotia  
in Partial Fulfillment of the Requirements for  
the Degree of Bachelor of Science with Honours in Chemistry.

April 18<sup>th</sup>, 2024, Halifax, Nova Scotia

Copyright Deana Symes, 2024

Approved: Dr. Jason Masuda  
Supervisor

---

Approved: Dr. Clarissa Sit  
Department Chairperson

---

Date: April 18, 2024

A Synthetic Investigation of Substituted Cyclopentadienyl Complexes of Bismuth and  
Germanium

By  
Deana Lillian Gladys Symes

A Thesis Submitted to  
Saint Mary's University, Halifax, Nova Scotia  
in Partial Fulfillment of the Requirements for  
the Degree of Bachelor of Science with Honours in Chemistry

April 2024, Halifax, Nova Scotia

Copyright Deana Symes, 2024

Approved: Dr. Jason Masuda  
Supervisor

Approved: Dr. Clarissa Sit  
Department Chairperson

Date: April 18<sup>th</sup>, 2024

# A Synthetic Investigation of Substituted Cyclopentadienyl Complexes of Bismuth and Germanium

by Deana Symes

## Abstract

A series of novel cyclopentadienyl bismuth and germanium metal complexes were prepared by using the sterically bulky 2,6-bis(2,4,6-trimethylphenyl)phenylcyclopentadienyl ( $^{\text{TerMes}}\text{Cp}$ ) ligand. Mono-, bis-, and tris-  $^{\text{TerMes}}\text{Cp}$  metal complexes were prepared by reacting  $^{\text{TerMes}}\text{Cp-K}$  with the metal halides:  $\text{GeCl}_2$ ,  $\text{BiCl}_3$ , and  $\text{BiI}_3$ . The bismuth complexes,  $^{\text{TerMes}}\text{CpBiI}_2$ ,  $(^{\text{TerMes}}\text{Cp})_2\text{BiI}$ , and  $(^{\text{TerMes}}\text{Cp})_3\text{Bi}$  contained trigonal pyramidal bismuth metal centers coordinated to the cyclopentadienyl ring with hapticities of  $\eta^1$ . The intermediate germanium complex,  $^{\text{TerMes}}\text{CpGeCl}$ , contained a germanium metal center coordinated to the cyclopentadienyl ring with a hapticity of  $\eta^1$ . Upon further reactivity, cationic germanium species  $[^{\text{TerMes}}\text{CpGe}][\text{GaCl}_4]$  and  $[^{\text{TerMes}}\text{CpGe}][\text{B}(3,5\text{-CF}_3\text{-C}_6\text{H}_3)]$  were synthesized with germanium metal centers coordinated to the cyclopentadienyl ring with hapticities of  $\eta^4$  and  $\eta^3$  respectively. In some cases, stabilizing aryl interactions with the mesityl ring of the  $^{\text{TerMes}}\text{Cp}$  ligand are present. Cationic germanium species,  $[^{\text{TerMes}}\text{Cp-Ge}]^+$ , were synthesized by chloride abstraction from the germanium chloride using  $\text{GaCl}_3$ , or by metathesis with  $\text{Na}[\text{B}(3,5\text{-CF}_3\text{-C}_6\text{H}_3)]$ .

April 18<sup>th</sup>, 2024

## Acknowledgements

To begin, I would like to acknowledge my supervisor, Dr. Jason Masuda for his endless support both in and outside of the lab. Thank you for the opportunity to work in your lab, for your guidance and patience throughout this project, and for sharing your passion and enthusiasm for chemistry with me. Having a supervisor who has been greatly accommodating to my way of learning and has taken the time to personally teach a variety of essential skills and knowledge has played a significant role in the success of this project and my growth as a chemist. Working on this project has allowed me to develop many useful skills and techniques that will be carried forward throughout my life and academic career, for which I am very grateful. Additionally, I would like to thank all the past Masuda group members, Alex Veinot, Bailey Mosher, and Thai Do, who worked on this project or related projects, provided materials, and developed some of the original syntheses used. I would also like to thank a current Masuda group member, Tanner George, for always encouraging me to be creative in the lab, for growing my interest in crystallography, for all your tips and suggestions in the lab, and for always being so kind and helpful in every way. I would also like to thank a recent addition to the Masuda group, Liam Hill. Thank you for aiding in the preparation of some of the materials used during the last and busiest few weeks of this project.

I would also like to give a special thanks to Dr. Mary Sheppard for revealing my love and passion for chemistry, convincing me to become a chemistry major during my first year, and continuing to support me throughout my undergraduate degree. Additionally, I would also like to thank Dr. Bitu Hurisso and Dr. Najwan Albarghouthi for their support throughout my research and for always providing positive words of encouragement.

I would also like to thank my dad, Dean Symes, for always supporting me, especially throughout my undergraduate degree. Thank you for forcing me to find a work-life balance, for always believing in my abilities to achieve my goals, and for raising me to always give my best efforts in everything I do.

Finally, I'd like to thank my partner, Dominick, for always reassuring me and bringing me back on track when life and school get overwhelming. Thank you for always being a positive influence in my life and for your continual love and support.

<b>Table of Contents</b>	<b>Page</b>
Abstract .....	ii
Acknowledgements .....	iii
Table of Contents .....	iv
Table of Figures .....	vii
Table of Schemes .....	ix
Table of Tables .....	x
List of Symbols and Abbreviations.....	xi
Compounds prepared .....	xiii
1.0 Introduction.....	1
1.1 Overview.....	1
1.2 Bonding in Cyclopentadienyl Complexes .....	4
1.3 Uses of Cyclopentadienyl Ligands and their Sterically Hindered Derivatives.....	7
1.4 Preparation of Cyclopentadienyl Metal Complexes .....	10
1.5 Bulky Cyclopentadienyl Bismuth Cations.....	11
1.6 Bulky Cyclopentadienyl Germanium Cations .....	13
2.0 Experimental .....	14
2.1 General Experimental Methods and Characterization .....	14
2.2 X-ray crystallography .....	16

2.3 Synthesis of TerMesI - 1 .....	16
2.4 Synthesis of TerMesLi - 2.....	20
2.5 Synthesis of $^{\text{TerMes}}\text{CpCoCp}$ - 3 .....	21
2.6 Synthesis of $^{\text{TerMes}}\text{CpH} - 4\text{a+b}$ .....	22
2.7 Synthesis of $^{\text{TerMes}}\text{CpK}$ - 5.....	23
2.8 Synthesis of $^{\text{TerMes}}\text{CpBiCl}_2$ - 6.....	24
2.9 Synthesis of $(^{\text{TerMes}}\text{Cp})_2\text{BiCl}$ -7.....	25
2.10 Synthesis of $^{\text{TerMes}}\text{CpBiI}_2$ - 8 .....	26
2.11 Synthesis of $(^{\text{TerMes}}\text{Cp})_2\text{BiI}$ - 9 .....	27
2.12 Synthesis of $(^{\text{TerMes}}\text{Cp})_3\text{Bi}$ - 10.....	29
2.13 Synthesis of $^{\text{TerMes}}\text{CpGeCl}$ - 11 .....	31
2.14 Synthesis of $[^{\text{TerMes}}\text{CpGe}][\text{GaCl}_4] - 12$ .....	32
2.15 Synthesis of $[^{\text{TerMes}}\text{CpGe}][\text{BARF}_{24}] - 13$ .....	33
3.0 Results and Discussion .....	34
3.1 Optimization of Multistep Synthesis .....	34
3.1.1 Optimization of TerMesI Synthesis .....	34
3.1.2 Optimization of TerMesLi Synthesis.....	36
3.1.3 Optimization of $^{\text{TerMes}}\text{CpCoCp}$ Synthesis .....	36

3.1.4 Optimization of $^{\text{TerMes}}\text{CpH}$ Synthesis .....	38
3.1.4.1 Utilizing Redox Chemistry for the Synthesis of $^{\text{TerMes}}\text{CpH}$ .....	38
3.1.4.2 Isomers of $^{\text{TerMes}}\text{CpH}$ .....	40
3.1.5 Optimization of $^{\text{TerMes}}\text{CpK}$ Synthesis.....	41
3.2 The Discovery of $^{\text{TerMes}}\text{Cp}$ Bismuth Complexes .....	43
3.2.1 Investigation of Cp- <i>H</i> resonances .....	43
3.2.2 Purification Attempts for $(^{\text{TerMes}}\text{Cp})_2\text{BiI}$ .....	48
3.3 The Discovery of $^{\text{TerMes}}\text{Cp}$ Germanium Complexes .....	50
3.3.1 Germanium precursor .....	50
3.3.2 Germanium Cations .....	50
4.0 Conclusions.....	53
5.0 Future Work .....	54
6.0 References.....	57
7.0 Appendix .....	65

## Table of Figures

<b>Figure 1.</b> The first metallocene complex, Ferrocene (left), and the first soluble organosamarium (II) complex isolated in 1981 (right).....	2
<b>Figure 2.</b> Targeted mono- (left) and bimetallic (right) bonding environments of <i>m</i> -Terphenyl Cp ligands.....	3
<b>Figure 3.</b> Different binding modes of Cp ligands with metal centers (M) (left) and illustration of metal slippage of a metal over a Cp ring (right) .....	4
<b>Figure 4.</b> Molecular orbitals of the Cp ligand.....	5
<b>Figure 5.</b> General molecular orbital diagram for Cp-main group element interactions, showing only occupied orbitals. ....	6
<b>Figure 6.</b> Pentamethylcyclopentadienyl (Cp*) ligand (left), a strong reducing agent derived from Cp*, decamethylcobaltocene (middle), and stabilized decamethyltitanocene (right). ....	7
<b>Figure 7.</b> Bulky alkyl-substituted Cp ligand (left) and a stabilized sandwich complex (right). ....	8
<b>Figure 8.</b> Commonly used <i>m</i> -Terphenyl ligands with substituted aryl groups. ....	8
<b>Figure 9.</b> Generic bismuth- $\pi$ -arene complex, X = halide.....	12
<b>Figure 10.</b> Germanium half sandwich complex characterized by Jutzi <i>et al.</i> ....	14
<b>Figure 11.</b> Molecular structure of <b>8</b> (left). Intermolecular Bi...I interactions (right). Ellipsoids are shown at the 50% probability level. Hydrogen atoms have been omitted for clarity.....	45
<b>Figure 12.</b> Molecular structure displaying the connectivity of <b>9</b> . Ellipsoids are shown at the 50% probability level. Hydrogen atoms have been omitted for clarity.. ....	46

<b>Figure 13.</b> Molecular structure of <b>10</b> . Ellipsoids are shown at the 50% probability level. Hydrogen atoms have been omitted for clarity.....	47
<b>Figure 14.</b> Space filling diagram of <b>10</b> . Ellipsoids are shown at the 50% probability level.....	48
<b>Figure 15.</b> Molecular structure of <b>12</b> . Ellipsoids are shown at the 50% probability level. Hydrogen atoms have been omitted for clarity.....	53
<b>Figure 16.</b> Molecular structure of <b>13</b> . Ellipsoids are shown at the 50% probability level. Hydrogen atoms have been omitted for clarity.....	53
<b>Figure 17.</b> Future directions to generate bismuth cations. ....	55
<b>Figure 18.</b> Future redox chemistry with <b>13</b> .....	56

## Table of Schemes

<b>Scheme 1.</b> Reaction of cyclopentadiene with an alkali metal to form cyclopentadienide..	1
<b>Scheme 2.</b> Synthesis of first known <i>m</i> -Terphenyl Cp metal complex.	9
<b>Scheme 3.</b> Synthetic preparation of <sup>TerMes</sup> CpH isomers from cobalt(I) Cp complex.	10
<b>Scheme 4.</b> General reaction schemes for the preparation of Cp metal complexes using standard synthetic routes. M is commonly an alkali metal salt in process (i) and commonly a Group 1 metal in process (iii), M' is any other metal, M <sup>m+</sup> is typically a low oxidation state metal (m=0-2), X is a halide, and L is typically CO in process (iii).	10
<b>Scheme 5.</b> Previously designed synthetic route to <i>m</i> -terphenyl substituted Cp compounds from the oxidative decomposition of <b>3</b> by FeCl <sub>3</sub> .	39
<b>Scheme 6.</b> Previously attempted synthetic route to <i>m</i> -terphenyl substituted Cp compounds from the oxidative decomposition of <b>3</b> by AgNO <sub>3</sub> in a binary solvent mixture of toluene and water.	39
<b>Scheme 7.</b> New synthetic route to <i>m</i> -terphenyl substituted Cp compounds from the oxidative decomposition of <b>3</b> by AgNO <sub>3</sub> in acetonitrile.	40
<b>Scheme 8.</b> Interconversion of alkyl substituted cyclopentadiene ring.	41

## Table of Tables

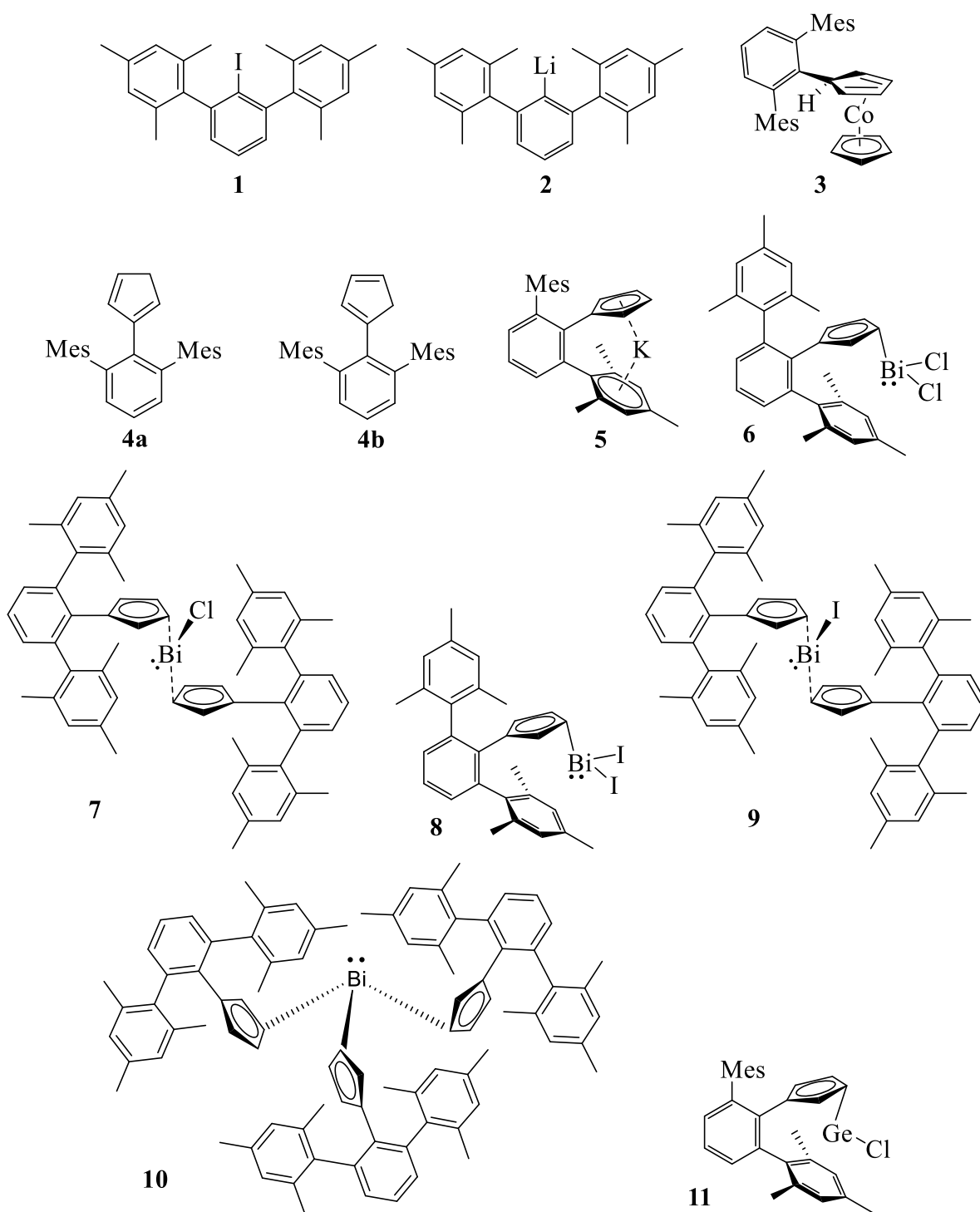
<b>Table 1.</b> Summary of the optimization of the multi-step synthesis of the <sup>TerMes</sup> Cp ligand compared to literature. ....	43
---	----

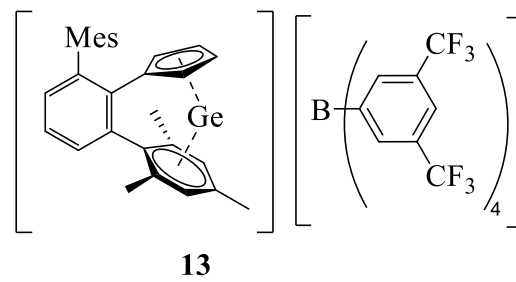
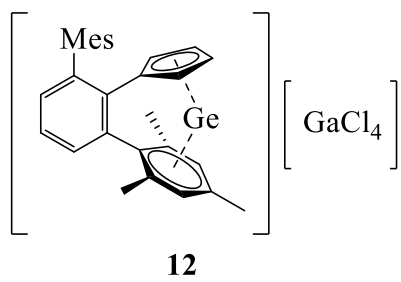
## List of Symbols and Abbreviations

°	degree
°C	degree Celsius
Å	Angstrom
aq	aqueous
Ar	aryl
BArF <sub>24</sub>	tetrakis[3,5-bis(trifluoromethyl)phenyl]borate
br	broad
Bu	butyl
<i>ca.</i>	approximately
cm	centimeter
Cp	cyclopentadienyl
Cp*	pentamethylcyclopentadienyl
d	doublet
D	deuterium
dd	doublet of doublets
dq	doublet of quartets
eq.	equivalent
g	gram
h	hour
Hz	hertz
<i>i-</i>	<i>ipso</i>
<i>in vacuo</i>	under vacuum
iPr	isopropyl
IR	infrared
<i>J</i>	coupling
K	Kelvin
kJ	kilojoule
L	liter
M	molarity
m	multiplet (NMR spectroscopy)
m	medium (IR spectroscopy)
<i>m-</i>	meta
m.p.	melting point
Me	methyl
Mes	mesityl
mg	milligram
MHz	MegaHertz
min	minute
mL	milliliter
mmol	millimole
NMR	nuclear magnetic resonance
<i>o-</i>	ortho
OTf	triflate
<i>p-</i>	para
Ph	phenyl
pKa	acidity measurement
ppm	parts per million

PTFE	polytetrafluoroethylene
q	quartet
r.t.	room temperature
s	singlet (NMR spectroscopy)
s	strong (IR spectroscopy)
t	triplet
tBu	tert-butyl
TerDipp	2,6-bis(2,6-diisopropylphenyl)phenyl
TerMes	2,6-bis(2,4,6-trimethylphenyl)phenyl
<sup>TerMes</sup> Cp	2,6-bis(2,4,6-trimethylphenyl)phenyl cyclopentadienyl
TerPh	2,6-di(phenyl)phenyl
THF	tetrahydrofuran
TMS	tetramethylsilane
vs	very strong
w	weak (IR spectroscopy)
$\delta$	delta (chemical shift)
$\Delta$	delta (heat)
$\eta$	hapticity
$\lambda$	wavelength
$\nu$	wavenumber

## Compounds Prepared

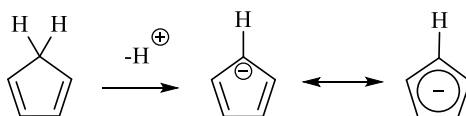




## Introduction

### 1.1 Overview

Dienes are an important class of compounds that have maintained attention throughout scientific history. Cyclopentadiene is a particular cyclic diene of interest with a molecular formula of  $C_5H_6$  and is generally produced by the pyrolysis of organic compounds.<sup>1</sup> This five-membered ring possesses a conjugated double-bond structure with an active methylene group and can spontaneously undergo a Diels-Alder reaction at room temperature with itself to form its corresponding dimer, dicyclopentadiene.<sup>1</sup> With a relatively low  $pK_a$  of approximately 15, cyclopentadiene can be deprotonated by bases such as alkali metal hydrides to generate the 6-electron aromatic cyclopentadienide ( $C_5H_5^-$ , abbreviated as Cp) (Scheme 1).<sup>2</sup>



**Scheme 1.** Reaction of cyclopentadiene with an alkali metal to form cyclopentadienide.<sup>2</sup>

In 1951, the unanticipated discovery of the first sandwich compound, ferrocene, was reported, incorporating two Cp rings (Figure 1).<sup>3</sup> The first proposed structure suggested covalent Fe-C  $\sigma$  bonds but it was later determined the six  $\pi$ -electrons of Cp participated in the bonding to the iron.<sup>4,5</sup> This discovery established a novel area of research for organometallic chemistry with Cp derivatives of various metals and metalloids gaining significant popularity. Between the years 1952 to 1954, the expeditious development of various metallocenes was driven by the competition between the research groups of Fischer and Wilkinson, resulting in the synthesis of Cp-incorporated metal complexes for nearly all the transition metals and many lanthanides.<sup>4,5</sup>

With the ease of modification regarding their electronic and steric properties, Cp ligands have been found advantageous in a variety of applications. Applications of these strongly electron-donating ligands include the previously discussed metallocenes, in half-sandwich complexes, as well as in homogeneous catalysis.<sup>6</sup> These ligands are particularly useful in catalysis as they contain the ability to tolerate a variety of substituents.<sup>6</sup> Incorporating bulkier substituents on Cp ligands has gained popularity as this has demonstrated additional bonding environments, spin states, and reactivity to be explored.<sup>7</sup>



**Figure 1.** The first metallocene complex, Ferrocene (left), and the first soluble organosamarium (II) complex isolated in 1981 (right).<sup>3,8</sup>

A widely popular Cp derivative used in organometallic chemistry is the permethylated analogue,  $C_5Me_5^-$ , commonly abbreviated as Cp\*.<sup>7</sup> Compared to the parent unsubstituted Cp ligand, Cp\* provides increased steric protection at the metal center, better electron-donating capabilities, and enhanced solubility in nonpolar organic solvents.<sup>7</sup> These factors have been especially useful in lanthanide chemistry whereas as a result of this increased solubility, the isolation of the first soluble organosamarium (II) complex was achievable (Figure 1). The accessibility of soluble complexes has allowed for further utility in research of reactivity and structural discoveries of metallocenes.<sup>8</sup>

Shortly after the discovery of sandwich complexes, the development of mixed Cp(arene) transition metal complexes became a topic of interest. The first compound of this sort to be prepared was diamagnetic  $(C_5H_4Me)Mn(C_6H_6)$ , followed by the synthesis of the paramagnetic

complex  $(C_5H_5)Cr(C_6H_6)$ .<sup>5</sup> In addition to this field of research, stable 18-electron salts of cationic compounds with the general composition of  $[(C_5H_5)Fe(arene)]^+$  were generated and subsequently reduced to 19-electron molecules,  $(C_5H_5)Fe(arene)$ . The derivatives that contained sterically unprotected arenes were found to be unstable, whereas the additional steric bulk of the arenes provided steric protection and improved the stability of these complexes.<sup>5</sup>

A particular Cp(arene) group of interest for metal complexes is the *m*-terphenyl Cp ligand. By incorporating larger substituents such as TerMes, (TerMes =  $C_6H_3-2,6-Mes$ , Mes = 2,4,6- $(CH_3)_3C_6H_2$ ), the desired Cp-M-Ar intramolecular bonding interactions can be promoted as the Cp attached to the *m*-terphenyl is forced to twist out of the plane of the central aromatic system by the sterically hindered aryl groups.<sup>7</sup> Targeting these interactions creates potential unique mono- or bimetallic environments that can undergo further investigation (Figure 2).

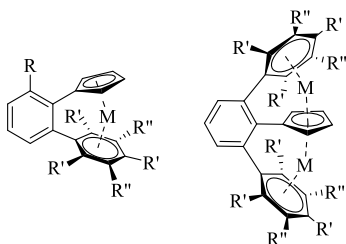


**Figure 2.** Targeted mono- (left) and bimetallic (right) bonding environments of *m*-Terphenyl Cp ligands.<sup>7</sup>

With growing interest in the literature on heavier Group 14 and 15 metal complexes, the development of organogermanium and organobismuth complexes with this framework is of interest. As a result of the additional aryl interactions from the mesityl substituents, germanium and bismuth complexes with this framework could generate stable intermediates, which can be

otherwise often difficult to isolate.<sup>9</sup> Furthermore, the metal- $\pi$  arene interactions are expected to support the formation of the corresponding metal cations with a broad potential of reactivity.

## 1.2 Bonding in Cyclopentadienyl Complexes

Cp ligands have a variety of binding modes to metal centers (Figure 3), however the most common is the symmetric  $\eta^5$  arrangement.<sup>10</sup> Most often Cp ligands are associated with transition metals where this trend is observed with minimal exceptions that can be easily explained using the electron-counting rule. However, with main group metals in addition to numerous bridging modes, there is a larger variety of binding modes ranging from slipped  $\eta^x$  arrangements to purely  $\sigma$ -bound (Figure 3) that can be difficult to anticipate.<sup>10,11</sup> This variety of bonding arrangements for main-group-metal Cp complexes is attributed to the difference in preferred metal-ring bonding arrangements of the  $ns$  and  $np$  orbitals of the metal. The metal orbitals are often more suitable for forming  $\sigma$ -bonds as opposed to  $\pi$ -bonds which may explain the formation of polymeric structures routinely observed in the solid state.<sup>10</sup>

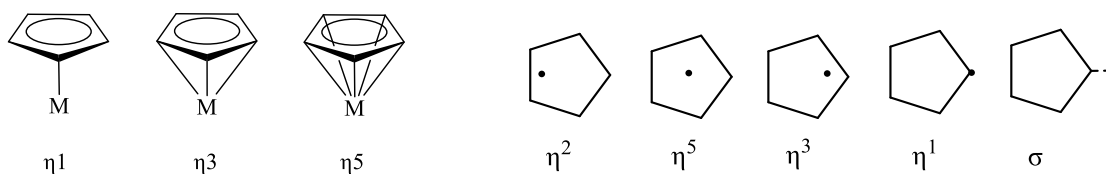


**Figure 3.** Different binding modes of Cp ligands with metal centers (M) (left) and illustration of metal slippage of a metal over a Cp ring (right).<sup>10,11</sup>

Cyclopentadienide is planar and in the  $D_{5h}$  point group.<sup>12</sup> Each carbon atom in this ring contains a p-orbital that is perpendicular to the molecular plane, and these combine to make the five  $\pi$  molecular orbitals of the Cp ligand.<sup>12,13</sup> Within these five molecular orbitals, there are three energy levels in which these orbitals reside. The lowest energy orbital is of the symmetry type  $a_1$

and contains no nodes, followed by a pair of degenerate orbitals of the symmetry type  $e_1$  containing one node, and then the final pair of degenerate orbitals of the symmetry type  $e_2$  containing 2 nodes (Figure 4).<sup>12,13</sup>

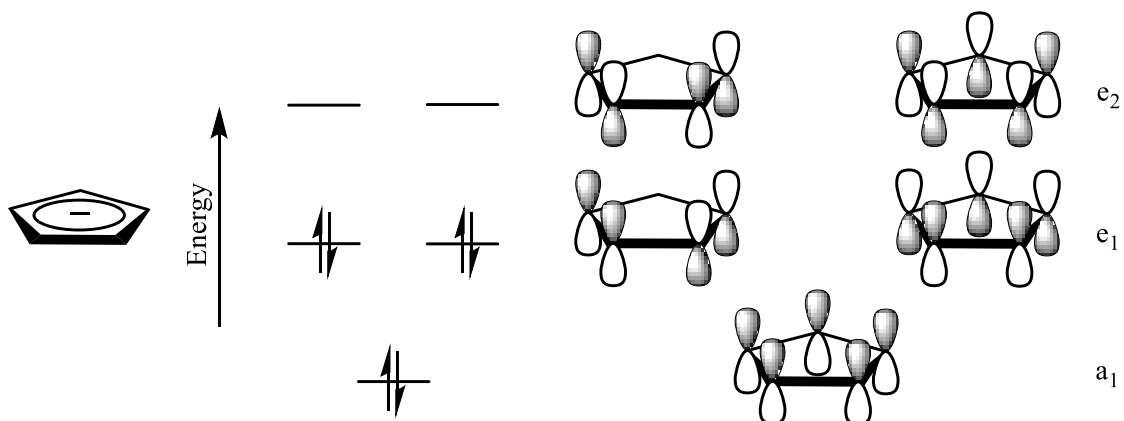


**Figure 4.** Molecular orbitals of the Cp ligand.<sup>12,13</sup>

When comparing transition metal-Cp bonding to main group metal-Cp bonding, the major difference in these interactions is related to the orbitals involved. For transition metal-Cp complexes, unlike main group metal-Cp complexes, there are valence d-orbitals that contribute to the bond formation.<sup>14</sup> For an interaction to be observed between a metal and a ligand, the ligand orbitals must be close in energy to those on the metal, and there must be substantial overlap.<sup>14</sup> For the main group metal-Cp complexes, the interactions observed are with the s- and p-orbitals on the metal, whereas the d-orbitals are either vacant or too low in energy to undergo an interaction with the Cp ligand.<sup>15</sup> A general representation of the molecular orbital energy diagram for the main group metal-Cp interactions can be seen in Figure 5.

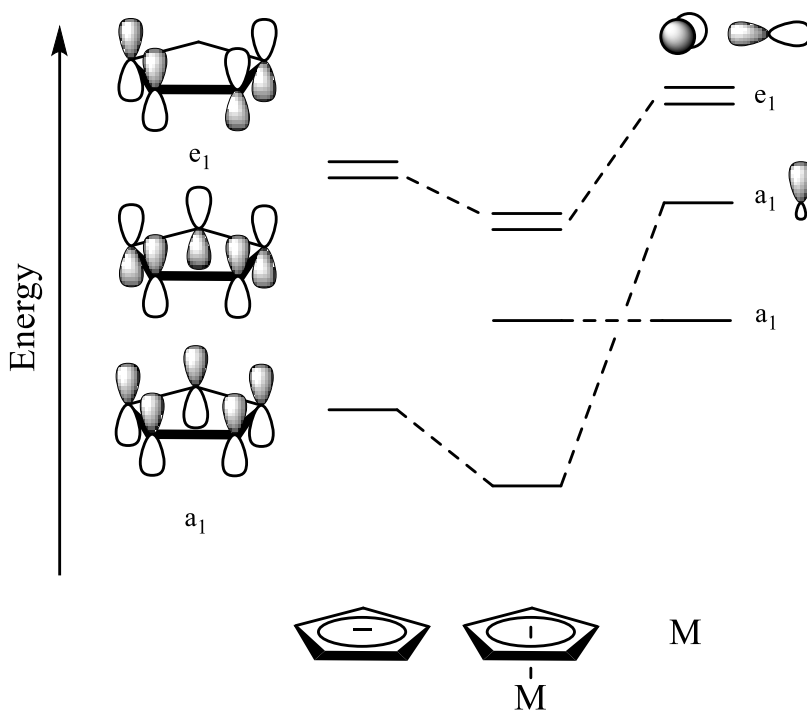


**Figure 5.** General molecular orbital diagram for Cp-main group element interactions, showing only occupied orbitals.<sup>15</sup>

Theoretical studies have focused on the bonding between main group metals and Cp ligands in terms of electrostatic and orbital contributions.<sup>10</sup> When observing Cp-main group metal complexes throughout the periodic table, trends in bonding arrangements are observed. Throughout the periodic table, it has been consistently observed that when going down a group, a “softer” Cp-metal bond occurs.<sup>10</sup> For the heavier elements, there is a tendency towards a lower hapticity, referring to the  $\pi$  coordination of the ligand to the metal center. In a few cases, there is an exception to this observation, particularly for the more electropositive elements such as Pb or Bi, where the opposite trend may be observed.<sup>10</sup> This wider range of electronegativities and hardness of main group metals allows for a varying degree of covalent character for main group metal complexes, where elements of groups 14 and 15 are predominantly covalent.<sup>15</sup>

### 1.3 Uses of Cyclopentadienyl Ligands and their Sterically Hindered Derivatives

As previously mentioned, Cp ligands are sterically and electronically easily modified by the addition of substituents.<sup>7</sup> The addition of substituents to Cp of metal complexes can display a variety of effects including improved steric protection of coordinated metal centers, increased stability, higher catalytic activity, and improvements in enantioselectivity as catalysts.<sup>16-18</sup> One of the simpler substituted Cp derivatives is pentamethylcyclopentadienyl with the molecular formula  $C_5Me_5$ , abbreviated as Cp\* (Figure 6). This derivative was produced in 1960 and led to the isolation of more stable Cp-metal complexes, some of which were otherwise previously unable to be isolated (Figure 6).<sup>16</sup>

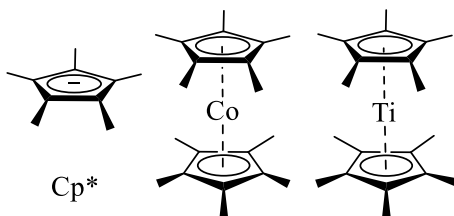


**Figure 6.** Pentamethylcyclopentadienyl (Cp\*) ligand (left), a strong reducing agent derived from Cp\*, decamethylcobaltocene (middle), and stabilized decamethyltitanocene (right).<sup>16-18</sup>

Increasingly bulkier alkyl substituents were introduced to Cp such as tert-butyl or isopropyl groups to further increase steric demands and investigate their new properties.<sup>16,17</sup> The ligand  $C_5H_2tBu_3$  (abbreviated Cp''') has been successfully used to synthesize unforeseen metallocene anions, whereas  $C_5iPr_5$  has stabilized additional metal sandwich complexes such as uranocene  $[(\eta^5-C_5iPr_5)_2U]$  (Figure 7).<sup>16</sup> An additionally useful Cp derivative is the indenyl ligand which contains a benzo ring fused to the Cp ligand. Metal indenyl complexes have been shown to accelerate organometallic reactions and have catalytic capabilities.<sup>19</sup> Chiral indenyltitanium and -zirconium complexes have been highly successful in stereoselective olefin polymerization and

catalytic transformation of small molecules that have otherwise been unsuccessfully attempted with the achiral  $\text{Cp}_2\text{TiCl}_2$  and  $\text{Cp}_2\text{ZrCl}_2$  parent analogues.<sup>19</sup>

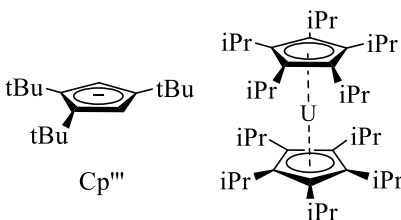


**Figure 7.** Bulky alkyl-substituted Cp ligand (left) and a stabilized sandwich complex (right).<sup>16</sup>

The versatility of Cp-metal derivatives has driven the desire to further extend the bulky aryl substituted ligand framework. An additional subset of bulky ligands is the *m*-terphenyl ligand. The terphenyl ligands are often designed with the general form of  $\text{C}_6\text{H}_3\text{-2,6Ar}_2$  (Ar=aryl).<sup>20</sup> The design of this general ligand type is one of the bulkiest and creates a sterically protected pocket between the two ortho aryl groups that often exhibits stabilizing  $\pi$ -arene interactions between the ortho aryl groups to the coordinated metal center.<sup>20,21</sup> The *m*-terphenyl ligand was further developed by the addition of ortho and occasionally para substituents to the flanking aryl rings to constrain the positions of these rings to be nearly perpendicular to the central aryl ring.<sup>20</sup> This conformation provides an enhanced sterically protected pocket for reactive metal centers and may alter the crystallization characteristics of these derivatives. Examples of commonly used aryl-substituted *m*-terphenyl ligands with the general form  $\text{C}_6\text{H}_3\text{-2,6Ar}_2$  are illustrated in Figure 8.<sup>20</sup>

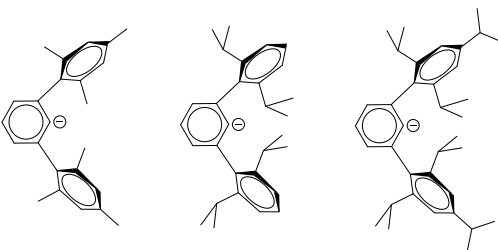
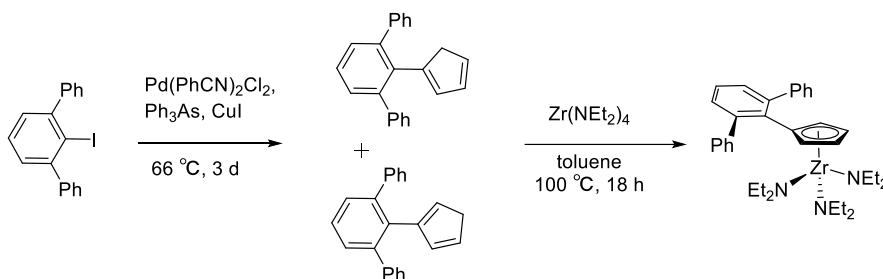


**Figure 8.** Commonly used *m*-Terphenyl ligands with substituted aryl groups.<sup>20</sup>

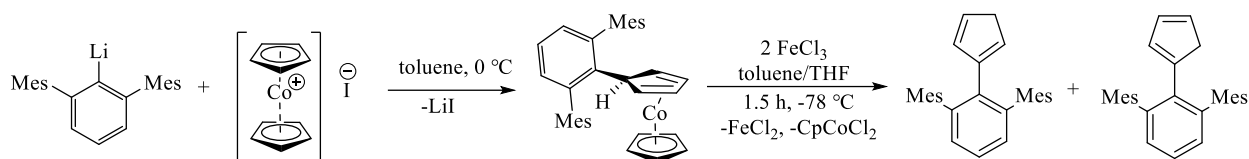
The first study to incorporate both the *m*-terphenyl ligand and the Cp ligand together was by Curnow *et al.* with the discovery of the *m*-terphenyl Cp ligand along with its tris(diethylamido)zirconium complex (Scheme 2).<sup>7,22</sup> Characterization of this novel metal complex demonstrated the significance of the bulky aryl group on its structure. Although there were no aryl-zirconium interactions, one of the phenyl groups on the central benzene ring was oriented towards the zirconium, creating a slip angle between the normal of the Cp plane and the Zr-CNT (CNT-centroid of the Cp ring).<sup>22</sup> Additionally, this phenyl ring has forced two of the amido groups coordinated to zirconium out of the ideal geometry. It is anticipated that the Zr metal center did not form interactions with the phenyl substituents as the Zr is previously electronically saturated with 18 electrons by the three amido groups, making the addition of electrons undesirable.<sup>22</sup>



**Scheme 2.** Synthesis of first known *m*-Terphenyl Cp metal complex.<sup>22</sup>

A more recent example of the utilization of the *m*-terphenyl Cp ligand in metal complexes has been done by Veinot *et al.*<sup>7</sup> The methodology of nucleophilic substitution reactions of unsaturated hydrocarbons such as benzene to produce the corresponding exo addition products when bound as ligands to cationic transition metals was used to their advantage in this work.<sup>7</sup> To synthesize the *m*-terphenyl Cp ligand, the organolithium reagent TerMesLi was treated with cobaltocenium iodide to afford the cobalt(I) Cp complex with an optimized yield of 66 % after recrystallization from cold pentane.<sup>7</sup> The cobalt (I) intermediate was then subsequently oxidized

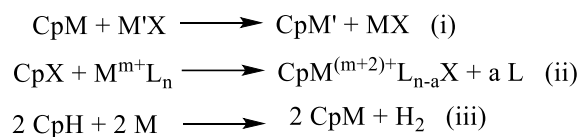
by FeCl<sub>3</sub> followed by column chromatography to yield a mixture of <sup>TerMes</sup>CpH isomers (Scheme 3). With the treatment of alkali-metal transfer reagents, the <sup>TerMes</sup>CpH isomer mixture was converted to the corresponding alkali-metal salts with the general form of [M(<sup>TerMes</sup>Cp)]<sub>n</sub>.<sup>7</sup> Using this framework, the goal is to further stabilize additional metal environments by utilizing the chelating Cp/Ar interactions.



**Scheme 3.** Synthetic preparation of <sup>TerMes</sup>CpH isomers from cobalt(I) Cp complex.<sup>7</sup>

#### 1.4 Preparation of Cyclopentadienyl Metal Complexes

To prepare Cp metal complexes, there are three synthetic routes that are most often used which are (i) salt metathesis, (ii) oxidative addition, and (iii) metalation/deprotonation (Scheme 4).<sup>23</sup> These synthetic routes were initially standardized for the synthesis of non-sterically hindered Cp complexes but were later determined to be adaptable to bulkier Cp derivatives.<sup>23</sup> As more sterically hindered Cp ligands are not readily commercially available, the ability to effectively synthesize these precursor metal complexes is essential for the progress of this work.



**Scheme 4.** General reaction schemes for the preparation of Cp metal complexes using standard synthetic routes. M is commonly an alkali metal salt in process (i) and commonly a Group 1 metal in process (iii), M' is any other metal, M<sup>m+</sup> is typically a low oxidation state metal (m=0-2), X is a halide, and L is typically CO in process (iii).<sup>23</sup>

The metalation/deprotonation route is key for the direct synthesis of Cp alkali salts from cyclopentadiene reactions with the respective metals or the respective hydrides or amides of these metals.<sup>23,24</sup> Additionally, the preparation of reagents such as KCp and NaCp have been successful using other strong bases such as KOH, and NaOH or NaOtBu respectively.<sup>24</sup> Salt metathesis is also significant for the preparation of most new Cp complexes due to its simplicity and high effectiveness whereas oxidative addition reactions are not as often utilized as they require bromine derivatives of highly substituted Cp ligands and are predominantly reserved for metals in low oxidation states.<sup>23</sup> In consideration of this project, methods (i) and (iii) are the most relevant for the desired metal complexes and will be utilized for the effective synthetic work of intermediates throughout as necessary.

### 1.5 Bismuth-Arene interactions Towards the Stabilization of Bismuth Cations

There are many advantages of bismuth-based compounds in chemical transformations including affordability, in some cases air and moisture stability, and functional group tolerance when compared to transition metal-based derivatives.<sup>25</sup> Bismuth is the heaviest stable element on the periodic table and is non-toxic and non-carcinogenic unlike other elements found in close proximity on the periodic table such as arsenic, antimony, lead, and tin which are highly toxic and hazardous to the environment.<sup>26</sup> With these characteristics in consideration, bismuth compounds have gained interest as a more environmentally friendly alternative reagent.

Organobismuth cations are a popular target in the literature due to their highly reactive nature but the difficulty in synthesizing stable intermediates and products has hindered the development of this research area.<sup>9</sup> To approach the instability issues,  $\pi$ -arene interactions have been demonstrated to provide a significant stabilizing effect on highly reactive bismuth cations.<sup>27</sup> Metal-arene  $\pi$ -coordination of the heavier pnictogens (As, Sb, Bi) with neutral aromatic hydrocarbons

was first investigated in the late 19<sup>th</sup> century and further developed at the beginning of the 20<sup>th</sup> century.<sup>28</sup> In 1986 the first evidence of bismuth-arene  $\pi$ -coordination was reported with the analysis of the X-ray single-crystal structures of  $\text{BiCl}_3 \cdot 1,3,5\text{-C}_6\text{H}_3\text{Me}_3$  followed by  $(\text{BiCl}_3)_2 \cdot \text{C}_6\text{H}_6$ .<sup>28-30</sup> The observed interactions were later classified as “Menshutkin” interactions, yielding Menshutkin-type complexes as Group 15 element (III) halide arene complexes.<sup>27,29,31</sup>

It has been suggested in the literature that the main contribution to the formation of the element- $\pi$ -system interactions is dispersion interactions with additional contributions from electron transfer in terms of  $\sigma$ -hole bonding.<sup>27</sup> Main Groups IV to VIII can participate in  $\sigma$ -hole bonding with one of their existing positively charged  $\sigma$ -hole interacting with a negatively charged electron donor or the  $\pi$ -electrons of unsaturated hydrocarbons and aromatic molecules (Figure 9).<sup>32</sup> The characterization of  $\sigma$ -holes is by its magnitude and size, where the magnitude represents the maximum positive electrostatic potential (ESP) of an electron density surface and the size refers to the positive spatial region.<sup>32,33</sup> The magnitude and size of a  $\sigma$ -hole increases proportionally with atomic size. Additionally, the bonding strength is proportional to its magnitude, suggesting these interactions are highly effective for heavier main Group IV-VIII elements.<sup>32</sup>

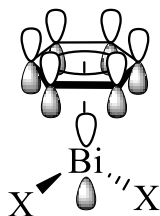


**Figure 9.** Generic bismuth- $\pi$ -arene complex, X = halide.<sup>27</sup>

For arene  $\pi$ -complexes of heavier Group 15 elements As, Sb, and Bi, the strongest complexes are formed with aromatic hydrocarbons with high donor strengths such as polyalkylated benzenes. Furthermore, the interactions for the corresponding metal cations of this type become more tightly

attached to the poly-methylated benzene rings than their parent metal complex due to the increase in Lewis acidity.<sup>27,30</sup> The Lewis acidity of cationic bismuth complexes arises from the large and diffuse empty bismuth-centered 6p-orbital that can accept electron density donated by a Lewis basic bonding partner.<sup>25</sup> Bismuth complexes have been shown to display a soft Lewis acidity character as these species show a high tolerance towards hard Lewis bases such that those containing oxygen-based functional groups, but can successfully coordinate and activate soft arene and olefin donor groups.<sup>25</sup> The <sup>TerMes</sup>Cp ligand will be exploited to synthesize the mono-, bis-, and tris-coordinated bismuth complexes, with the intent of then isolating cationic bismuth species that will be stabilized through metal-arene interactions with the mesityl groups of the ligand.

## 1.6 Bulky Cyclopentadienyl Germanium Cations

Germanium is a non-toxic metal that displays high thermal conductivity and is most commonly found in nature with oxidation states of Ge(II) and Ge(IV).<sup>34</sup> Organogermanium compounds have gained significant interest due to their applications in a variety of industries such as pharmacology, cosmetics, chemotherapy, and nanotechnology.<sup>34,35</sup> With such a wide application of organic germanium, further investigation of these species is of interest.

The ability to synthesize divalent germanium compounds containing organic ligands, (germylenes) has been a major goal in organometallic research. However, the development of germylenes has been hindered by the polymerization of these species.<sup>36,37</sup> This issue of polymerization can be overcome by both kinetic and thermodynamic stabilization. Kinetic and thermodynamic stabilization of these complexes to prevent dimerization, oligomerization, or polymerization of these species can be achieved through steric effects, which has generally been done in the literature using bulky aryl/silyl amine ligands.<sup>36-40</sup> Thermodynamic stabilization can also be achieved by using  $\eta$ - or  $\pi$ -donor ligands, which donate electron density to the vacant 4p-

orbital of the germanium center, therefore reducing the electron deficiency which can lead to the polymerization of these materials.<sup>36,37</sup> The general class of donor-stabilized germylenes of interest that has previously been studied by Jutzi *et al.* is half-sandwich compounds of the type Cp\*GeR, where Cp\* = pentamethylcyclopentadienyl and R = Cl (Figure 10).<sup>36,37,41,42</sup>



**Figure 10.** Germanium half sandwich complex characterized by Jutzi *et al.*<sup>36,37,41,42</sup>

By changing the Cp\* group in the germanium half-sandwich complex to incorporate the bulky TerMes ligand as <sup>TerMes</sup>Cp, the intention is to generate metal- $\pi$ -arene interactions through the mesityl groups of the *m*-terphenyl ligand. Assuming a germanium cation is formed, it is presumed that the germanium center will have metal-arene interactions with the nearby mesityl ring from the TerMes ligand which will provide stabilization of the cation. In this project, the synthesis of cationic germanium species will be investigated by chloride ion abstraction with the Lewis acid GaCl<sub>3</sub> and by salt metathesis with a weakly coordinating anion.

## 2.0 Experimental

### 2.1 General Experimental Methods and Characterization

For this project, all manipulations were carried out under an inert atmosphere of dry nitrogen gas using a mBraun inert atmosphere glovebox or standard Schlenk techniques unless otherwise stated. Glassware was dried for a minimum of four hours in an oven at 120 °C before use. Alumina and 4 Å molecular sieves were pre-dried in an oven at 120 °C for a minimum of three days before drying at 300 °C *in vacuo*. Celite<sup>®</sup> (diatomaceous earth) and silica gel were dried

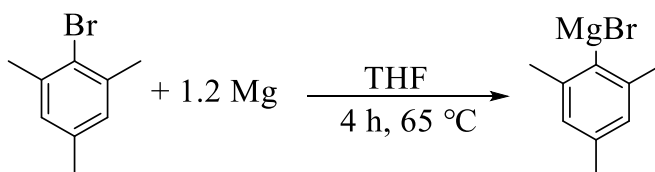
by storing in an oven at 120 °C for a minimum of three days before drying at 300 °C *in vacuo*. NMR solvents were purchased from Cambridge Isotope Laboratories, Inc. and stored over 4 Å molecular sieves for a minimum of three days before use. For deuterated benzene, the bottle was pre-dried with potassium hydride for a minimum of one day and then filtered through Celite® before storing over 4 Å molecular sieves. NMR spectra were recorded at 298 K on a 300 MHz spectrometer. Chemical shifts are reported in ppm, and coupling constants are reported in Hz and given as absolute values. <sup>1</sup>H NMR spectra are collected in deuterated solvents (<sup>2</sup>H defined as D) and referenced<sup>43</sup> to internal references of protonated solvents relative to tetramethyl silane, TMS ( $\delta = 0.00$  ppm), or by using an internal TMS standard found only in CDCl<sub>3</sub>. <sup>13</sup>C{<sup>1</sup>H} NMR spectra were referenced<sup>43</sup> internally to their respective deuterated solvents relative to TMS ( $\delta = 0.00$  ppm). <sup>19</sup>F NMR was referenced to external  $\alpha,\alpha,\alpha$ -trifluorotoluene ( $\delta = -63.72$  ppm) and <sup>11</sup>B NMR was referenced to external BF<sub>3</sub>·OEt<sub>2</sub> ( $\delta = 0.00$  ppm). IR spectra were collected using a Bruker ALPHA Platinum ATR unless otherwise indicated. Melting points were recorded on an Electrothermal MEL-Temp 3.0 using glass capillaries sealed under inert conditions. Dichloromethane (Fisher Scientific), diethyl ether (Fisher Scientific), THF (Sigma Aldrich), toluene (Fisher Scientific), and pentane (Fisher Scientific) were dried using an alumina-based solvent purification system from Vacuum Atmospheres. Diethyl ether, THF, toluene, and pentane were further dried using potassium hydride followed by filtration through alumina and stored over 4 Å molecular sieves overnight in the glovebox before use. Dichloromethane was stored over 4 Å molecular sieves for a minimum of three days before use. Acetonitrile (Fisher Scientific) and hexanes (Fisher Scientific) were used without further purification. All reagents were purchased from Sigma-Aldrich and used as they were received unless otherwise stated. Bismuth trichloride was purchased from Sigma-Aldrich and doubly sublimed prior to use. Potassium hydride was purchased as a

mineral oil dispersion (30%) from Sigma-Aldrich and washed a minimum of three times with sufficient pentane then dried *in vacuo* until a free-flowing powder was obtained.

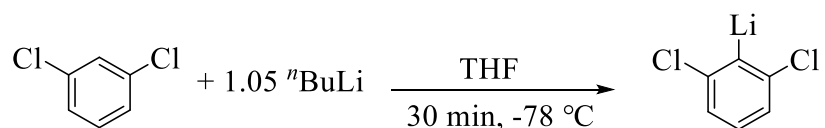
## 2.2 X-ray crystallography

Under inert conditions, crystals were prepared for mounting by suspending them in Paratone-N oil on a microscope slide. The crystal chosen was attached to the tip of a MicroLoop with Paratone-N oil. Measurements were made on a Bruker D8 VENTURE diffractometer equipped with a PHOTON III CMOS detector using monochromated Mo K $\alpha$  radiation ( $\lambda = 0.71073 \text{ \AA}$ ) from an Incoatec micro-focus sealed tube at 125 K.<sup>44</sup> The initial orientation and unit cell were indexed using a least-squares analysis of the reflections collected from a complete 180° phi-scan with 1° per frame. For data collection, a strategy was calculated to maximize data completeness and multiplicity, in a reasonable amount of time, and then implemented using the Bruker Apex 4 software suite.<sup>44</sup> The crystal to detector distance was set to 4 cm. Data collection, unit cell refinement, data processing and multi-scan absorption correction were applied using the APEX4<sup>44</sup> software package. The structures were solved using SHELXT<sup>45</sup> and all non-hydrogen atoms were refined anisotropically with SHELXL<sup>46</sup> using a combination of shelXle<sup>47</sup> and OLEX2<sup>48</sup> graphical user interfaces. Unless otherwise noted, all hydrogen atom positions were idealized and ride on the atom to which they were attached. The final refinement included anisotropic displacement factors on all non-hydrogen atoms.

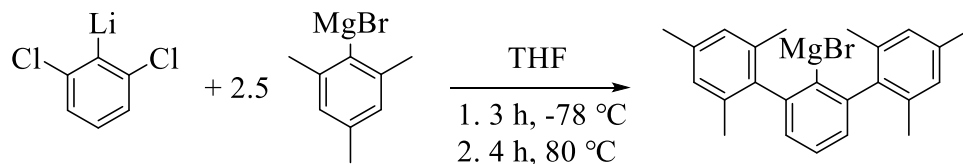
## 2.3 Synthesis of TerMesI - 1



Following a similar procedure as those reported in the literature<sup>23,49</sup>, 7.315 g of magnesium turnings (301 mmol, 1.19 eq.) and a PTFE-coated magnetic stir bar were added to a 500 mL 3-necked round bottom flask equipped with a 125 mL pressure-equalizing dropping funnel capped with a rubber septum on one of the side necks, a reflux condenser capped with a gas adaptor on the center neck, and a glass stopper on the final neck. The magnesium turnings were heated to 100 °C and stirred vigorously for *ca.* 30 minutes. The flask was then removed from the heat and allowed to cool. Once the flask was cooled to about 50-60 °C, 20 mL of THF was added through the dropping funnel to produce a magnesium slurry. While heating at 60 °C, 1-2 large crystals of I<sub>2</sub> (*ca.* 100 mg) was added to the slurry to activate the magnesium. With the addition of I<sub>2</sub>, the slurry went through a series of colour changes from yellow to orange to red, which dissipated within a few minutes of stirring and returned to a colourless slurry to show the magnesium had been successfully activated. In the closed dropping funnel, 38.5 mL of 2-bromomesitylene (50.1 g, 252 mmol, 1.0 eq) and 40 mL of THF were combined to produce a 1:1 MesBr:THF solution. This solution was added dropwise to the magnesium slurry over 30 minutes to produce a dark brown coloured mixture. After the complete addition of the MesBr:THF solution, the temperature was slowly increased until reaching reflux temperature, then heated under reflux for 4 hours. After 4 hours, the reaction was removed from the heat and allowed to cool. An aliquot of *ca.* 0.25 mL of the mixture was quenched with wet diethyl ether, filtered, and then dried *in vacuo*. The aliquot was then redissolved in C<sub>6</sub>D<sub>6</sub> and analyzed by <sup>1</sup>H NMR to ensure no 2-bromomesitylene remained unreacted. The reaction flask was brought into the glovebox under an inert atmosphere and then topped up with 250 mL of THF and allowed to stir overnight at room temperature.

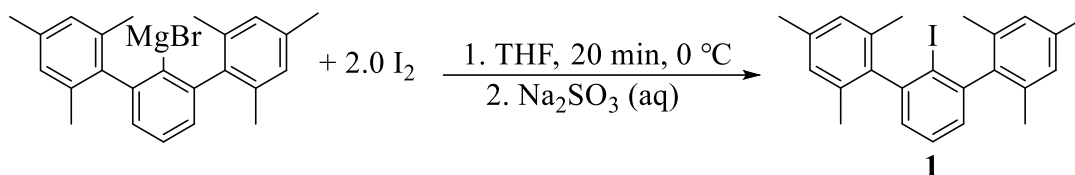


The following day, a 1L 3-neck round bottom flask equipped with a PTFE-coated magnetic stir bar, a 500 mL pressure-equalizing dropping funnel sealed off with a rubber septum, a rubber septum on the center neck, and a gas adaptor was set up under an inert atmosphere. Through the septum, 11.4 mL (14.7 g, 99.9 mmol, 1.0 eq) of pale yellow coloured 1,3-dichlorobenzene was added to the round bottom flask followed by 160 mL of THF to dilute the contents of the reaction flask. The reaction flask was then cooled to -78 °C using an acetone/liquid nitrogen bath while periodically adding dry ice to maintain the low temperature. To the reaction flask, 42.5 mL of a pale yellow solution of n-BuLi (2.5 M in hexanes, 106 mmols, 1.06 eq.) was added *via* syringe dropwise over 30 minutes through the center septum to produce a peach coloured mixture. After the complete addition, the reaction was left to stir for an additional 30 minutes at -78 °C. During that time, the dark brown coloured MesMgBr Grignard solution was transferred to the 500 mL dropping funnel *via* cannula.



To the pale yellow coloured reaction mixture, the MesMgBr Grignard solution was added dropwise over 3 hours while maintaining a temperature of -78 °C. Throughout the addition, the reaction mixture transitioned from the initial peach colour to yellow, then orange, then to a red-orange, before reaching the final dark brown colour. After the addition was complete, the reaction mixture was left to warm up to room temperature. Once the reaction mixture reached room temperature, a reflux condenser fitted with a gas adaptor was swapped in place of the center septum, and the side neck was closed off with a glass stopper. The reaction was then slowly heated in increments of 10 °C until reaching reflux temperature, and then allowed to reflux for 4 hours. After

4 hours, the reaction was removed from heat and allowed to cool to room temperature. Once the reaction mixture reached room temperature, an aliquot of *ca.* 0.25 mL was quenched and extracted with wet diethyl ether, filtered, dried, and then redissolved in C<sub>6</sub>D<sub>6</sub> and analyzed by <sup>1</sup>H NMR to ensure the reaction had gone to completion.



The dark brown reaction mixture was then cooled to 0 °C using an ice-water bath. The reflux condenser was removed, and the dropping funnel was replaced by a gas adaptor, leaving the center neck open to the atmosphere. With the aid of a funnel, 50.9 g of purple coloured I<sub>2</sub> crystals (201 mmol, 2.01 eq.) was slowly added to the reaction mixture, causing the reaction mixture to become dark reddish-brown in colour. This mixture was left to stir in the ice-water bath for 20 minutes. The excess I<sub>2</sub> remaining in the mixture was then quenched using 500 mL of 1 M aqueous solution of Na<sub>2</sub>SO<sub>3</sub>. The addition of the colourless solution of Na<sub>2</sub>SO<sub>3</sub> caused the reaction mixture to change colour from the reddish-brown to reddish-orange, then orange-yellow, until finally producing a pale yellow mixture that was left to slowly warm up to room temperature overnight.

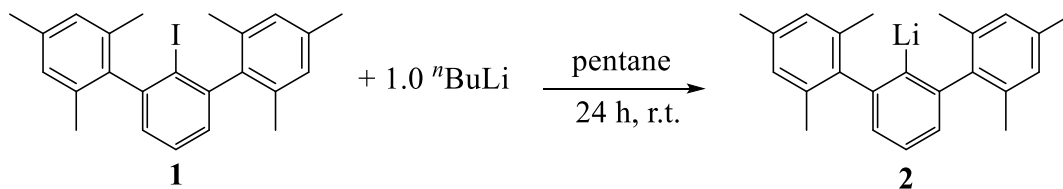
The following morning, the yellow mixture was left to separate into a bright yellow top organic layer and a pale yellow aqueous fraction along with some colourless precipitate at the bottom of the flasks. The reaction mixture was transferred into a 1 L separatory funnel and the aqueous layer was removed. Once the yellow organic fraction was isolated, it was then washed once with 200 mL of a saturated aqueous solution of NaCl. The yellow organic fraction was then dried with MgSO<sub>4</sub> for 20 minutes prior to removing the solids by vacuum filtration. The yellow filtrate was collected in a 1 L round bottom flask and the solvent was removed *in vacuo* to yield a

pale yellow solid. A PTFE-coated stir bar and *ca.* 300 mL of methanol were added to the round bottom flask containing the solids to produce a yellow mixture. A reflux condenser was attached to the flask then the reaction mixture was heated under reflux for 4 hours. The precipitate was then separated *via* hot vacuum filtration and the solids were washed with 150 mL of cold methanol and dried *in vacuo* to yield shiny white crystals of TerMesI, **1**. Before discarding the filtrate,  $^1\text{H}$  NMR analysis was done to ensure no significant quantity of **1** remained.

Yield: 25.8 g (59 % yield)

$^1\text{H}$  NMR ( $\text{C}_6\text{D}_6$ , 300 MHz):  $\delta$  7.09 (t,  $^3J_{\text{HH}} = 7.1$  Hz, 1H, *p*- $\text{C}_6\text{H}_3$ ), 6.88 (d,  $^3J_{\text{HH}} = 7.1$  Hz, 2H, *m*- $\text{C}_6\text{H}_3$ ), 6.84 (s, 4H, *m*- $\text{C}_6\text{H}_2(\text{CH}_3)_3$ ), 2.21 (s, 6H, *p*- $\text{CH}_3$ ), 2.07 (s, 12H, *o*- $\text{CH}_3$ ). The  $^1\text{H}$  NMR matches those previously described in the literature.<sup>23,49</sup>

## 2.4 Synthesis of TerMesLi - **2**



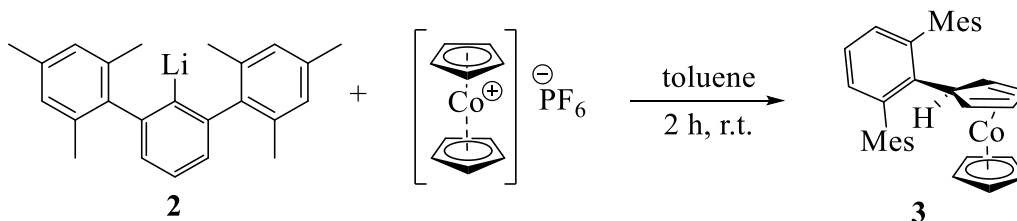
Following a similar procedure previously described in the literature<sup>23,50</sup>, 4.141 g (9.404 mmol, 1.0 eq.) of **1** was weighed out into a 20 mL scintillation vial equipped with a small PTFE-coated magnetic stir bar. To this vial, 10 mL of pentane was added to produce a colourless paste of **1**. While the stirring was off, a thin top layer of pentane was added, followed by 3.8 mL of a pale yellow *n*BuLi solution (2.5 M in hexanes, 9.5 mmol, 1.0 eq.) to produce a yellow-coloured mixture. This mixture was topped off with pentane, sealed, shaken, and left to stir overnight. The following day the mixture was transferred using a disposable glass Pasteur pipette and divided equally into two glass centrifuge tubes and centrifuged for 5 minutes. The resulting dark yellow

supernatant was decanted into a 250 mL round bottom flask then the original vial was rinsed with pentane and transferred to the centrifuge tubes for any residual product. After adding more pentane to the centrifuge for the next wash cycle, the mixture was vortexed until the solids were completely suspended in solution. This mixture was then centrifuged again for 5 minutes, and the resulting supernatant was a paler yellow colour and combined with the first wash. Following this, one more wash cycle with pentane was done for a total of three washes. The resulting solids were then dried *in vacuo* to yield a colourless powder.

Yield: 2.647 g (88 % yield)

$^1\text{H NMR}$  ( $\text{C}_6\text{D}_6$ , 300 MHz):  $\delta$  7.24 (t,  $^3J_{\text{HH}} = 7.5$  Hz, 1H, *p*- $\text{C}_6\text{H}_3$ ), 6.84 (s, 4H, *m*- $\text{C}_6\text{H}_2(\text{CH}_3)_3$ ), 6.83 (d,  $^3J_{\text{HH}} = 7.5$  Hz, 2H, *m*- $\text{C}_6\text{H}_3$ ), 2.17 (s, 6H, *p*- $\text{CH}_3$ ), 1.83 (s, 12H, *o*- $\text{CH}_3$ ). The  $^1\text{H NMR}$  matches those previously described in the literature.<sup>23,50</sup>

## 2.5 Synthesis of $^{\text{TerMes}}\text{CpH}(\text{CoCp})$ - **3**



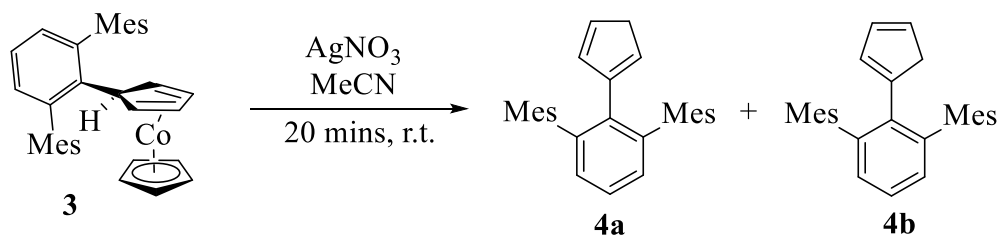
Following a similar procedure previously described in the literature<sup>7,23</sup> 4.997 g (15.6 mmol, 1.0 eq.) of **2**, a colourless powder, was weighed into a 20 mL scintillation vial and dissolved in approximately 20 mL of toluene to produce a beige coloured mixture. In a 250 mL round bottom flasks equipped with a PTFE-coated magnetic stir bar, 5.213 g (15.6 mmol, 1.0 eq.) of a bright yellow  $[\text{Cp}_2\text{Co}][\text{PF}_6]$  powder was suspended in approximately 20 mL of toluene to produce a tan coloured mixture. The mixture of **2** was added dropwise over 5 minutes to the stirring

[Cp<sub>2</sub>Co][PF<sub>6</sub>] suspension to produce a beige coloured mixture. After stirring for 10 minutes, the mixture went from beige to a copper-orange coloured mixture, followed by a dark red coloured mixture. The reaction was then left to stir for 2 hours and then an aliquot was removed for <sup>1</sup>H NMR analysis which indicated the reaction was complete and that *ca.* 20 % of TerMesH was formed as a by-product. The dark red mixture was then filtered through Celite<sup>®</sup> into a 250 mL Schlenk flask. The solvent was then removed *in vacuo* to afford the crude product as a shiny red solid. The crude product could then be crystallized by redissolving in a minimal amount of pentane and placed in the freezer at -30 °C overnight, however, this led to much lower yields and only reduced the presence of TerMesH, and therefore the crude was used for further reactions.

Yield: 7.279 g (93 %) as a mixture of **3** (80 %) and TerMesH (20 %) by <sup>1</sup>H NMR spectroscopy.

<sup>1</sup>H NMR (C<sub>6</sub>D<sub>6</sub>, 300 MHz): δ 7.03 (t, <sup>3</sup>J<sub>HH</sub> = 7.4 Hz, 1H, *p*-C<sub>6</sub>H<sub>3</sub>), 6.93 (s, 4H, *m*-C<sub>6</sub>H<sub>2</sub>(CH<sub>3</sub>)<sub>3</sub>), 6.78 (d, <sup>3</sup>J<sub>HH</sub> = 7.4 Hz, 2H, *m*-C<sub>6</sub>H<sub>3</sub>), 4.55 (m, <sup>4</sup>J<sub>HH</sub> = 1.9 Hz, 2H, Cp-CH), 4.32 (s, 5H, C<sub>5</sub>H<sub>5</sub>), 4.19 (t, <sup>4</sup>J<sub>HH</sub> = 2.5 Hz, 1H, Cp-CH), 2.50 (m, <sup>4</sup>J<sub>HH</sub> = 1.5 Hz, 2H, Cp-CH<sub>2</sub>), 2.28 (s, 6H, *p*-CH<sub>3</sub>) 2.10 ppm (s, 12H, *o*-CH<sub>3</sub>). The <sup>1</sup>H NMR matches those previously described in the literature.<sup>7,23</sup>

## 2.6 Synthesis of TerMesCpH – 4a+b



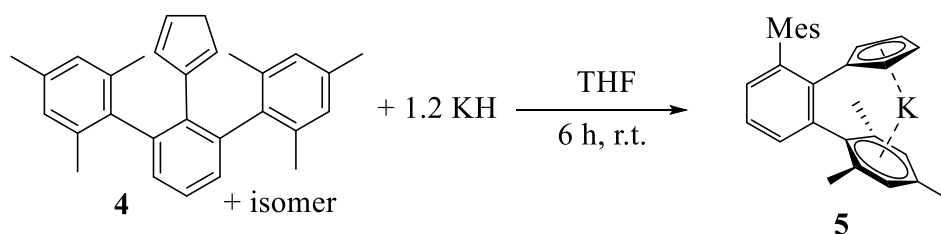
In a 250 mL round bottom flask equipped with a PTFE-coated magnetic stir bar, 3.944 g (7.8 mmol, 1.0 eq.) of crude **3** (77 % **3**, 23 % TerMesH) was suspended in *ca.* 80 mL of acetonitrile to produce a dark red suspension. In a 25 mL round bottom flask or beaker, 1.334 g (7.9 mmol, 1.0 eq.) of silver nitrate, AgNO<sub>3</sub>, was dissolved in 10 mL of acetonitrile to produce colourless

solution. The  $\text{AgNO}_3$  solution was added dropwise to the stirring suspension of **3** to instantly produce a dark grey/black coloured mixture with a grey/silver precipitate. The reaction was allowed to stir for *ca.* 20 minutes after the complete addition of the  $\text{AgNO}_3$  solution then sufficient  $\text{MgSO}_4$  was added to pre-dry the mixture. The solvent was removed *in vacuo* then the product was extracted with hexanes and filtered through Celite<sup>®</sup> into a pre-weighed 250 mL round bottom flask. The solvent was then removed *in vacuo* to obtain a pale yellow powder. This powder contained a mixture of two isomers of the product, as well as the TerMesH carried over from the previous reaction. On occasion when analyzing the product by  $^1\text{H}$  NMR it was observed that a single isomer was formed, however would quickly equilibrate with the other isomer in solution.

Yield: 2.697 g as a mixture of **4a+b** (85 %), and TerMesH (15 %) by  $^1\text{H}$  NMR spectroscopy.

$^1\text{H}$  NMR ( $\text{C}_6\text{D}_6$ , 300 MHz):  $\delta$  7.19 (dd,  $^3J_{\text{HH}} = 8.1$  Hz,  $^3J_{\text{HH}} = 1.44$  Hz, 1H, *p*- $\text{C}_6\text{H}_3$ ), 7.15 (dd, (overlapping with  $\text{C}_6\text{D}_5\text{H}$ , 1H, *p*- $\text{C}_6\text{H}_3$ ), 7.04 (m, 4H, *m*- $\text{C}_6\text{H}_3$  **4a+b**), 6.79 (s, 4H, *m*- $\text{C}_6\text{H}_2(\text{CH}_3)_3$ , **4a+b**), 6.22 (dq,  $^3J_{\text{HH}} = 5.13$  Hz,  $^4J_{\text{HH}} = 1.5$  Hz, 1H, Cp-CH, **4b**), 6.04 (m, 2H, Cp-CH, **4a**), 5.90 (dq,  $^3J_{\text{HH}} = 5.19$  Hz,  $^4J_{\text{HH}} = 1.44$  Hz, 1H, Cp-CH, **4a**), 5.81 (m, 2H, Cp-CH, **4b**), 2.72 (d,  $^3J_{\text{HH}} = 1.4$  Hz, 2H, Cp- $\text{CH}_2$ , **4a**), 2.40 (d,  $^3J_{\text{HH}} = 1.4$  Hz, 2H, Cp- $\text{CH}_2$ , **4b**), 2.13 ppm (s, 24H, *o*- $\text{C}_6\text{H}_2(\text{CH}_3)_3$ , **4a+b**), 2.09 ppm (s, 12H, *p*- $\text{C}_6\text{H}_2(\text{CH}_3)_3$ , **4a+b**). The  $^1\text{H}$  NMR matches those previously described in the literature.<sup>7,23</sup>

## 2.7 Synthesis of $\text{Ter}^{\text{Mes}}\text{CpK}$ - **5**

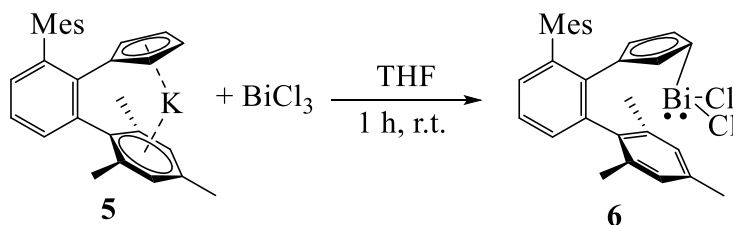


Following a similar procedure previously described in the literature<sup>7,23</sup>, 0.135 g (3.4 mmol, 1.2 eq.) of potassium hydride was weighed into a 250 mL round bottom flask equipped with a PTFE-coated magnetic stir bar and suspended in 30 mL of THF. In a 20 mL scintillation vial, 1.093 g (2.9 mmol, 1.0 eq.) of a crude mixture of **4a+b** (82 % **4a+b**, 18 % TerMesH) was dissolved in 20 mL of THF. Compound **4a+b** was then added dropwise to the stirring potassium hydride suspension to produce a yellow coloured solution shortly followed by a light orange coloured solution and then a dark brown coloured solution. The scintillation vial was rinsed with 3 x 5 mL of THF to ensure an appropriate concentration for the reaction and then left to stir overnight. The following day, the dark brown coloured solution was filtered through Celite<sup>®</sup> to remove the excess KH. The solvent was removed *in vacuo* to obtain a pale brown coloured solid.

Yield: 1.141 g as a mixture of **5** (85 %) and (15 % TerMesH) by <sup>1</sup>H NMR spectroscopy.

<sup>1</sup>H NMR (C<sub>6</sub>D<sub>6</sub>, 300 MHz): δ 7.25 (t, <sup>3</sup>J<sub>HH</sub> = 7.6, 1H, *p*-C<sub>6</sub>H<sub>3</sub>), 7.05 (s, 2H, *m*-C<sub>6</sub>H<sub>2</sub>(CH<sub>3</sub>)<sub>3</sub>), 6.93 (d, <sup>3</sup>J<sub>HH</sub> = 7.6 Hz, 2H, *m*-C<sub>6</sub>H<sub>3</sub>), 6.55 (s, 2H, *m*-C<sub>6</sub>H<sub>2</sub>(CH<sub>3</sub>)<sub>3</sub>), 5.71 (s, br, 3H, Cp-CH), 5.64 (s, br, 1H, Cp-CH), 2.37 (s, 6H, *o*-CH<sub>3</sub>), 2.27 (s, 6H, *o*-CH<sub>3</sub>), 2.11 (s, 6H, *p*-CH<sub>3</sub>). The <sup>1</sup>H NMR matches those previously described in the literature.<sup>7,23</sup>

## 2.8 Synthesis of <sup>TerMes</sup>CpBiCl<sub>2</sub> - **6**



In a 20 mL scintillation vial equipped with a small PTFE-coated magnetic stir bar, 0.175 g (0.55 mmol, 1.0 eq.) of BiCl<sub>3</sub> was dissolved in 1 mL of THF to produce a colourless solution. In a separate 20 mL scintillation vial, 0.228 g (0.55 mmol, 1.0 eq.) of **5** was dissolved in 2 mL of THF

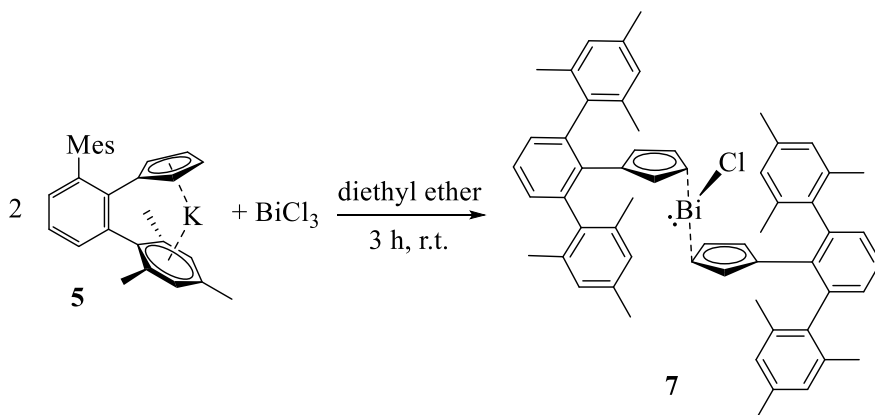
to produce a brown coloured solution. The solution of **5** was added dropwise to the stirring BiCl<sub>3</sub> solution, causing the clear solution to become an orange coloured mixture. The vial was then rinsed with 3 x 1 mL of THF to ensure complete transfer. The mixture was allowed to stir for 1 hour and then filtered through Celite<sup>®</sup> into a clean 20 mL scintillation vial. The solvent was then removed *in vacuo* to yield the crude orange-red coloured solids. The resulting solids were then washed with pentane then dried *in vacuo* to afford the desired product as a yellow-orange solid.

Yield: 0.270 g (75 %)

m.p. (°C): 111.2-112.5 °C

<sup>1</sup>H NMR (C<sub>6</sub>D<sub>6</sub>, 300 MHz): δ 7.12 (t, (overlapping with C<sub>6</sub>D<sub>5</sub>H) <sup>3</sup>J<sub>HH</sub> = 7.6, 1H, *p*-C<sub>6</sub>H<sub>3</sub>), 6.89 (d, <sup>3</sup>J<sub>HH</sub> = 7.6 Hz, 2H, *m*-C<sub>6</sub>H<sub>3</sub>), 6.66 (s, 4H, *m*-C<sub>6</sub>H<sub>2</sub>(CH<sub>3</sub>)<sub>3</sub>), 6.56 (pseudo-t, <sup>3</sup>J<sub>HH</sub> = 2.6 Hz, 2H, Cp-CH), 5.14 (pseudo-t, <sup>3</sup>J<sub>HH</sub> = 2.5 Hz, 2H, Cp-CH), 2.08 (s, 6H, *p*-CH<sub>3</sub>), 1.90 (s, 12H, *o*-CH<sub>3</sub>).

## 2.9 Synthesis of (Ter<sup>Mes</sup>Cp)<sub>2</sub>BiCl - **7**



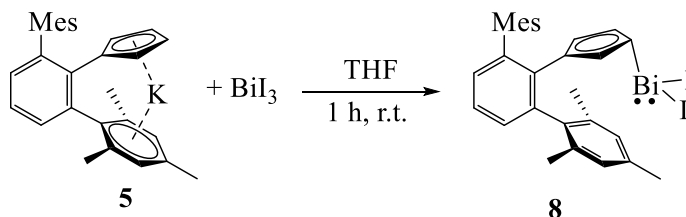
In a 20 mL scintillation vial equipped with a small PTFE-coated magnetic stir bar, 0.3649 g (0.87 mmol, 2.0 eq.) of **5** was dissolved in 4 mL of diethyl ether to produce a brown coloured suspension. In a separate 20 mL scintillation vial, 0.1376 g (0.44 mmol, 1.0 eq.) of BiCl<sub>3</sub> was dissolved in 2 mL of diethyl ether to produce a colourless solution. The BiCl<sub>3</sub> solution was added

dropwise to the stirring solution of **5**, causing the brown mixture to become an orange-brown coloured mixture. The vial was then rinsed with 3 x 1 mL of diethyl ether to ensure complete transfer. The mixture was allowed to stir for 3 hours and then filtered through Celite® into a clean 20 mL scintillation vial. The solvent was then removed *in vacuo* to yield the crude orange coloured solids. The product was then extracted with pentane, filtered through a fresh plug of Celite® then dried *in vacuo* to afford a yellow-orange foamy solid crude mixture. The pure product has not yet been obtained. The reported proton NMR lists only the peaks attributed by **7**.

Yield: 0.2273 g as a mixture of **6** (61 %), and **7** (39 %).

<sup>1</sup>H NMR (C<sub>6</sub>D<sub>6</sub>, 300 MHz): δ 7.11 (t, (overlapping with C<sub>6</sub>D<sub>5</sub>H), 1H, *p*-C<sub>6</sub>H<sub>3</sub>), 6.99 (m, 4H, *m*-C<sub>6</sub>H<sub>3</sub>), 6.55 (s, 8H, *m*-C<sub>6</sub>H<sub>2</sub>(CH<sub>3</sub>)<sub>3</sub>), 6.22 (pseudo-t, <sup>3</sup>J<sub>HH</sub> = 2.0 Hz, 2H, Cp-CH), 4.23 (pseudo-t, <sup>3</sup>J<sub>HH</sub> = 2.0 Hz, 2H, Cp-CH), 2.2 (s, 12H, *p*-CH<sub>3</sub>), 2.05 (s, 24H, *o*-CH<sub>3</sub>).

## 2.10 Synthesis of <sup>Ter</sup>MesCpBiI<sub>2</sub> - **8**



In a 20 mL scintillation vial equipped with a small PTFE-coated magnetic stir bar, 0.697 g (1.2 mmol, 1.0 eq.) of BiI<sub>3</sub> was dissolved in 4 mL of THF to produce a bright orange coloured solution. In a separate 20 mL scintillation vial, 0.494 g (1.2 mmol, 1.0 eq.) of **5** was dissolved in 3 mL of THF to produce a brown coloured solution. The solution of **5** was added dropwise to the stirring solution of BiI<sub>3</sub>, causing the solution to gradually darken from an orange coloured mixture to a dark blood-red coloured mixture. The vial was then rinsed with 3 x 1 mL of THF to ensure a

complete transfer of **5**. The mixture was allowed to stir for 1 hour and then filtered through a Celite<sup>®</sup> pipette filter into a clean 20 mL scintillation vial to yield a dark red solution. The solvent was then removed *in vacuo* to yield the crude red coloured solids. The resulting solids were then washed with pentane then dried *in vacuo* to afford the desired product as a maroon-red solid. Crystals suitable for X-ray diffraction were isolated from dissolving the product in minimal pentane and placed in the freezer at -35 °C overnight.

Yield: 0.8885 g (89 %)

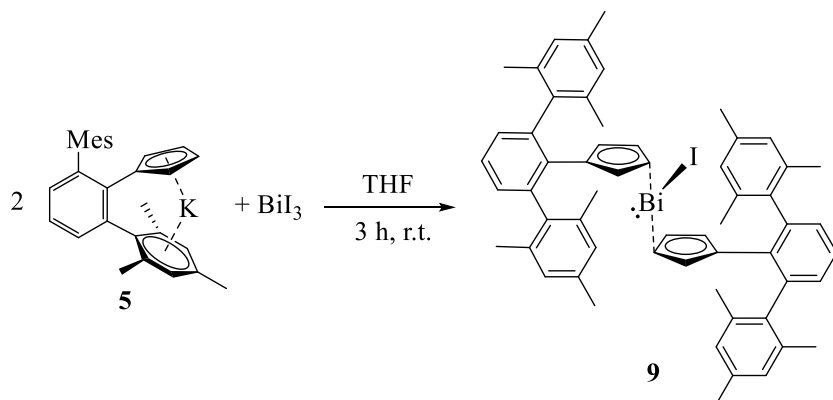
m.p. (°C): begins to decompose at 185 °C into a black solid.

<sup>1</sup>H NMR (C<sub>6</sub>D<sub>6</sub>, 300 MHz): δ 7.15 (t, (overlapping with C<sub>6</sub>D<sub>5</sub>H) <sup>3</sup>J<sub>HH</sub> = 7.6 Hz, 1H, *p*-C<sub>6</sub>H<sub>3</sub>), 6.89 (d, <sup>3</sup>J<sub>HH</sub> = 7.6 Hz, 2H, *m*-C<sub>6</sub>H<sub>3</sub>), 6.67 (s, 4H, *m*-C<sub>6</sub>H<sub>2</sub>(CH<sub>3</sub>)<sub>3</sub>), 6.54 (t, <sup>3</sup>J<sub>HH</sub> = 2.5 Hz, 2H, Cp-CH), 5.39 (t, <sup>3</sup>J<sub>HH</sub> = 2.5 Hz, 2H, Cp-CH), 2.1 (s, 6H, *p*-CH<sub>3</sub>), 1.92 (s, 12H, *o*-CH<sub>3</sub>).

<sup>13</sup>C {<sup>1</sup>H} NMR (C<sub>6</sub>D<sub>6</sub>, 75 MHz): δ 141.88, 140.41, 138.91, 136.91, 135.81, 128.56, 128.35, 127.86, 118.95, 103.02, 20.63, 20.51. The quaternary Cp carbon is not found on the <sup>13</sup>C spectrum.

FT-IR (ATR, cm<sup>-1</sup>): ν 2910 (m), 2849 (w), 2318 (w), 1734 (w), 1604 (w), 1566 (w), 1484 (w), 1447 (m), 1373 (m), 1303 (w), 1253 (w), 1182 (w), 1075 (m), 1035 (w), 1008 (w), 979 (w), 852 (s), 814 (vs), 785 (m), 755 (vs), 736 (m), 665 (w), 578 (w), 461 (w).

## 2.11 Synthesis of (Ter<sup>Mes</sup>Cp)<sub>2</sub>BiI - **9**



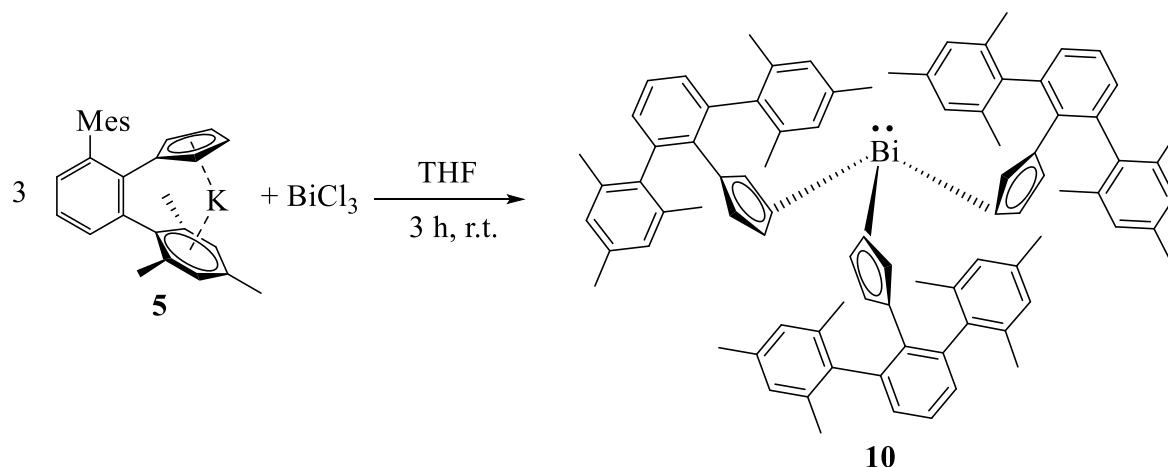
In a 20 mL scintillation vial equipped with a small PTFE-coated magnetic stir bar, 0.1974 g (0.33 mmol, 1.0 eq.) of BiI<sub>3</sub> was dissolved in 3 mL of THF to produce a bright orange coloured solution. In a separate 20 mL scintillation vial, 0.2801 g (0.67 mmol, 2.0 eq.) of **5** was dissolved in 3 mL of THF to produce a brown coloured solution. The solution of **5** was added dropwise to the stirring solution of BiI<sub>3</sub>, causing the reaction mixture to gradually darken from an orange coloured solution to a dark blood-red coloured mixture. The vial was then rinsed with 3 x 1 mL of THF to ensure a complete transfer of **5**. The mixture was allowed to stir for 3 hours and then filtered through a Celite<sup>®</sup> pipette filter into a clean 20 mL scintillation vial to yield a dark red-orange solution. The solvent was then removed *in vacuo* to yield the crude red coloured solids. The product was then extracted with pentane, filtered through a new plug of Celite<sup>®</sup> then dried *in vacuo* to afford an orange-red foamy solid mixture. An early attempt to purify the product by recrystallization from pentane yielded a small amount of material for analysis by <sup>1</sup>H NMR. All other subsequent attempts to obtain pure material have not been successful. Crystals suitable for X-ray diffraction were isolated from a mixture of compounds **8** and **9** by slow evaporation of a pentane solution containing a few drops of toluene. A mixture of **8** and **9** were present in the sample, and the best crystal of **9** was of low quality and therefore only atom connectivity could be obtained.

Yield: 0.2491 (68 %) as a mixture of **8** (47 %) and **9** (53 %)

<sup>1</sup>H NMR (C<sub>6</sub>D<sub>6</sub>, 300 MHz): δ 7.15 (t, (overlapping with C<sub>6</sub>D<sub>5</sub>H) <sup>3</sup>J<sub>HH</sub> = 7.6 Hz, 1H, *p*-C<sub>6</sub>H<sub>3</sub>), 7.02 (d, <sup>3</sup>J<sub>HH</sub> = 7.6 Hz, 2H, *m*-C<sub>6</sub>H<sub>3</sub>), 6.79 (s, 4H, *m*-C<sub>6</sub>H<sub>2</sub>(CH<sub>3</sub>)<sub>3</sub>), 6.20 (t, <sup>3</sup>J<sub>HH</sub> = 2.5 Hz, 2H, Cp-CH), 4.38 (t, <sup>3</sup>J<sub>HH</sub> = 2.5 Hz, 2H, Cp-CH), 2.17 (s, 6H, *p*-CH<sub>3</sub>), 2.08 (s, 12H, *o*-CH<sub>3</sub>).

## 2.12 Synthesis of $(\text{Ter}^{\text{Mes}}\text{Cp})_3\text{Bi}$ - **10**

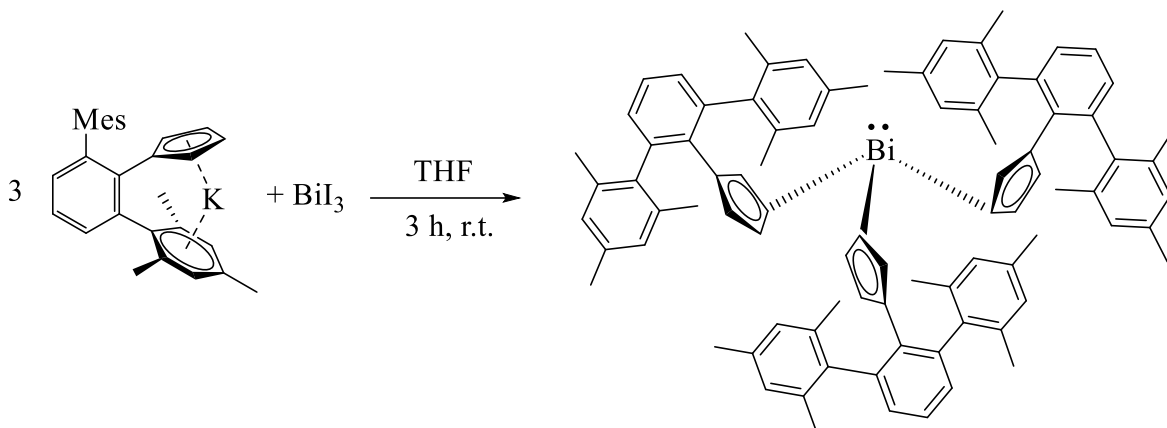
### Route A



In a 20 mL scintillation vial equipped with a small PTFE-coated magnetic stir bar, 0.0590 g (0.187 mmol, 1.0 eq.) of  $\text{BiCl}_3$  was dissolved in 3 mL of THF to produce a colourless solution. In a separate 20 mL scintillation vial, 0.2366 g (0.567 mmol, 3.0 eq.) of **5** was dissolved in 6 mL of THF to produce a brown coloured solution. The solution of **5** was added dropwise to the stirring solution of  $\text{BiCl}_3$ , producing an orange-brown coloured mixture. The vial was then rinsed with 3 x 1 mL of THF to ensure a complete transfer of **5**. The reaction was left to stir overnight and then filtered through a Celite<sup>®</sup> pipette filter into a clean 20 mL scintillation vial to yield a bright orange coloured solution. The solvent was then removed *in vacuo* to yield the crude orange solids. The resulting solids were then washed with pentane then dried *in vacuo* to afford the desired product as a pale yellow-orange solid. Crystals suitable for X-ray diffraction were isolated from the evaporation of pentane in a small test tube.

Yield: 0.1079 g (43 %)

## Route B



In a 20 mL scintillation vial equipped with a small PTFE-coated magnetic stir bar, 0.095 g (0.161 mmol, 0.99 eq.) of BiI<sub>3</sub> was dissolved in 2 mL of THF to produce a bright orange coloured solution. In a separate 20 mL scintillation vial, 0.2046 g (0.490 mmol, 3.0 eq.) of **5** was dissolved in 10 mL of THF to produce a brown coloured solution. The solution of **5** was added dropwise to the stirring solution of BiI<sub>3</sub>, producing an orange-brown coloured mixture. The vial was then rinsed with 3 x 1 mL of THF to ensure a complete transfer of **5**. The reaction was left to stir overnight and then filtered through a Celite<sup>®</sup> pipette filter into a clean 20 mL scintillation vial to yield a bright orange coloured solution. The solvent was then removed *in vacuo* to yield the crude orange solids. The resulting solids were then washed with pentane then dried *in vacuo* to afford the desired product as a pale yellow-orange solid.

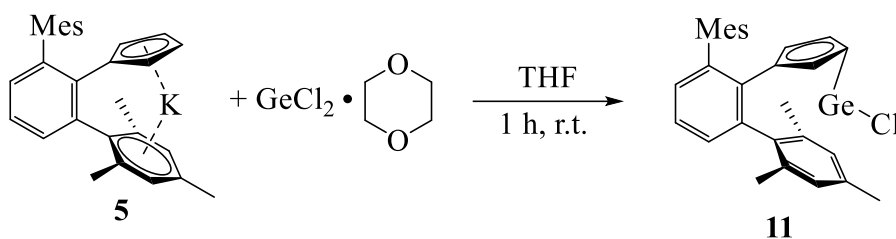
Yield: 0.0855 g (40%)

m.p. (°C): starts to decompose at 134 °C into a black solid/tar.

<sup>1</sup>H NMR (C<sub>6</sub>D<sub>6</sub>, 300 MHz): δ 7.13 (t, (overlapping with C<sub>6</sub>D<sub>5</sub>H), 3H, *p*-C<sub>6</sub>H<sub>3</sub>), 7.04 (d, <sup>3</sup>J<sub>HH</sub> = 6.8 Hz, 6H, *m*-C<sub>6</sub>H<sub>3</sub>), 6.74 (s, 12H, *m*-C<sub>6</sub>H<sub>2</sub>(CH<sub>3</sub>)<sub>3</sub>), 5.97 (pseudo-t, <sup>3</sup>J<sub>HH</sub> = 2.3 Hz, 6H, Cp-CH), 4.03 (pseudo-t, <sup>3</sup>J<sub>HH</sub> = 2.2 Hz, 6H, Cp-CH), 2.15 (s, 18H, *p*-CH<sub>3</sub>), 2.08 (s, 36H, *o*-CH<sub>3</sub>).

$^{13}\text{C}$   $\{^1\text{H}\}$  NMR ( $\text{C}_6\text{D}_6$ , 75 MHz):  $\delta$  141.88, 140.41, 138.91, 136.91, 135.81, 128.56, 128.35, 127.86, 118.95, 103.02, 20.63, 20.51. The quaternary Cp carbon is not found on the  $^{13}\text{C}$  spectrum. FT-IR (ATR,  $\text{cm}^{-1}$ ):  $\nu$  2947 (w), 2916 (w), 2855 (w), 1611 (w), 1485 (w), 1455 (m), 1376 (m), 1350 (w), 1033 (w), 1006 (w), 978 (m), 890 (w), 871 (m), 849 (vs), 817 (s), 804 (s), 782 (m), 760 (vs), 745 (w), 737 (w), 727 (w), 714 (w), 651 (w), 622 (m), 586 (w), 574 (w).

### 2.13 Synthesis of $\text{Ter}^{\text{Mes}}\text{CpGeCl}$ - **11**

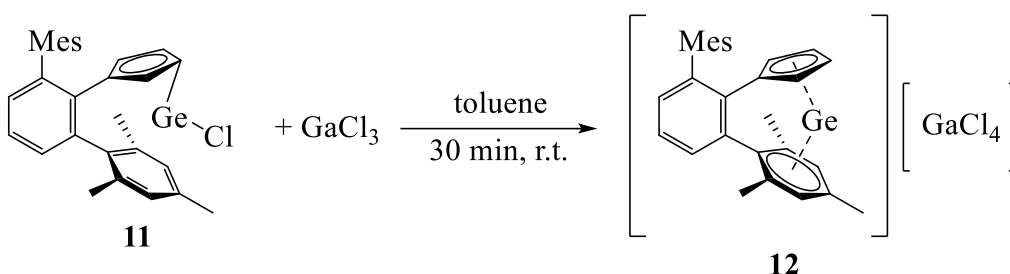


In a 20 mL scintillation vial equipped with a small PTFE-coated magnetic stir bar, 0.123 g (0.531 mmol, 1.0 eq.) of  $\text{GeCl}_2 \cdot \text{dioxane}$  was dissolved in 8 mL of THF producing a colourless solution. In a separate 20 mL scintillation vial, 0.224 g (0.536 mmol, 1.0 eq.) of **5** was dissolved in 2 mL of THF producing a brown solution. The  $\text{GeCl}_2 \cdot \text{dioxane}$  solution was added dropwise to the stirring solution of **5** to produce a light brown solution with half the addition, followed by a light orange coloured solution with the complete addition. The vial was then rinsed with 3 x 1 mL of THF to ensure the complete transfer. This was left to stir for 1 hour and then filtered through Celite<sup>®</sup>. The solvent was then removed *in vacuo* to afford the desired product as a light brown coloured solid.

Yield: 0.2052 g (78 %)

$^1\text{H}$  NMR ( $\text{C}_2\text{D}_2\text{Cl}_2$ ):  $\delta$  7.42 (t,  $^3J_{\text{HH}} = 7.7$  Hz, 1H,  $p\text{-C}_6\text{H}_3$ ), 7.16 (d,  $^3J_{\text{HH}} = 7.6$  Hz, 2H,  $m\text{-C}_6\text{H}_3$ ), 6.89 (s, 4H,  $m\text{-C}_6\text{H}_2(\text{CH}_3)_3$ ), 5.90 (pseudo-t,  $^3J_{\text{HH}} = 2.5$  Hz, 2H, Cp-CH), 5.86 (pseudo-t,  $^3J_{\text{HH}} = 2.4$  Hz, 2H, Cp-CH), 2.3 (s, 6H,  $p\text{-CH}_3$ ), 2.01 (s, 12H,  $o\text{-CH}_3$ ).

#### 2.14 Synthesis of $\text{Ter}^{\text{Mes}}\text{CpGe-GaCl}_4$ - **12**



In a 20 mL scintillation vial equipped with a small PTFE-coated magnetic stir bar, 0.2052 g (0.42 mmol, 1.0 eq.) of **11** was dissolved in 3 mL of toluene producing a tan coloured solution. In a separate 20 mL scintillation vial, 0.0965 g (0.54 mmol, 1.3 eq) of  $\text{GaCl}_3$  was dissolved in 2 mL of toluene to produce a colourless solution. The solution of  $\text{GaCl}_3$  was added dropwise to the stirring solution of **11** which instantly formed a beige solid precipitate. The vial was then rinsed with 2 x 1 mL of toluene to ensure the complete transfer. The reaction was left to stir for 30 minutes then the solvent was decanted to yield the crude free flowing beige solid. The solids were washed with 3 x 1 mL of toluene and then dried *in vacuo* to yield a shiny sand coloured solid. Crystals suitable for X-ray diffraction were isolated by performing a separate reaction. A test tube was first filled with a solution of  $\text{GaCl}_3$  (0.0425 g, 0.241 mmol, 1.0 eq.) dissolved in *ca.* 1 mL of toluene, then layered with 3-4 mL of pure toluene, followed by a solution of **11** (0.1176 g, 0.242 mmol, 1.0 eq.) dissolved in *ca.* 1 mL of toluene. Slow diffusion of reagents deposited crystals of compound **12** into the middle toluene layer.

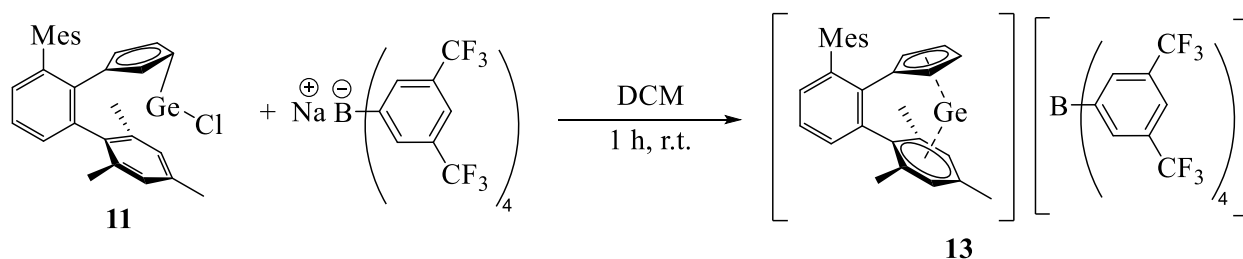
Yield: 0.1628 g (58 %).

m.p. (°C): 218.2-219.3 °C. Upon melting, the solid transitions to a grey liquid.

$^1\text{H}$  NMR ( $\text{C}_2\text{D}_2\text{Cl}_2$ , 300 MHz):  $\delta$  7.70 (t,  $^3J_{\text{HH}} = 7.8$  Hz, 1H,  $p\text{-C}_6\text{H}_3$ ), 7.34 (d,  $^3J_{\text{HH}} = 7.8$  Hz, 2H,  $m\text{-C}_6\text{H}_3$ ), 7.02 (s, 4H,  $m\text{-C}_6\text{H}_2(\text{CH}_3)_3$ ), 6.40 (pseudo-t,  $^3J_{\text{HH}} = 2.4$  Hz, 2H, Cp-CH), 6.35 (pseudo-t,  $^3J_{\text{HH}} = 2.5$  Hz, 2H, Cp-CH), 2.3 (s, 6H,  $p\text{-CH}_3$ ), 2.04 (s, 12H,  $o\text{-CH}_3$ ).

$^{13}\text{C}$   $\{^1\text{H}\}$  NMR ( $\text{C}_2\text{D}_2\text{Cl}_2$ , 75 MHz):  $\delta$  140.48, 139.56, 136.94, 130.66, 130.56, 129.65, 128.78, 128.15, 112.88, 110.94, 20.81, 20.48. The quaternary Cp carbon is not found on the  $^{13}\text{C}$  spectrum. FT-IR (ATR,  $\text{cm}^{-1}$ ):  $\nu$  3120 (w), 3106 (w), 2973 (m), 2917 (m), 2852 (w), 1602 (w), 1573 (w), 1494 (w), 1453 (m), 1415 (m), 1391 (m), 1375 (m), 1267 (w), 1182 (w), 1163 (w), 1104 (w), 1073 (w), 1061 (w), 1037 (m), 1014 (w), 943 (w), 900 (w), 883 (m), 868 (m), 841 (vs), 811 (s), 791 (m), 761 (s), 734 (m), 666 (w), 585 (m), 574 (m), 524 (w), 465 (w).

### 2.15 Synthesis of $\text{Ter}^{\text{Mes}}\text{CpGeBARF}_{24}$ - **13**



In a 20 mL scintillation vial, 0.1092 g (0.224 mmol, 1.0 eq) of **11** was dissolved in 4 mL of dichloromethane to produce a tan coloured solution. In a separate 20 mL scintillation vial equipped with a small PTFE-coated magnetic stir bar, 0.2002 g (0.226 mmol, 1.0 eq.) of NaBARF<sub>24</sub> dissolved in 3 mL of dichloromethane to produce a white cloudy mixture. The solution of **11** was added dropwise to the NaBARF<sub>24</sub> mixture, producing a tan coloured mixture that rapidly went grey with a fine precipitate. The reaction was left to stir for 1 hour. The solution was filtered then the solvent was removed *in vacuo* to yield the crude as a silver coloured solid. The solids were then redissolved in approximately 2 mL of dichloromethane and filtered into a clean 20 mL

scintillation vial then layered with 2 mL of pentane. After one week, large colourless crystals suitable for X-ray diffraction were formed. The crystals were then isolated by decanting off the solvent and rinsing with 4 x 1 mL of pentane.

Yield: 0.075 g (25 %)

m.p. (°C): 214.2-215.6 °C. Upon melting, the crystals transition to a blue-grey liquid.

$^1\text{H}$  NMR ( $\text{C}_2\text{D}_2\text{Cl}_2$ , 300 MHz):  $\delta$  7.76 (br s, 8H, *o*- $\text{C}_6\text{H}_3(\text{CF}_3)_2$ ), 7.73 (t (overlapping with *o*- $\text{C}_6\text{H}_3(\text{CF}_3)_2$ ), 1H, *p*- $\text{C}_6\text{H}_3$ ), 7.60 (br s, 4H, *p*- $\text{C}_6\text{H}_3(\text{CF}_3)_2$ ), 7.38 (d,  $^3J_{\text{HH}} = 7.7$  Hz, 2H, *m*- $\text{C}_6\text{H}_3$ ), 7.02 (s, 4H, *m*- $\text{C}_6\text{H}_2(\text{CH}_3)_3$ ), 6.40 (pseudo-t,  $^3J_{\text{HH}} = 2.5$  Hz, 2H, Cp-CH), 6.32 (pseudo-t,  $^3J_{\text{HH}} = 2.6$  Hz, 2H, Cp-CH), 5.37 (s, 1H, 0.5 eq of co-crystallized  $\text{CH}_2\text{Cl}_2$ ), 2.31 (s, 6H, *p*- $\text{CH}_3$ ), 2.03 (s, 12H, *o*- $\text{CH}_3$ ).

$^{13}\text{C}$  { $^1\text{H}$ } NMR ( $\text{C}_2\text{D}_2\text{Cl}_2$ , 75 MHz):  $\delta$  161.74 (q,  $^1J_{\text{C-F}} = 49.5$  Hz), 140.17, 140.06, 137.51, 136.79, 134.79, 131.36, 129.82, 128.97, 128.66 (q,  $^2J_{\text{C-F}} = 3.2$  Hz), 126.39, 122.78, 117.47, 113.59, 110.42, 20.68, 20.42. The quaternary Cp carbon is not found on the  $^{13}\text{C}$  spectrum.

$^{11}\text{B}$  NMR ( $\text{C}_2\text{D}_2\text{Cl}_2$ , 96 MHz):  $\delta$  -6.60 (s).

$^{19}\text{F}$  NMR ( $\text{C}_2\text{D}_2\text{Cl}_2$ , 283 MHz):  $\delta$  -62.77 (s).

FT-IR (ATR,  $\text{cm}^{-1}$ ):  $\nu$  2924 (w), 1610 (w), 1454 (w), 1352 (s), 1270 (vs), 1159 (s), 1114 (vs), 1057 (m), 1035 (w), 1014 (w), 931 (w), 912 (w), 865 (m), 854 (w), 837 (w), 808 (s), 788 (w), 760 (w), 742 (m), 714 (m), 681 (m), 669 (s), 583 (w), 573 (w), 447 (w).

### 3.0 Results and Discussion

#### 3.1 Optimization of Multistep Synthesis

##### 3.1.1 Optimization of TerMesI Synthesis

Previously, the work done related to this project was not easily accessible to others due to the difficulty in some of the required synthetic techniques as well as prolonged reaction durations of intermediate steps. To alleviate these issues, prior to probing for new discoveries, there has been a great focus on optimizing the multistep synthesis of the required starting reagents including the search for less challenging alternative synthetic routes to afford these materials. The first series of reactions are done on a large scale to yield a crucial reagent in this work known as TerMesI, **1**. The synthesis of **1** is well described in the literature<sup>23,49</sup> but often not with the greatest yields. For example, this synthesis is described by past Masuda group members and in the literature with an isolated yield of 44 % and 36 % respectively for **1**.<sup>23,49</sup>

For simplicity of the synthesis, the required THF was removed from the glovebox with 60 mL syringes as necessary for the reactions. Overall, for the synthesis of **1**, slight changes were made which included altering the initial reaction from refluxing for 6 hours with the heating mantle set at 65 °C to refluxing the reaction for 4 hours with the heating mantle set at 95 °C. The next change that was made for this synthesis was instead of allowing the MesMgBr Grignard solution to stir overnight while warming up to room temperature, once the addition was complete, the reaction was first removed from the dry ice liquid nitrogen/acetone bath and then the heating mantle was slowly heated to 80 °C and the reaction was refluxed for 4 hours. For the final step in the synthesis of **1**, the reaction duration was reduced from 90 minutes to 20 minutes after the addition of iodine to the TerMesMgBr Grignard reagent. Additionally for this step, the reflux was done using a more concentrated solution going from a solution with 500 mL of methanol to a solution with 300 mL. The resulting solids were then filtered hot and washed by stirring well with a spatula in the filter frit with a reduced amount of cold methanol from 300 mL to 100-150 mL. After thoroughly washing the product with cold methanol, the solvent was removed *via* vacuum

filtration, and the solids were dried *in vacuo* in a Schlenk flask with the aid of a hot water bath. With these minimal changes to the procedure, shiny white crystals were afforded rather than the typical beige/pale yellow coloured powder with a consistent average yield of  $57\pm 2$  % over three trials. These small changes have reduced the solvent waste, allowing for a greener synthetic approach with an appreciable increase in yield and purity of the product, which is imperative for large-scale reactions.

### 3.1.2 Optimization of TerMesLi Synthesis

The next step is making the lithium derivative, TerMesLi, **2**. When using the beige-coloured powder provided by a previous group member, the isolated yield was on average  $59\pm 4$  % over three trials. When converting the entire first batch of TerMesI of the white crystalline material to **2**, the average yield was  $85\pm 2$  % over five trials, and over the course of 14 trials including reactions from all three batches of TerMesI, the average yield was  $82\pm 1$  %. A yield of 78 % for this step was previously reported by a past member of the Masuda research group<sup>23</sup>, which still suggests an improvement, especially when considering the higher end of the newly isolated yields of 88%. This variation in yields demonstrates the importance of the purity of the starting material for this synthetic work.

### 3.1.3 Optimization of <sup>TerMes</sup>CpCoCp Synthesis

For the synthesis of <sup>TerMes</sup>CpCoCp, **3**, a variation of solvents, solvent pairs, and concentrations were investigated. For the first set of reactions, TerMesLi, **2**, was dissolved in pentane and [Cp<sub>2</sub>Co][PF<sub>6</sub>] was dissolved in toluene. As the concentration was increased for each reagent in their respective solvents, the overall yield for the formation of **3** decreased from 52 % to 38 % overall with an increase in the formation of TerMesH, according to <sup>1</sup>H NMR. This suggests

that increased concentrations of the reagents in the reaction displayed negative effects on the formation of **3**. The next reaction was done by diluting both reagents in THF, which resulted in an overall yield of 35 % for **3**, with a significant increase in the formation of TerMesH. Another solvent variation used was both reagents slightly diluted in pentane which resulted in the lowest yield of **3** with 11 % overall. The reaction was then attempted with both reagents dissolved in toluene. The first reaction was done at a concentration of 0.5 g of reagent per 10 mL of toluene which gave a yield of 73 % for **3** with a reduced contamination of TerMesH according to <sup>1</sup>H NMR analysis.

Following this reaction, a more dilute and a more concentrated reaction was conducted by decreasing and increasing the mass by a factor of two while maintaining the same volume of solvent. As the reaction was diluted, the yield decreased to 63 % overall for **3**, whereas the increased concentration stayed the same at 73 % overall for **3**. The reaction was then scaled up to a 5 g scale reaction using the concentration of 1 g of reagent per 10 mL of toluene. On average the yield for the scaled-up reactions was 70-75 % overall for **3**. Going forward all reactions were done on this scale following the suggested optimized concentrations of the reagents.

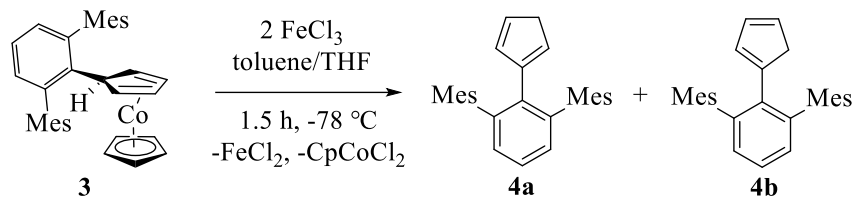
The formation of the TerMesH by-product is first observed in the synthesis of **3**. It is not understood mechanistically how this by-product is formed but it is suggested that the organolithium reagent, which is a strong base, reacts with an acidic proton from either an intermediate species in the reaction, or from the product of the reaction. To gain some insight into this problem, this was investigated by an NMR scale reaction of **2** and **3**. In a J-Young NMR tube, 6.4 mg of **2** (0.02 mmol, 1.0 eq.) and 10 mg of **3** (0.02 mmol, 1.0 eq.) were dissolved in 0.6 mL of deuterated benzene. Before mixing, **3** contained *ca.* 7 % TerMesH according to <sup>1</sup>H NMR analysis. The NMR tube was left in the glovebox overnight and then re-analyzed immediately the following

morning. Overnight there appeared to be minimal change in the concentration of TerMesH from *ca.* 7 % to 9 %. The reaction was then heated at 40 °C for 2 hours and analyzed once again by <sup>1</sup>H NMR which suggested no change. To test the limits of the reaction, the reaction was then heated at 80 °C for 4 hours, which showed a significant increase in the concentration of TerMesH from 9 % to 25 %. Although during the synthesis of **3** there is no heat involved, this supports the presence of both reagents in solution can form the TerMesH by-product. Since this test reaction was also done on a significantly smaller scale than what is used for the synthesis of **3**, this isn't an ideal representation of the reactivity between these two reagents as their concentrations vary throughout the progression of the synthesis of **3**. To arrive at a more conclusive understanding of their reactivity, additional studies of varied concentrations of the reagents in solution should be investigated.

### **3.1.4 Optimization of <sup>TerMes</sup>CpH Synthesis**

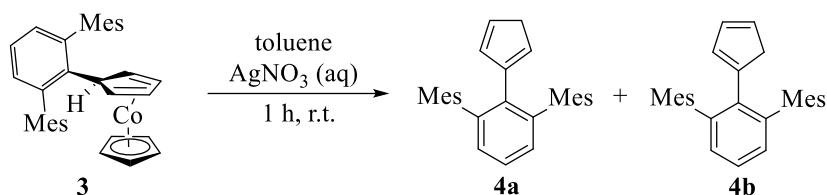
#### **3.1.4.1 Utilizing Redox Chemistry for the Synthesis of <sup>TerMes</sup>CpH**

The following step in this multi-step synthesis is to synthesize <sup>TerMes</sup>CpH, **4**. Previously this synthetic step used FeCl<sub>3</sub> and column chromatography (Scheme 5) which required a complicated setup, prolonged reaction durations, and dry ice to maintain proper reaction conditions.<sup>7,23</sup> Prior to finding an alternative synthetic route, this reaction was not feasible for undergraduate students due to the precise requirements of techniques and reaction conditions. With many factors to consider throughout the reaction, the yield was very inconsistent and would range anywhere from 0-82%. With complete failure of the reaction being a common occurrence using this method, this created a restraint for the progress of this project in the past.



**Scheme 5.** Previously designed synthetic route to *m*-terphenyl substituted Cp compounds from the oxidative decomposition of **3** by FeCl<sub>3</sub>.<sup>7,23</sup>

Alternatively, the reaction was done by past group members using toluene to dissolve **3** and reacted with an aqueous solution of AgNO<sub>3</sub> (Scheme 6). This reaction was repeated and a yield of 64 % was obtained. The reaction conditions were then altered and **3** was dissolved in acetonitrile and AgNO<sub>3</sub> remained dissolved in water. This reaction resulted in a 90 % crude yield but when extracted with hexanes, the final yield significantly decreased to 36 %.



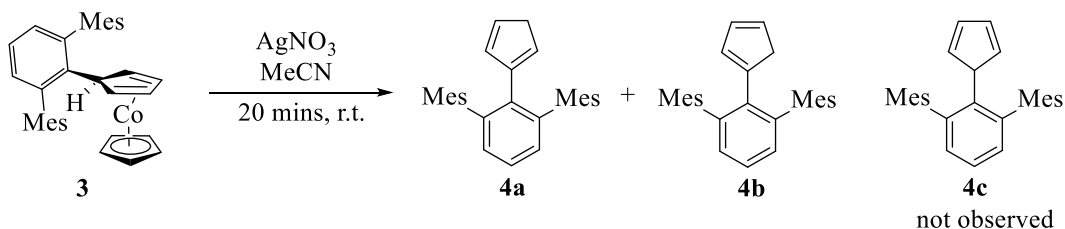
**Scheme 6.** Previously attempted synthetic route to *m*-terphenyl substituted Cp compounds from the oxidative decomposition of **3** by AgNO<sub>3</sub> in a binary solvent mixture of toluene and water.

One final attempt to improve the reaction conditions was made by dissolving both **3** and AgNO<sub>3</sub> in acetonitrile. Compound **3** is only slightly soluble in acetonitrile but as the reaction progressed, more of this reagent was able to dissolve and further react. The reaction mixture was first vacuum-filtered through Celite<sup>®</sup> to remove the solid by-products, dried *in vacuo* then the product was extracted with hexanes and gravity-filtered into a pre-weighed round bottom flask and

pumped to dryness again to afford the final product. Using this very simple, newly developed method allowed for a consistently high yield of  $81 \pm 2$  % over five trials. When gravity filtering in the final step, it was observed that some of the product was precipitating on the filter paper which caused a reduced yield for the reaction. To approach this problem and improve the yields, rather than filtering the reaction twice, the reaction was pumped to dryness prior to filtration then the product was extracted with hexanes. The hexanes solution was then vacuum filtered through Celite<sup>®</sup> and then pumped to dryness to obtain the final product. This slight alteration to the synthesis, increased the yield to 89 %. With high yields and a relatively simplistic synthetic route, this reaction went from a very technical, difficult synthesis with inconsistent results to a reaction that could easily be performed by undergraduates.

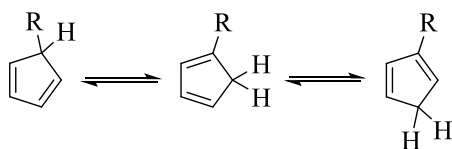
### 3.1.4.2 Isomers of <sup>Ter</sup>MesCpH

From the oxidation reaction of <sup>Ter</sup>MesCpCoCp with 1 equivalent of AgNO<sub>3</sub> followed by the previously described workup, the resulting Cp ligand precursor is isolated in the form of two isomers, **4a+b** as confirmed by comparing the <sup>1</sup>H NMR to the literature (Scheme 7).<sup>7,23</sup> Based on <sup>1</sup>H NMR analysis, there has been no indication of the formation of the allylic isomer, **4c**.



**Scheme 7.** New synthetic route to *m*-terphenyl substituted Cp compounds from the oxidative decomposition of **3** by AgNO<sub>3</sub> in acetonitrile.

A highly recognized phenomenon in the literature that supports this observation is the intramolecular migration of atoms or groups from  $sp^3$  hybridized carbons to nearby  $sp^2$  hybridized atoms contained in a five-membered, four- $\pi$  electron ring.<sup>51</sup> The most commonly observed example of this phenomenon is the rearrangement of a hydrogen atom around a cyclopentadiene ring, which leads to the rapid interconversion of 5-alkyl-cyclopentadienes to the respective 1-alkyl and 2-alkyl isomers (Scheme 8).<sup>51-53</sup> Previous kinetic studies of methyl-cyclopentadiene suggest a factor that contributes to this observation is the free energy difference between the given isomers. When comparing the 1-methyl isomer to the 5-methyl isomer, there is an approximate 8-10 kJ/mol energy difference, allowing for the spontaneous first-order decay of the 5-methyl isomer, to achieve a more stable conformation.<sup>52</sup> When comparing this to the rate of rearrangement from the 1-methyl isomer to the 2-methyl isomer, the rate of rearrangement of the latter is much smaller, which may be attributed to the fact that the free energy difference between the two isomers is much less at approximately 0-4 kJ/mol.<sup>52</sup> For further investigation of the **4a+b** mixture, DFT calculations have been performed, revealing that **4b** is less than 1 kJ/mol lower in energy than **4a**, and *ca.* 33 kJ/mol more stable than **4c**.<sup>7,23</sup> These findings agree with the experimental observations where the **4a** and **4b** isomers are obtained without **4c**.



**Scheme 8.** Interconversion of alkyl substituted cyclopentadiene ring.<sup>51-53</sup>

### 3.1.5 Optimization of <sup>TerMes</sup>CpK Synthesis

The final step of the multistep synthesis is the synthesis of <sup>TerMes</sup>CpK, **5**. Previously this reaction was done in a mixture of THF and toluene for the solvents and had a reaction duration of

*ca.* four days. Changing the solvent from a mixture of THF and toluene to pure THF, rapidly increased the reaction rate and decreased the reaction duration to within six hours. The yield for this reaction when performed on a 0.5-1g scale of  $\text{Ter}^{\text{Mes}}\text{CpH}$ , **4a+b**, has been 95-97 % however when done on a larger scale or a more concentrated scale, the yields have been much lower with an average of 49 % over three trials. It appears that as the reaction is done on a larger scale, even while maintaining the same concentration, a  $\text{Ter}^{\text{Mes}}\text{Cp}$  containing byproduct is formed that becomes insoluble in THF, toluene, and pentane. Additionally, the same issue is observed if the reaction is allowed to stir for an extended period after the reaction has gone to completion. To maximize the yield, the reaction is most consistent with the highest yields when done between a 0.5-0.75 g scale of **4a+b** with roughly 40 mL of THF per 0.5 g of **4a+b**.

A summary of the overall optimization of the multi-step synthesis can be seen in Table 1. From the optimization of the multi-step synthesis, the final yield has increased by greater than fivefold compared to the previously described synthesis in the literature<sup>7,23</sup>, giving an overall yield of 33.6 %, compared to the previous yield of 5.9 %. In addition to the significant increase in yield, the overall synthetic route has been simplified and the scale of the reactions have also been increased, which has saved an exceptional amount of time for the synthesis of the  $\text{Ter}^{\text{Mes}}\text{Cp}$  ligand. Although the optimization of this multi-step synthesis may still have some areas to further improve, this current state has allowed for further investigation to be done with the  $\text{Ter}^{\text{Mes}}\text{Cp}$  ligand framework in this project.

**Table 1.** Summary of the optimization of the multi-step synthesis of the  $\text{TerMesCp}$  ligand compared to literature.<sup>7,23</sup>

	<b>TerMesI</b> yield (%)	<b>TerMesLi</b> yield (%)	<b>TerMesCpCoCp</b> yield (%)	<b>TerMesCpH</b> yield (%)	<b>TerMesCpK</b> yield (%)	<b>Overall</b> yield (%)
<b>Literature</b> <sup>7,23</sup>	44	79	66	83	31	5.9
<b>Optimized Reactions</b>	59	88	75	89	97	33.6

## 3.2 The Discovery of $\text{TerMesCp}$ Bismuth Complexes

### 3.2.1 Investigation of Cp-*H* resonances

For this project, a series of  $\text{TerMesCp}$  bismuth halide complexes were synthesized. The first two complexes made in this work were  $\text{TerMesCpBiCl}_2$  followed by  $\text{TerMesCpBiI}_2$ . The synthesis of  $\text{TerMesCpBiCl}_2$  had previously been done by a past Masuda group member<sup>23</sup> by mixing 1 equivalent of  $\text{BiCl}_3$  with 1 equivalent of **5** in THF however, this work only contained preliminary, incomplete results.<sup>23</sup> The previous analysis done on this complex described the presence of four unique Cp-*H* resonances visible in the  $^1\text{H}$  NMR spectrum run in benzene ( $\delta$  6.55 ppm, 6.22 ppm, 5.10 ppm, and 4.23 ppm).<sup>23</sup>

In the previous procedure, the reaction was filtered to remove any salts formed, dried *in vacuo*, and then the product was extracted with pentane. The same procedure was used for the original synthesis of  $\text{TerMesCpBiI}_2$ , **8**, which also resulted in four Cp-*H* resonances at 6.54 ppm, 6.20 ppm, 5.39 ppm, and 4.38 ppm in the crude reaction mixture. Upon further investigation of the remaining solids left behind after the pentane extraction, the  $^1\text{H}$  NMR spectrum showed only two unique Cp-*H* resonances at 6.54 ppm and 5.39 ppm. From this discovery, it was suggested that in addition to the formation of **8**, a second equivalent of **5** was able to react with **8** in solution to form

(<sup>TerMes</sup>Cp)<sub>2</sub>BiI, **9**. When repeating for the chloride derivative, the same results were observed, with only two Cp-*H* resonances at 6.56 ppm and 5.14 ppm. This also explains the previously poor yields for this reaction due to the low solubility of the di-halide-bismuth complexes in pentane, where most of the product remained behind after the pentane extractions. Additionally, the previously reported yields were for a mixture of products, therefore the desired product was present in a much lower yield than reported. Going forward, to purify **6** and **8**, the solids were washed with pentane rather than extracted with pentane to remove the mono-halide-bismuth, **7** and **9** respectively.

In addition to <sup>1</sup>H NMR spectroscopy, **8** was also characterized by X-ray crystallography. The molecular structure of **8** features a trigonal pyramidal bismuth center bound to two iodides and an η<sup>1</sup>-coordinated Cp ring (Figure 11). In compound **8**, the bismuth-<sup>13</sup>C bond length (2.338(5) Å) is shorter than the shortest bismuth-Cp carbon bond length in η<sup>3</sup>-(iPr<sub>4</sub>Cp)-BiI<sub>2</sub> (2.48(2) Å)<sup>54</sup> but similar to the η<sup>1</sup>-Cp\*-bismuth bond length (2.397(6) Å) in Bi(Me<sub>2</sub>Si{NAr}<sub>2</sub>)(Cp\*).<sup>11</sup> The Bi-I bond lengths (2.8827(4) Å and 2.8450(5) Å) in **8** are similar to those in TerMesBiI<sub>2</sub> (2.8649(10) Å and 2.8302(10) Å) and the I-Bi-I bond angle (92.828(15) °) in **8** is smaller than that of TerMesBiI<sub>2</sub> (101.26(3) °).<sup>55</sup>

Furthermore, when analyzing the molecular structure of **8**, there are intermolecular interactions between the bismuth of one molecule and the iodine of a second molecule (3.7563(6) Å) as shown in Figure 11. Another key structural component to note of **8** is the angle between the mean plane of the central aromatic ring (C6-C11) of the TerMes group and the mean plane of the Cp ring (C1-C5) is 114.06(16) °. Additionally, the lone pair of electrons on bismuth are directed towards one of the mesityl rings and are suspected to be occupying a low lying 6s orbital.<sup>56,57</sup> This electron pair is stereochemically active; however, these electrons are not easily accessible due to the inert pair effect.<sup>56,57</sup>

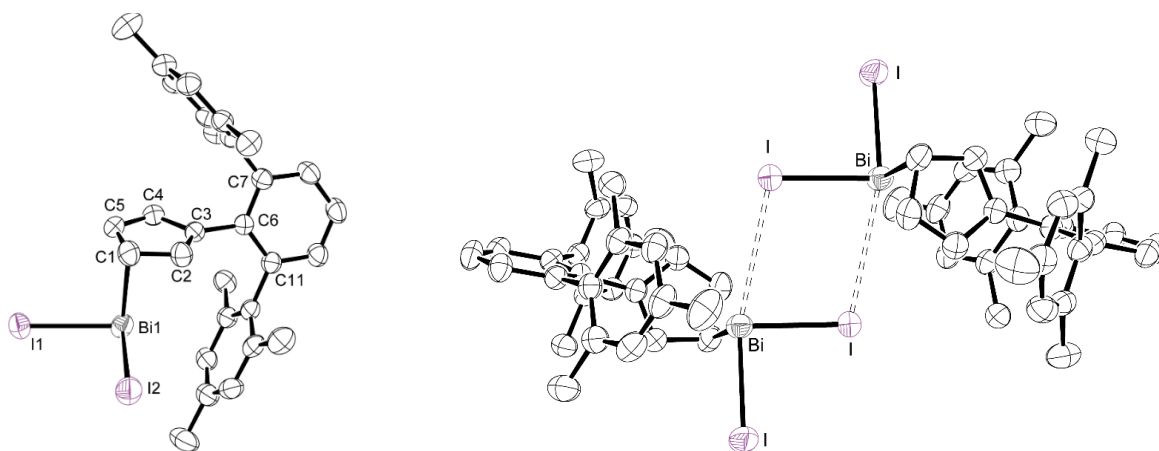


**Figure 11.** Molecular structure of **8** (left). Intermolecular Bi $\cdots$ I interactions (right). Ellipsoids are shown at the 50% probability level. Hydrogen atoms have been omitted for clarity.

After discovering the potential for two equivalents of the  $\text{Ter}^{\text{Mes}}\text{Cp}$  ligand to exchange with the bismuth halides, this reaction was attempted by mixing two equivalents of **5** with one equivalent of  $\text{BiI}_3$ . Following the original procedure, the reaction mixture was filtered, dried *in vacuo*, then the product was extracted with pentane to reduce the contamination of **8** in the product. The solvent was removed again *in vacuo* then the product was redissolved in minimal pentane and placed in the freezer at  $-35\text{ }^\circ\text{C}$  overnight. The following morning there were orange-red solids lining the bottom of the vial and an orange solution above. The solvent was decanted off and the solids were dried *in vacuo*. Since the reaction was performed on a small scale, the crystallization yielded only a small amount of material sufficient for analysis by  $^1\text{H}$  NMR. The  $^1\text{H}$  NMR spectrum showed only two unique Cp-*H* resonances at 6.20 ppm and 4.38 ppm, suggesting the successful isolation of  $(\text{Ter}^{\text{Mes}}\text{Cp})_2\text{BiI}$ , **9**. Unfortunately, subsequent attempts to purify **9** were all unsuccessful in the complete removal of **8**. The crude  $^1\text{H}$  NMR in all sequential attempts contained either contamination from  $\text{Ter}^{\text{Mes}}\text{CpBiI}_2$ ,  $(\text{Ter}^{\text{Mes}}\text{Cp})_3\text{Bi}$ , or both, which have not been easily separated. In

addition to  $^1\text{H}$  NMR spectroscopy, **9** was also characterized by X-ray crystallography, however, due to poor crystal quality only atom connectivity could be determined, and no metrical parameters will be discussed (Figure 12). However, it should be noted that no Bi-I intermolecular interactions were observed for this compound.

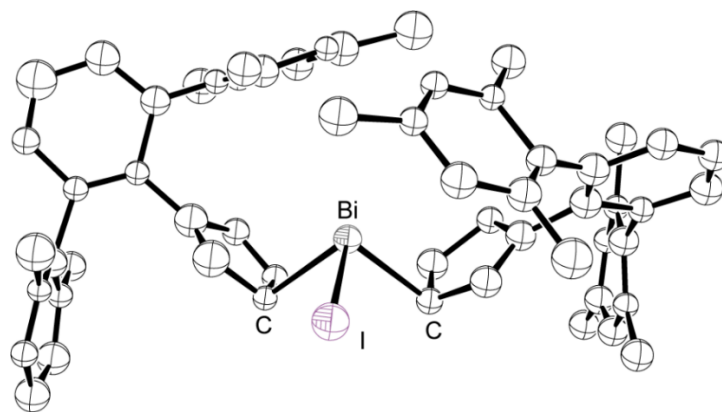


**Figure 12.** Molecular structure displaying the connectivity of **9**. Ellipsoids are shown at the 50% probability level. Hydrogen atoms have been omitted for clarity.

After a few additional attempts to synthesize **9**, when analyzing the  $^1\text{H}$  NMR spectrum, the presence of what appeared to be two additional Cp-*H* resonances was observed. It was previously assumed that three equivalents of the  $^{\text{TerMes}}\text{Cp}$  ligand may undergo unfavourable steric interactions, preventing the formation of  $(^{\text{TerMes}}\text{Cp})_3\text{Bi}$ , **10**, however, the additional Cp-*H* resonances indicated this product may be possible. To further investigate, three equivalents of **5** were mixed with one equivalent of  $\text{BiI}_3$ , to successfully yield **10**. For compound **10**, the Cp-*H* resonances were observed at 5.97 ppm and 4.03 ppm. A trend in the Cp-*H* resonances shows going from the mono- $^{\text{TerMes}}\text{Cp}$  to the bis- $^{\text{TerMes}}\text{Cp}$  to the tris- $^{\text{TerMes}}\text{Cp}$ , the two Cp-*H* chemical shifts gradually decrease in chemical shift with the addition of an equivalent of  $^{\text{TerMes}}\text{Cp}$  to the bismuth center, while the gap in chemical shifts of the two Cp-*H* resonances in the given complex increases from *ca* 1.15 ppm to 1.82 ppm to 1.94 ppm respectively.

To further characterize **10**, crystals suitable for X-ray diffraction were grown by slow pentane evaporation to yield orange needle-like crystals. The molecular structure of compound **10** features a trigonal pyramidal bismuth center bound to three  $\eta^1$ -coordinated cyclopentadienyl rings (Figure 14). In compound **10**, the three bismuth- $\eta^1$ C bond lengths (2.346(5) Å, 2.344(4) Å, and 2.380(5) Å) are similar to the three  $\eta^1$ -Cp bismuth bond lengths (2.34(2) Å, 2.37(2) Å, and 2.41(2) Å) in BiCp<sub>3</sub>.<sup>11,58</sup> A notable feature of **10**, which is also seen in BiCp<sub>3</sub>, is that when the <sup>TerMes</sup>Cp ligand is pointing down and the hydrogen atom is pointed towards the direction of the lone pair of electrons on the bismuth center, that Cp-bismuth bond length (2.380(5) Å) is slightly longer than when the hydrogen atom is pointed away from the lone pair of electrons (2.346(5) Å and 2.344(4) Å). The Cp-Bi-Cp bond angles (91.89(17) °, 93.32(16) °, and 97.50(16) °) in **10** are similar to the Cp-Bi-Cp bond angles (91.7(7) °, 94.3(7) °, and 98.0(6) °) in BiCp<sub>3</sub>.<sup>58</sup>

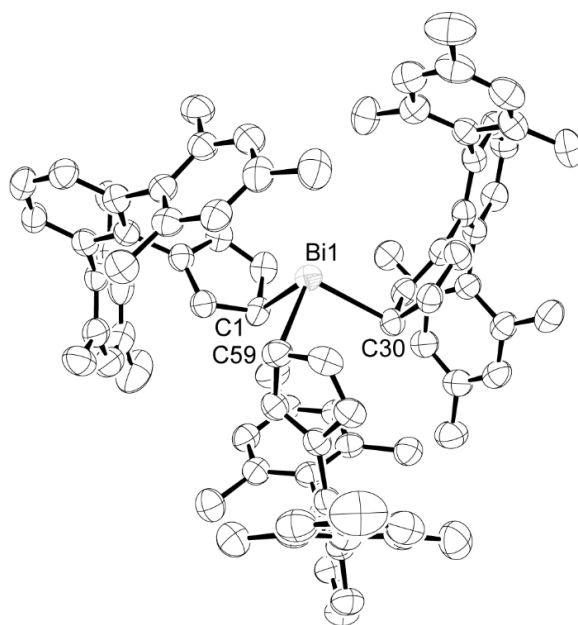


**Figure 13.** Molecular structure of **10**. Ellipsoids are shown at the 50% probability level. Hydrogen atoms have been omitted for clarity.

For compound **10**, an additional interesting feature is the encapsulation of the bismuth center by the three <sup>TerMes</sup>Cp groups as seen in Figure 14.

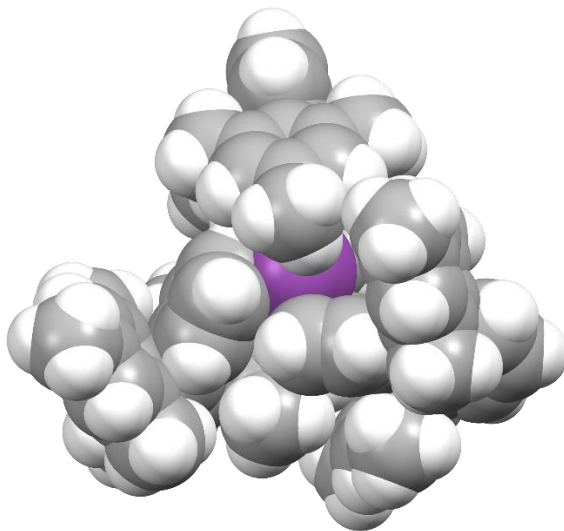


**Figure 14.** Space filling diagram of **10**. Ellipsoids are shown at the 50% probability level.

### 3.2.2 Purification Attempts for (<sup>TerMes</sup>Cp)<sub>2</sub>BiI

With the highest interest in (<sup>TerMes</sup>Cp)<sub>2</sub>BiI, **9**, for further reactivity studies, a great effort went into finding a reliable method to purify this compound. First, a variety of solvents including pentane, toluene, and a mix of pentane and toluene at varied ratios were used in attempt to selectively crystallize **9** from the other derivatives in the freezer at -35 °C overnight. Based on <sup>1</sup>H NMR analysis of these samples, no significant change was observed in the ratio of products. Other attempts for purification included slow evaporation from pentane which also led to a mixture of products. A consecutive series of three recrystallizations were done, however, the ratio of the mono-, bis-, and tris-<sup>TerMes</sup>Cp bismuth complexes only slightly differed between each recrystallization from the initial ratio of 65:31:4, to then a ratio of 52:44:3, to a final ratio 50:47:3. Aside from crystallization, a small-scale trial using a pipette column packed with silica gel was

used in an attempt to separate a mixture of the mono-, bis-, and tris-<sup>TerMes</sup>Cp complexes. This separation was attempted on a very small scale and only three separate fractions were collected, however, this showed potential in the ability to separate the mono-<sup>TerMes</sup>Cp complex from the bis- and tris-complexes. Due to time constraints, this has yet to be attempted on a larger scale, however, shows promising potential for separating samples that contain only the mono- and bis-<sup>TerMes</sup>Cp complexes.

In consideration of the failed attempts to purify **9**, different approaches to the synthesis were taken in an attempt to preferentially form **9**. One of the early attempts included performing the reaction at -35 °C. In this reaction, the ratio of the mono-, bis-, and tris-<sup>TerMes</sup>Cp bismuth complexes formed was 46:40:14, which showed some improvement towards favouring the bulkier products, but still lacked selectivity for the targeted bis-<sup>TerMes</sup>Cp bismuth complex. A similar attempt was also done at -78 °C under inert conditions using Schlenk techniques outside of the glovebox, however, it appeared that water managed to enter the reaction, which resulted in the formation of <sup>TerMes</sup>CpH and other unfamiliar impurities and has yet to be repeated. An additional attempt was made by adding the first equivalent of **5**, allowing the reaction to occur, and then later adding the second equivalent of **5**. For this reaction, the ratio of the mono-, bis-, and tris-<sup>TerMes</sup>Cp bismuth complexes was 57:34:9, which showed minimal improvement towards selectively synthesizing **9**.

Since it appeared that the selective formation of **9** was not easily attainable, a redistribution reaction of **10** and BiI<sub>3</sub> overnight in THF was attempted. In this reaction, the ratio of the mono-, bis-, and tris-<sup>TerMes</sup>Cp bismuth complexes was 46:46:8. This ratio of products is still not the greatest, however, the mono- and bis-<sup>TerMes</sup>Cp bismuth complexes are formed in equal ratios, which is improvement compared to the previous attempts. A similar issue was observed in the literature<sup>59</sup>

for the synthesis of  $\text{Dipp}_2\text{BiI}$ , which could not be separated from  $\text{DippBiI}_2$  in the product mixture. The closest to achieving a pure product was a ratio of 75:25 of  $\text{Dipp}_2\text{BiI}$  and  $\text{DippBiI}_2$  respectively.<sup>59</sup> With this being a common issue in the literature, it is important to determine a proper method of separation in the future to obtain the isolated desired product.

### 3.3 The Discovery of $\text{Ter}^{\text{Mes}}\text{Cp}$ Germanium Complexes

#### 3.3.1 Germanium precursor

The final part of this project shifted to reacting other main group metals with the  $\text{Ter}^{\text{Mes}}\text{Cp}$  ligand. With the difficulties faced for the purification of the bismuth mono-halide derivatives with the  $\text{Ter}^{\text{Mes}}\text{Cp}$  ligand,  $\text{Ter}^{\text{Mes}}\text{CpGeCl}$ , **11**, a known mono-halide main group metal complex incorporating the  $\text{Ter}^{\text{Mes}}\text{Cp}$  ligand in the Masuda group, was used for further reactivity studies. This complex could be easily synthesized from the reaction between **5** and  $\text{GeCl}_2(\text{dioxane})$  without further reacting with a second equivalent of **5**.

#### 3.3.2 Germanium Cations

With the ease in accessing the mono-halide germanium complex, the investigation of germanium cations became of interest. Cationic germanium species were synthesized by abstracting a chloride ion utilizing a Lewis acid or salt metathesis using sodium salts of weakly coordinating anions. The first reaction that underwent investigation was the reaction between **11** and the Lewis acid,  $\text{GaCl}_3$ . The product obtained by the reaction between **11** and  $\text{GaCl}_3$  was characterized by  $^1\text{H}$  NMR spectroscopy and X-ray crystallography.

When first analyzing the reaction by  $^1\text{H}$  NMR spectroscopy in  $\text{CD}_2\text{Cl}_2$ , a notable shift in the Cp-*H* resonances was observed, showing an increase in chemical shifts from 5.90 ppm and

5.86 ppm to 6.40 ppm and 6.35 ppm. The structure was then confirmed by X-ray crystallography to show the generation of the germanium (II) cation in the form of [<sup>TerMes</sup>CpGe][GaCl<sub>4</sub>], **12**.

To further characterize **12** crystals suitable for X-ray diffraction were grown by slow diffusion of reagents dissolved in toluene in a test tube separated by a middle layer of pure toluene to yield colourless crystals. The molecular structure of compound **12** features a bent germanium center bound to an η<sup>4</sup>-coordinated cyclopentadienyl ring (Figure 15). In compound **12** the germanium-<sup>n</sup>4C bond lengths (2.276(3) Å, 2.280(3) Å, 2.294(3) Å and 2.286(3) Å) are slightly longer than the η<sup>1</sup>-Cp germanium bond length (2.171(3) Å) in <sup>TerMes</sup>CpGeCl, a germanium complex previously synthesized in the Masuda group lab by Thai Do and similar to the η<sup>5</sup>-Cp germanium bond lengths (2.258(7) Å, 2.279(6) Å, 2.302(7) Å, 2.308(6) Å, and 2.281(7) Å) in [Cp\*Ge][SnCl<sub>3</sub>].<sup>60</sup> Another key structural component of **12** is the angle between the mean plane of the central aromatic ring of the TerMes defined by C6-C11 and the mean plane of the Cp ring defined by C1-C5, which is 82.88(11) °. Additionally, the cationic germanium center exhibits metal-arene interactions (Ge-centroid<sub>Mes</sub> = 2.84434(7) Å) and short distance interactions with the GaCl<sub>4</sub> anion (Ge-Cl1 = 3.39746(7) Å). Although it appears in Figure 15 that there may be an interaction between Ge and Cl4, the distance Ge-Cl4 (4.01073(8) Å), which is outside of the sum of the van derWaals radii (3.86 Å).

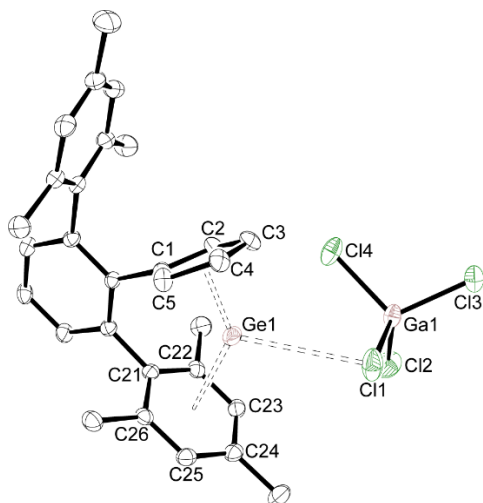


**Figure 15.** Molecular structure of **12**. Ellipsoids are shown at the 50% probability level. Hydrogen atoms have been omitted for clarity.

The next reaction that underwent investigation was between **11** and NaBArF<sub>24</sub>. The driving force for this metathesis reaction is the formation of the NaCl salt which precipitates out of solution, pushing the reaction in the forward direction. When analyzing the reaction by <sup>1</sup>H NMR spectrum in CD<sub>2</sub>Cl<sub>2</sub>, a similar shift in the Cp-*H* resonances to **12** was observed, where the chemical shifts increased from 5.90 ppm and 5.86 ppm to 6.40 ppm and 6.32 ppm. The structure for this product was then confirmed by X-ray crystallography, showing the generation of another germanium (II) cation in the form [<sup>TerMes</sup>CpGe][BArF<sub>24</sub>], **13**.

To further characterize **13** crystals suitable for X-ray diffraction were grown by slow diffusion of a dichloromethane solution layered with pentane to yield colourless crystals co-crystallized with half of an equivalent of dichloromethane. The molecular structure of **13** features a bent germanium center bound to an η<sup>3</sup>-coordinated cyclopentadienyl ring (Figure 16). In **13** the germanium-<sup>13</sup>C bond lengths (2.2592(12) Å, 2.2560(14) Å, and 2.2642(15) Å) are slightly longer than the η<sup>1</sup>-Cp germanium bond length (2.171(3) Å) in <sup>TerMes</sup>CpGeCl, a germanium complex

previously discussed and similar to the  $\eta^5$ -Cp germanium bond lengths (2.258(7) Å, 2.279(6) Å, 2.302(7) Å, 2.308(6) Å, and 2.281(7) Å) in [Cp\*Ge][SnCl<sub>3</sub>] previously discussed.<sup>60</sup> Another key structural component of **13** is the angle between the mean plane of the central aromatic ring of the TerMes defined by C6-C11 and the mean plane of the Cp ring defined by C1-C5, which is 89.84(6) °. Additionally, the cationic germanium center exhibits metal-arene interactions (Ge-centroid<sub>Mes</sub> = 2.7443(6) Å) and short distance interactions with the BARF<sub>24</sub> anion (Ge-C41 = 3.3047(12) Å).

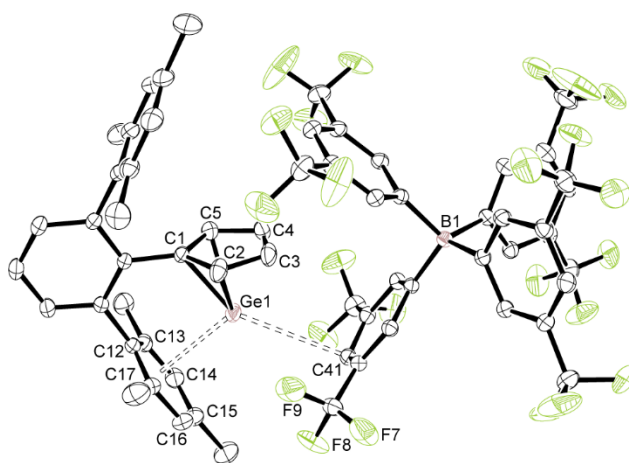


**Figure 16.** Molecular structure of **13**. Ellipsoids are shown at the 50% probability level. Hydrogen atoms have been omitted for clarity.

#### 4.0 Conclusions

The multistep synthesis up to and including the synthesis of <sup>TerMes</sup>CpK, **5**, has been optimized in consideration of yields, reaction duration, solvent waste, and simplicity of the synthetic route. The corresponding mono-, bis-, and tris-<sup>TerMes</sup>Cp bismuth complexes **8**, **9**, and **10** were prepared using routine synthetic approaches and were characterized by multinuclear NMR spectroscopy and X-ray crystallography. The full characterization for **9** has not been completed due to the inability to find a reliable purification method.

The synthesis of  $^{\text{TerMes}}\text{Cp}$ -germanium derivatives was investigated in addition to this project. The germanium (II) species **11** was prepared *via* salt metathesis with **5** and  $\text{GeCl}_2(\text{dioxane})$ . Compound **11** was then further reacted with  $\text{GaCl}_3$  and  $\text{NaBArF}_{24}$  to yield the germanium (II) cations **12**, and **13** respectively. Compounds **12** and **13** were characterized by multinuclear NMR spectroscopy and X-ray crystallography to confirm the identity of the cationic germanium species.

## 5.0 Future Work

Overall, there are many directions in which this project may progress or may have applications in related projects. The immediate priority for this project is to determine a consistent purification process for  $(^{\text{TerMes}}\text{Cp})_2\text{BiI}$ , **9**, to allow for further investigation of the targeted bismuth (III) cations. Once a consistent purification process is established, the synthesis of the bismuth (III) cations will be done following similar methods used for the germanium (II) cation derivatives including halide abstraction with Lewis acids or salt metathesis with weakly coordinating anions.

Furthermore, if unable to purify **9**, other methods to generate the bismuth cation will be investigated. One method includes the use of an oxonium acid,  $[\text{H}(\text{OEt}_2)_2][\text{B}(\text{C}_6\text{F}_5)_4]$ , designed by Jutzi *et al.* to react with  $(^{\text{TerMes}}\text{Cp})_3\text{Bi}$ , **10**, resulting in the loss of  $^{\text{TerMes}}\text{CpH}$  and producing  $[(^{\text{TerMes}}\text{Cp})_2\text{Bi}][\text{B}(\text{C}_6\text{F}_5)_4]$  (Figure 17).<sup>61</sup> Another similar method using the silver salt,  $[\text{Ag}(\text{arene})_3][\text{B}(\text{C}_6\text{F}_5)_4]$ , where arene is benzene or substituted benzene derivatives, could be used to oxidize the bismuth center to generate a radical cation from **10** (Figure 17).<sup>62</sup> If the product from the silver reaction were to decompose, this may ultimately lead to the generation of the desired bismuth cation  $[(^{\text{TerMes}}\text{Cp})_2\text{Bi}][\text{B}(\text{C}_6\text{F}_5)_4]$  (Figure 17).

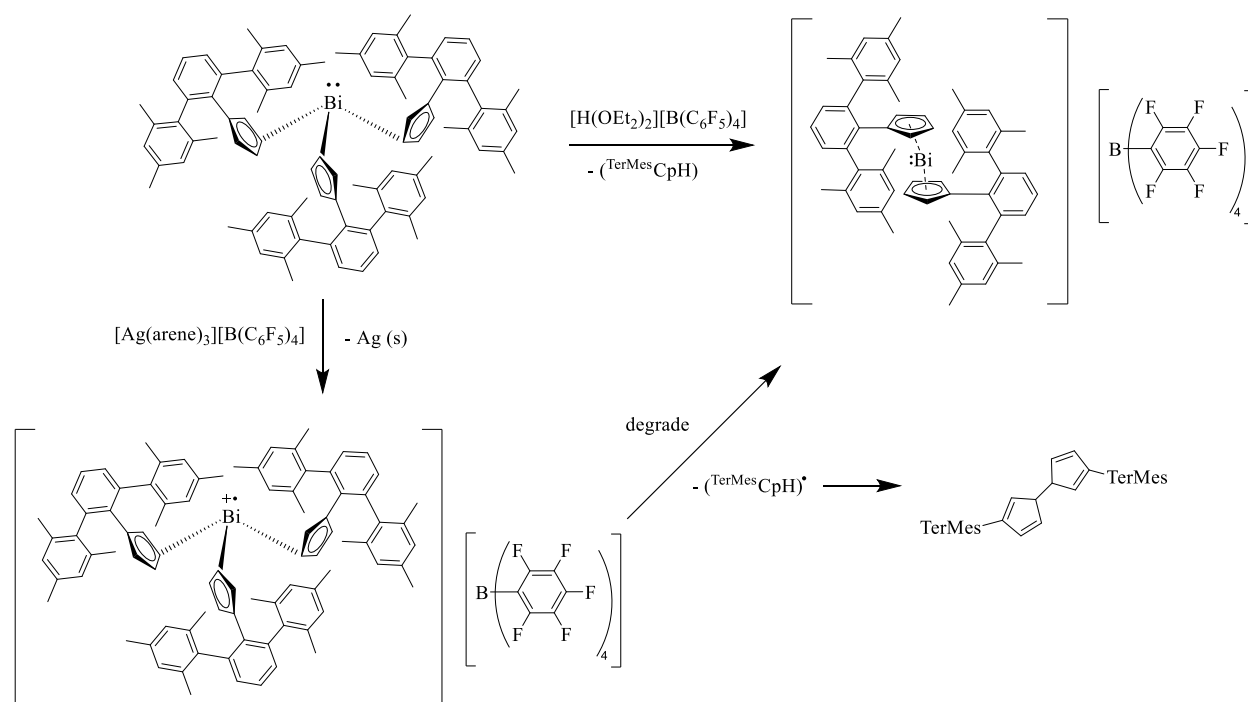


**Figure 17.** Future directions to generate bismuth cations.

For the germanium (II) cations **12** and **13**, the investigation of further reactivity including coordination chemistry or redox chemistry is the next step of this work. A reaction of interest is the addition of trimethylamine *N*-oxide to oxidize the germanium center of **13** from Ge (II) to Ge (IV) by inserting the cationic germanium center into the nitrogen-oxygen bond (Figure 18).<sup>63</sup> Additionally, there is interest in attempting to reduce the germanium (II) cation to germanium (I). It is suspected that the germanium (I) cation may not be sufficiently stable and either dimerize or generate a germanium (III) species by reducing the mesityl ring and oxidizing the metal (Figure 18), similar to related work with titanium (IV) species in the literature.<sup>64</sup>

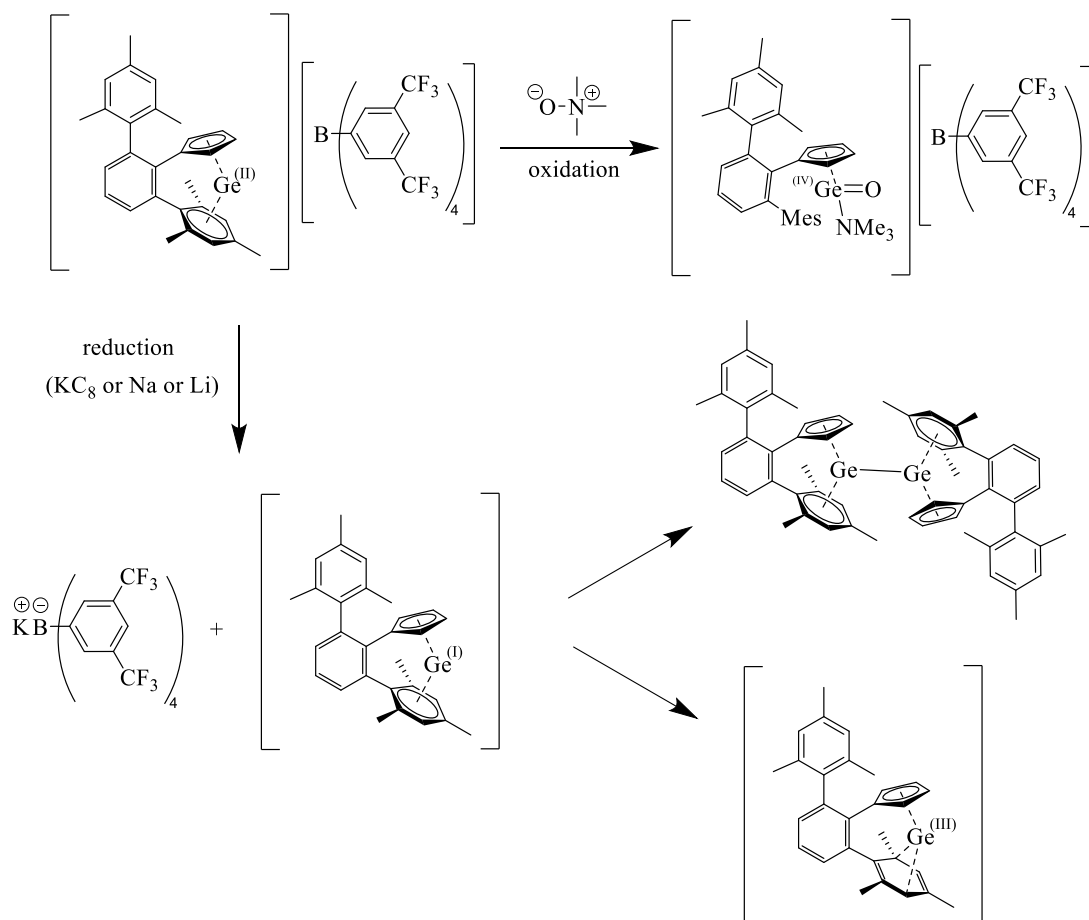


**Figure 18.** Future redox chemistry with **13**.

Aside from the  $\text{Ter}^{\text{Mes}}\text{Cp}$  project, the developed synthesis of  $\text{Ter}^{\text{Mes}}\text{CpH}$  may apply to related past projects in the Masuda group, including the BiphenylCp and the  $\text{Ter}^{\text{Dipp}}\text{Cp}$  projects. The synthesis of the Cp derivatives of the various ligands has been a common setback in these projects, but now with the newly developed synthetic route, these projects may be investigated in further detail. For the  $\text{Ter}^{\text{Dipp}}\text{Cp}$  project, it would be of interest to investigate any conformation changes due to the smaller substituents. For example, for the  $\text{Ter}^{\text{Mes}}\text{Cp}$  derivative, the potassium salt is a tetramer in the solid state, and investigating the effects of the ligand on this conformation could be conducted.

## References

1. Wilson, P. J.; Wells, J. H. The Chemistry and Utilization of Cyclopentadiene. *Chem. Rev.* **1944**, *34*, 1-50.
2. Breton, G. W. Generation and Observation of the Cyclopentadienyl Anion: A Negatively Charged Aromatic Molecule. *Chem. Educ.* **1997**, *2*, 1-8.
3. Kauffman, G. B. The Discovery of Ferrocene, the First Sandwich Compound. *J. Chem. Educ.* **1983**, *60* (3), 185.
4. Werner, H. At Least 60 Years of Ferrocene: The Discovery and Rediscovery of the Sandwich Complexes. *Angew. Chem. Int. Ed.* **2012**, *51* (25), 6052–6058.
5. Werner, H.; Werner, H. A Scientific Revolution: The Discovery of the Sandwich Complexes. *Landmarks in Organo-Transition Metal Chemistry: A Personal View* **2009**, 1–48.
6. Muthig, A. M. T.; Wieland, J.; Koop, S.; Lenczyk, C.; Kerner, F.; Hupp, B.; Steffen, A. Synthesis and Photophysical Studies of Copper (I) CAAC Half-Sandwich Complexes as a Highly Modifiable Class of Emitters. *Inorg Chem* **2022**, *61* (44), 17427–17437.
7. Veinot, A. J.; Todd, A. D.; Masuda, J. D. A Bulky m-Terphenyl Cyclopentadienyl Ligand and Its Alkali-Metal Complexes. *Angew. Chem. Int. Ed.* **2017**, *56*, 11615-11619. <https://doi.org/10.1002/ange.201706398>
8. Evans, W. J.; Davis, B. L. Chemistry of tris(pentamethylcyclopentadienyl) f-Element Complexes,  $(C_5Me_5)_3M$ . *Chem. Rev.* **2002**, *102* (6), 2119-2136. <https://doi.org/10.1021/cr010298r>.
9. Wiacek, R. J.; Jones, J. N.; Macdonald, C. L.; Cowley, A. H. Structural Interrelationships between the Bis(pentamethylcyclopentadienyl) Arsenic (III) and Antimony (III) Cations

- and their Precursor Chlorides. *Can. J. Chem.* **2002**, *80* (11), 1518-1523.  
<https://doi.org/10.1139/v02-075>.
10. Budzelaar, P. H. M.; Engelberts, J. J.; Lenthe, J. H. Van. Trends in Cyclopentadienyl–Main-Group-Metal Bonding. *Organometallics* **2003**, *22* (8), 1562–1576.
  11. Day, B. M.; Coles, M. P. Assigning Hapticity to Cyclopentadienyl Derivatives of Antimony and Bismuth. *Organometallics* **2013**, *32* (15), 4270–4278.
  12. Hosmane, N. S. In *Chapter 4 - Group Theory: Matrix Representation and Character Tables*; Elsevier Inc: 2017; pp 43-71.
  13. Liddle, S. T. Inverted Sandwich Arene Complexes of Uranium. *Coord Chem Rev* **2015**, *293*, 211–227.
  14. Jean, Y. In *Chapter 1- Molecular orbitals of transition metal complexes*; Oxford University Press: Oxford: 2005; pp 4-32.
  15. Jutzi, P.; Burford, N. Structurally Diverse  $\pi$ -Cyclopentadienyl Complexes of the Main Group Elements. *Chem Rev* **1999**, *99* (4), 969–990. <https://doi.org/10.1021/cr941099t>.
  16. Hierlmeier, G.; Wolf, R. Bulking up Cp<sup>BIG</sup>: A Penta-Terphenyl Cyclopentadienyl Ligand. *Organometallics* **2022**, *41* (6), 776–784. <https://doi.org/10.1021/acs.organomet.2c00009>.
  17. Erker, G.; Nolte, R.; Aul, R.; Wilker, S.; Krueger, C.; Noe, R. Cp-Substituent Additivity Effects Controlling the Stereochemistry of the Propene Polymerization Reaction at Conformationally Unrestricted (Cp-CHR<sub>1</sub>R<sub>2</sub>)<sub>2</sub>ZrCl<sub>2</sub>/Methylalumoxane Catalysts. *J Am Chem Soc* **1991**, *113* (20), 7594–7602.
  18. Ruble, J. C.; Latham, H. A.; Fu, G. C. Effective Kinetic Resolution of Secondary Alcohols with a Planar– Chiral Analogue of 4-(Dimethylamino) Pyridine. Use of the Fe (C<sub>5</sub>Ph<sub>5</sub>) Group in Asymmetric Catalysis. *J Am Chem Soc* **1997**, *119* (6), 1492–1493.

19. Trost, B. M.; Ryan, M. C. Indenylmetal Catalysis in Organic Synthesis *Angew. Chem. Int. Ed.* **2017**, *56* (11), 2862–2879.
20. Ni, C.; Power, P. P. Transition Metal Complexes Stabilized by Bulky Terphenyl Ligands: Application to Metal–Metal Bonded Compounds. *Metal-Metal Bonding* **2010**, 59–111.
21. Clyburne, J. A. C.; McMullen, N. Unusual Structures of Main Group Organometallic Compounds Containing *m*-Terphenyl Ligands. *Coord Chem Rev* **2000**, *210* (1), 73–99.
22. Curnow, O. J.; Fern, G. M.; Wöll, D. Synthesis of the Sterically Constrained Ligand Precursor Cyclopentadienyl-2,6-Diphenylbenzene and Structure of [(2,6-Ph<sub>2</sub>-C<sub>6</sub>H<sub>3</sub>-η<sup>5</sup>-C<sub>5</sub>H<sub>4</sub>)Zr(NEt<sub>2</sub>)<sub>3</sub>]. *Inorg Chem Commun* **2003**, *6* (9), 1201–1204.
23. Veinot, A. J. Phosphorus Cations and Bulky Cyclopentadienyl Ligands. Master's Degree. Thesis, Saint Mary's University, CA, 2017.
24. Panda, T. K.; Gamer, M. T.; Roesky, P. W. An Improved Synthesis of Sodium and Potassium Cyclopentadienide. *Organometallics* **2003**, *22* (4), 877–878.
25. Ramler, J.; Lichtenberg, C. Molecular Bismuth Cations: Assessment of Soft Lewis Acidity. *Chem. Eur. J.* **2020**, *26* (45), 10250–10258. <https://doi.org/10.1002/chem.202001674>.
26. Leonard, N. M.; Wieland, L. C.; Mohan, R. S. Applications of Bismuth (III) Compounds in Organic Synthesis. *Tetrahedron* **2002**, *58*, 8373-8397.
27. Bresien, J.; Hering-Junghans, C.; Schulz, A.; Thomas, M.; Villinger, A. Reactivity of TerN(SiMe<sub>3</sub>)BiCl<sub>2</sub>—Synthesis of an Aminobismuthenium Cation and TerN(SiMe<sub>3</sub>)Bi(N<sub>3</sub>)<sub>2</sub>. *Organometallics* **2018**, *37* (15), 2571–2580.
28. Auer, A. A.; Nolde, C.; Mansfeld, D.; Schneider, W.; Schürmann, M.; Mehring, M. Bismuth-Arene π-Interaction: A Combined Experimental and Theoretical Approach. *Organometallics* **2009**, *28* (18), 5405–5411. <https://doi.org/10.1021/om900536r>.

29. Preda, A. M.; Schneider, W. B.; Schaarschmidt, D.; Lang, H.; Mertens, L.; Auer, A. A.; Mehring, M. The Role of Dispersion Type Metal $\cdots\pi$  Interaction in the Enantiotropic Phase Transition of Two Polymorphs of Tris-(Thienyl) Bismuthine. *Dalton Trans.* **2017**, 46 (39), 13492–13501.
30. Schmidbaur, H.; Schier, A.  $\pi$ -Complexation of Post-Transition Metals by Neutral Aromatic Hydrocarbons: The Road from Observations in the 19th Century to New Aspects of Supramolecular Chemistry. *Organometallics* **2008**, 27 (11), 2361–2395.
31. Frank, W.; Weber, J.; Fuchs, E.  $[\text{CH}_3\text{C}_6\text{H}_5\text{BiCl}_2][\text{AlCl}_4]$  and  $[(\text{CH}_3)_6\text{C}_6\text{BiCl}_2][\text{AlCl}_4]$ -Compounds Containing  $\eta^6$ -Arene-Complexed BiCl Units. *Angew. Chem., Int. Ed Engl.* **1987**, 26 (1), 74–75.
32. Lo, R.; Švec, P.; Růžicková, Z.; Růžicka, A.; Hobza, P. On the Nature of the Stabilisation of the E $\cdots\pi$  Pnicogen Bond in the SbCl<sub>3</sub> $\cdots$  Toluene Complex. *Chem. Comm.* **2016**, 52 (17), 3500–3503.
33. Kolář, M.; Hostaš, J.; Hobza, P. The Strength and Directionality of a Halogen Bond Are Co-Determined by the Magnitude and Size of the  $\sigma$ -Hole. *Phys. Chem. Chem. Phys.* **2014**, 16 (21), 9987–9996. <https://doi.org/10.1039/c3cp55188a>.
34. Zheng, J.; Yang, L.; Deng, Y.; Zhang, C.; Zhang, Y.; Xiong, S.; Ding, C.; Zhao, J.; Liao, C.; Gong, D. A Review of Public and Environmental Consequences of Organic Germanium. *Crit Rev Environ. Sci Technol* **2020**, 50 (13), 1384–1409.
35. Dobrzyński, D.; Boguszewska-Czubara, A.; Sugimori, K. Hydrogeochemical and Biomedical Insights into Germanium Potential of Curative Waters: A Case Study of Health Resorts in the Sudetes Mountains (Poland). *Environ. Geochem Health* **2017**, 40 (4), 1335–1375. <https://doi.org/10.1007/s10653-017-0061-0>.

36. Jutzi, P.; Schmidt, H.; Neumann, B.; Stammer, H.-G. Bis(2,4,6-Tri-Tert-Butylphenyl) Germylene Reinvestigated: Crystal Structure, Lewis Acid Catalyzed C–H Insertion, and Oxidation to an Unstable Germanone. *Organometallics* **1996**, *15* (2), 741–746.
37. Winter, J. G.; Portius, P.; Kociok-Köhn, G.; Steck, R.; Filippou, A. C. Insertion of Cp\*GeCl into a Tungsten–Chlorine Bond and Crystal Structures of the Germylenes Cp\*GeCl, [Cp\*GeBr]<sub>2</sub>, and [Cp\*Ge][BF<sub>4</sub>] (Cp\* = Pentamethylcyclopentadienyl). *Organometallics* **1998**, *17* (19), 4176–4182.
38. Garg, P.; Dange, D.; Jones, C. Development of a Library of Extremely Bulky Amide Ligands, and Their Use for the Stabilization of Germanium (I) and Germanium (II) Compounds. *Z Anorg Allg Chem* **2023**, *649* (4), e202200303.
39. Hadlington, T. J.; Li, J.; Jones, C. Synthesis and Characterization of Extremely Bulky Amido-Germanium (II) Halide Complexes. *Can J Chem* **2014**, *92* (6), 427–433.
40. Pineda, L. W.; Jancik, V.; Colunga-Valladares, J. F.; Roesky, H. W.; Hofmeister, A.; Magull, J. Lewis Base Character of Hydroxygermylenes for the Preparation of Heterobimetallic LGe(OH)M Systems (M = Fe, Mn, L = HC [(CMe)(NAr)]<sub>2</sub>, Ar = 2,6-iPr<sub>2</sub>C<sub>6</sub>H<sub>3</sub>). *Organometallics* **2006**, *25* (9), 2381–2383.
41. Jutzi, P.  $\pi$  Bonding to Main-Group Elements; *Advances in organometallic chemistry*; Elsevier, 1986; Vol. 26, pp 217–295.
42. Jutzi, P. Cyclopentadienyl Complexes with Main-Group Elements as Central Atoms—a Decade of Research. *J Organomet Chem* **1990**, *400* (1–2), 1–17.
43. Fulmer, G. R.; Miller, A. J. M.; Sherden, N. H.; Gottlieb, H. E.; Nudelman, A.; Stoltz, B. M.; Bercaw, J. E.; Goldberg, K. I. NMR Chemical Shifts of Trace Impurities: Common Laboratory Solvents, Organics, and Gases in Deuterated Solvents Relevant to the

Organometallic Chemist. *Organometallics* **2010**, 29 (9), 2176–2179.

<https://doi.org/10.1021/om100106e>.

44. APEX 4 (Bruker, 2018) Bruker AXS Inc., Madison, Wisconsin, USA.
45. Sheldrick, G.M. (2015) *Acta Cryst.*, A71, 3-8.
46. Sheldrick, G.M. (2015) *Acta Cryst.*, C71, 3-8.
47. C. B. Hübschle, G. M. Sheldrick and B. Dittrich, *J. Appl. Crystallogr.*, 2011, **44**, 1281-1284 (DOI:10.1107/S0021889811043202).
48. O. V. Dolomanov, L. J. Bourhis, R. J. Gildea, J. A. K. Howard and H. Puschmann, *J. Appl. Crystallogr.*, 2009, **42**, 339-341 (DOI:10.1107/S0021889808042726).
49. Power, P. P. Homoleptic, Two-Coordinate Open-Shell 2,6-Dimesitylphenyl Complexes of Lithium, Manganese, Iron, and Cobalt. In *Inorganic Syntheses*, Vol 37; John Wiley & Sons, Incorporated: 2018; pp 47-83.
50. Ruhlandt-Senge, K.; Ellison, J. J.; Wehmschulte, R. J.; Pauer, F.; Power, P. P. Isolation and Structural Characterization of Unsolvated Lithium Aryls. *J. Am. Chem. Soc.* **1993**, *115*, 11353-11357.
51. Majchrzak, M. W.; Jefferson, E.; Warkentin, J. Stepwise Mechanism of Formal 1, 5-Sigmatropic Rearrangement of Dimethyl 3,3-Dialkyl-3H-Pyrazole-4,5-Dicarboxylates. *J Am Chem Soc* **1990**, *112* (6), 2449–2451.
52. McLean, S.; Haynes, P. Hydrogen Migration in Cyclopentadienes. *Tetrahedron* **1965**, *21* (9), 2329–2342.
53. McLean, S.; Webster, C. J.; Rutherford, R. J. D. Kinetic Isotope Effect for the Thermally-Induced Migration of Hydrogen in Cyclopentadienes. *Can J Chem* **1969**, *47* (9), 1555–1559.

54. Sitzmann, H.; Wolmershäuser, G. Wismutverbindungen Mit Voluminösen, Mehrfach Alkylierten Cyclopentadienyl-Liganden. *Chem Ber* **1994**, *127* (8), 1335–1342.
55. Breunig, H. J.; Haddad, N.; Lork, E.; Mehring, M.; Mügge, C.; Nolde, C.; Raț, C. I.; Schürmann, M. Novel Sterically Congested Monoorganobismuth (III) Compounds: Synthesis, Structure, and Bismuth–Arene  $\pi$  Interaction in  $\text{ArBiXY}$  (X, Y = Br, I, OH, 2, 6-Mes<sub>2</sub>-4-*t*-Bu-C<sub>6</sub>H<sub>2</sub>PHO<sub>2</sub>). *Organometallics* **2009**, *28* (4), 1202–1211.
56. Lyczko, K. Tropolone as Anionic and Neutral Ligand in Lead (II) and Bismuth (III) Complexes: Synthesis, Structure, Characterization and Computational Studies. *J Mol Struct* **2017**, *1127*, 549–556.
57. Kyono, A.; Kimata, M. Structural Variations Induced by Difference of the Inert Pair Effect in the Stibnite-Bismuthinite Solid Solution Series (Sb,Bi)<sub>2</sub>S<sub>3</sub>. *Am. Min.* **2004**, *89* (7), 932–940.
58. Lorberth, J.; Massa, W.; Wocadlo, S.; Sarraje, I.; Shin, S.-H.; Li, X.-W. Synthesis and Crystal Structure of EO Fischer’s “Red Crystalline Modification of Tris-Cyclopentadienylbismuth, (1<sup>h</sup>-C<sub>5</sub>H<sub>5</sub>)<sub>3</sub>Bi.” *J Organomet Chem* **1995**, *485* (1–2), 149–152.
59. Dunaj, T.; Dollberg, K.; Ritter, C.; Dankert, F.; von Hänisch, C. 2,6-Diisopropylphenyl-Substituted Bismuth Compounds: Synthesis, Structure, and Reactivity. *Eur J Inorg Chem* **2021**, *2021* (9), 870–878. <https://doi.org/10.1002/ejic.202001019>.
60. Rouzaud, J.; Joudat, M.; Castel, A.; Delpech, F.; Rivière, P.; Gornitzka, H.; Manriquez, J. M.; Chavez, I. New Linked Di-Germanocenes and Di-Stannocenes. *J Organomet Chem* **2002**, *651* (1–2), 44–51.

61. Jutzi, P.; Müller, C.; Stammler, A.; Stammler, H. G. Synthesis, Crystal Structure, and Application of the Oxonium Acid  $[\text{H}(\text{OEt}_2)_2]^+[\text{B}(\text{C}_6\text{F}_5)_4]^-$ . *Organometallics* **2000**, *19* (7), 1442–1444. <https://doi.org/10.1021/om990612w>.
62. Ibad, M. F.; Schulz, A.; Villinger, A. Facile Route to Silver Triarene Borate Salts,  $[\text{Ag}(\text{Arene})_3][\text{B}(\text{C}_6\text{F}_5)_4]$ : Thermodynamics, Structure, and Bonding. *Organometallics* **2019**, *38* (7), 1445–1458. <https://doi.org/10.1021/acs.organomet.8b00873>.
63. Hendsbee, A. D.; Giffin, N. A.; Zhang, Y.; Pye, C. C.; Masuda, J. D. Lewis Base Stabilized Oxophosphonium Ions. *Angew. Chem. Int. Ed* **2012**, *51* (43), 10836–10840. <https://doi.org/10.1002/anie.201206112>.
64. Graham, T. W.; Kickham, J.; Courtenay, S.; Wei, P.; Stephan, D. W. Reduction of Titanium(IV)-Phosphinimide Complexes: Routes to Ti(III) Dimers, Ti(IV)-Metallacycles, and Ti(II) Species. *Organometallics* **2004**, *23* (13), 3309–3318. <https://doi.org/10.1021/om049826q>.

## Appendix A

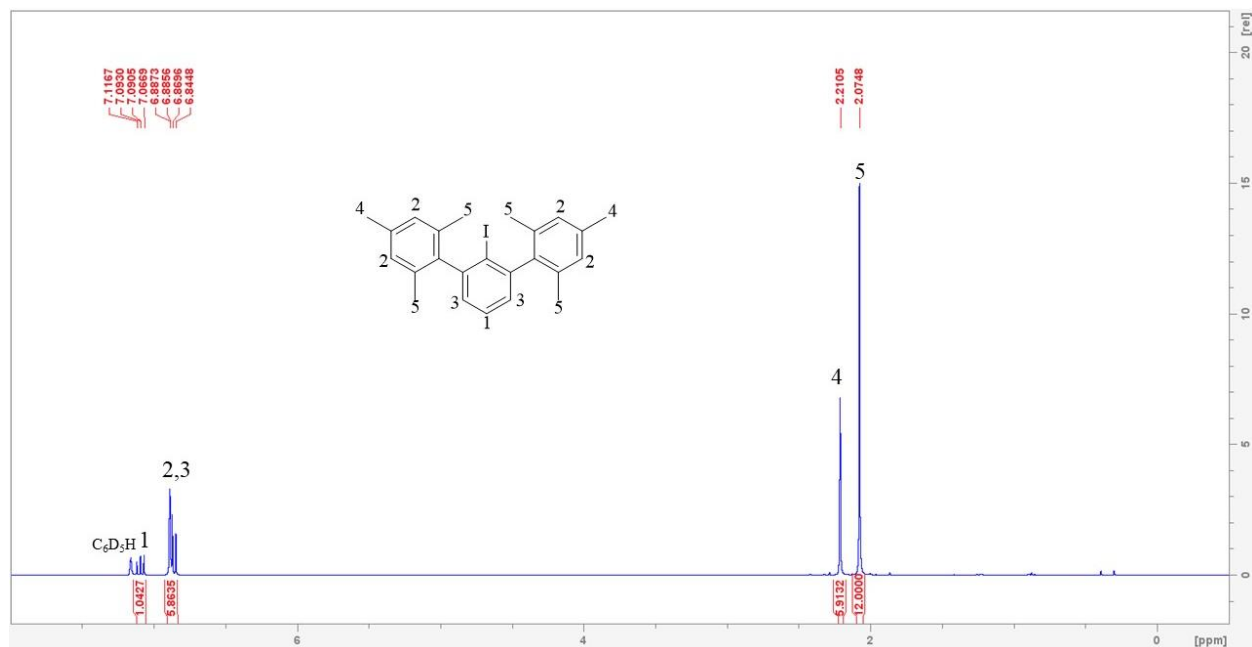


Figure A1. <sup>1</sup>H NMR Spectrum for TerMesI.

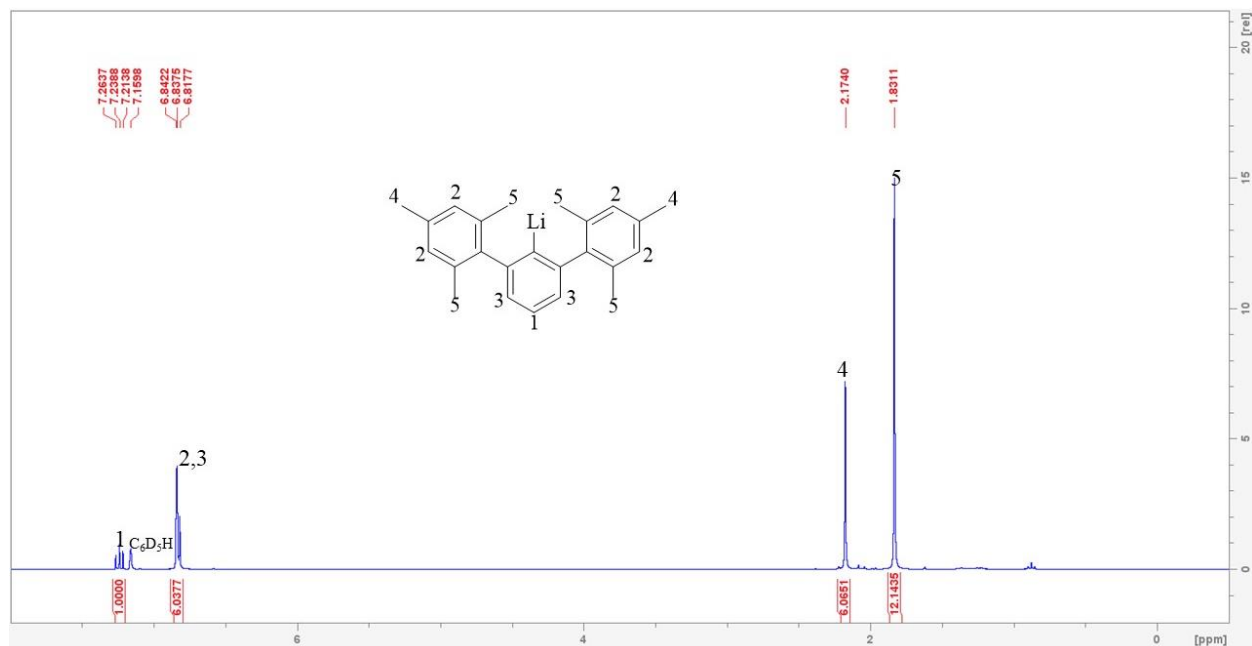
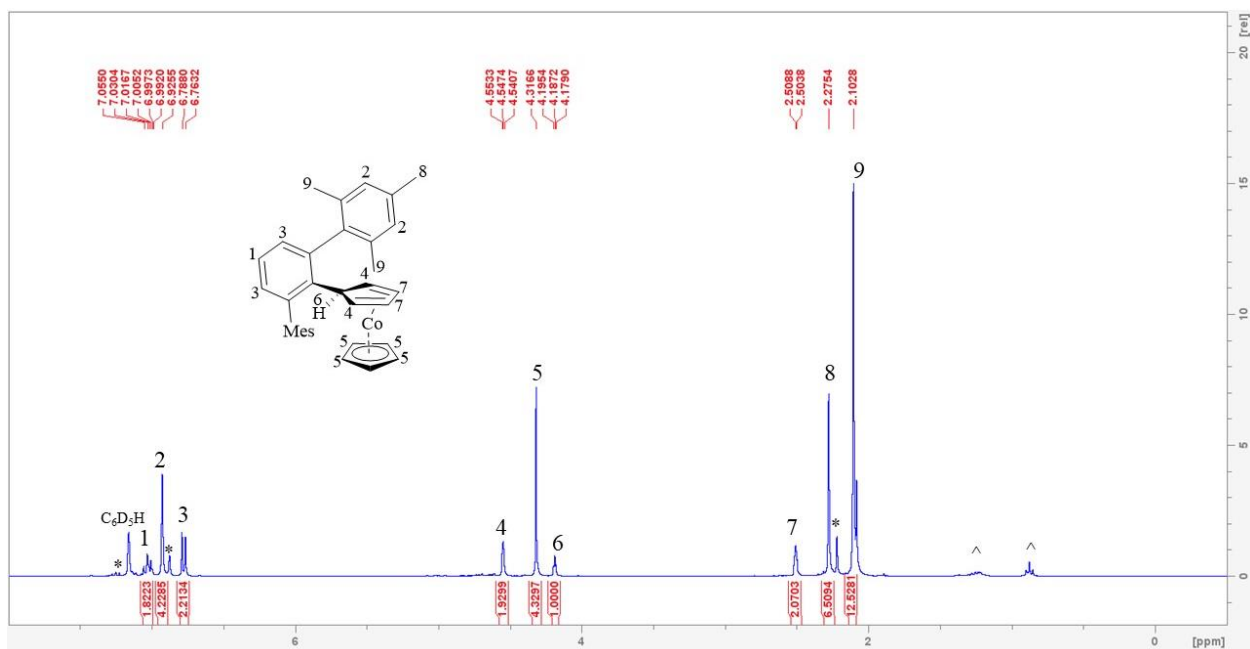
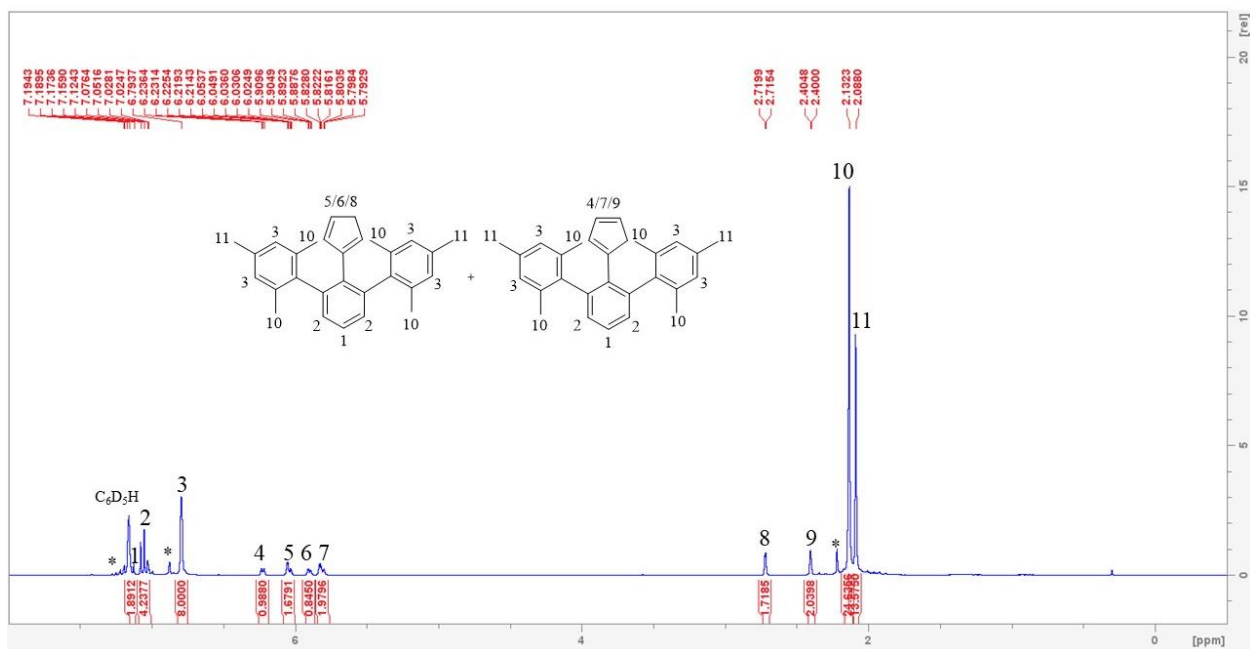


Figure A2. <sup>1</sup>H NMR Spectrum for TerMesLi.



**Figure A3.** <sup>1</sup>H NMR Spectrum for <sup>TerMes</sup>CpCo(I). \* Denotes signals from TerMesH impurities, ^ denotes pentane.



**Figure A4.** <sup>1</sup>H NMR Spectrum for <sup>TerMes</sup>CpH. \* Denotes signals from TerMesH impurities.

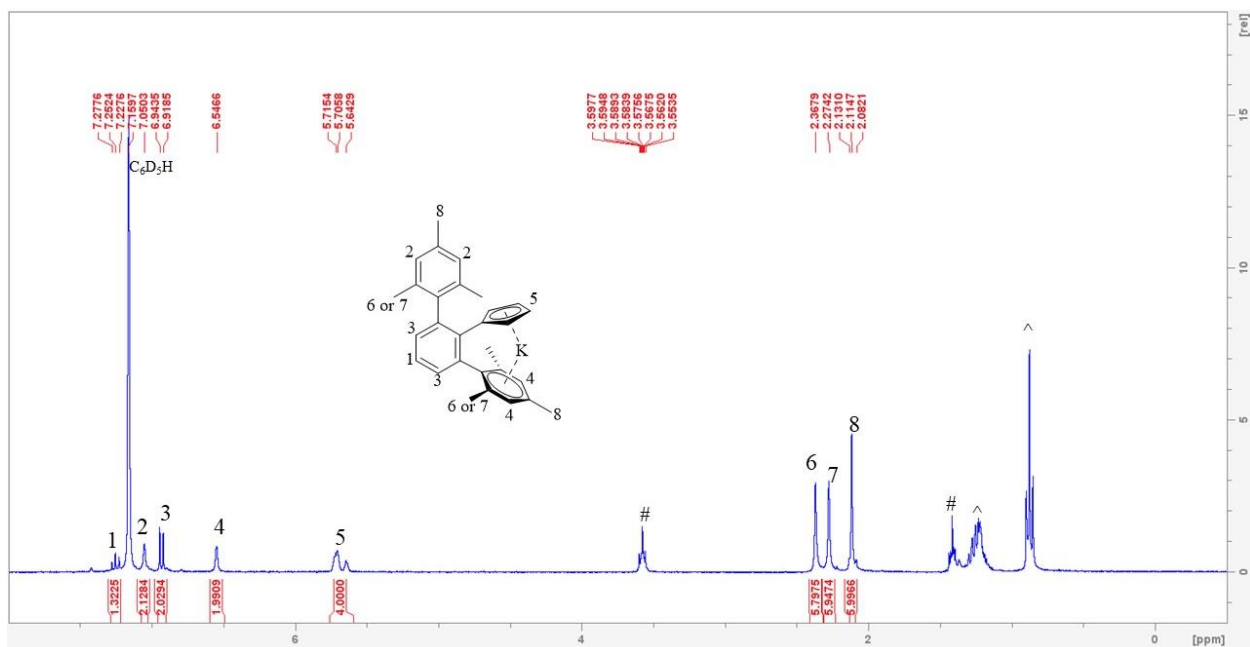


**Figure A5.**  $^1\text{H}$  NMR Spectrum for  $\text{TerMesCpK}$ . ^ denotes pentane, # denotes THF.

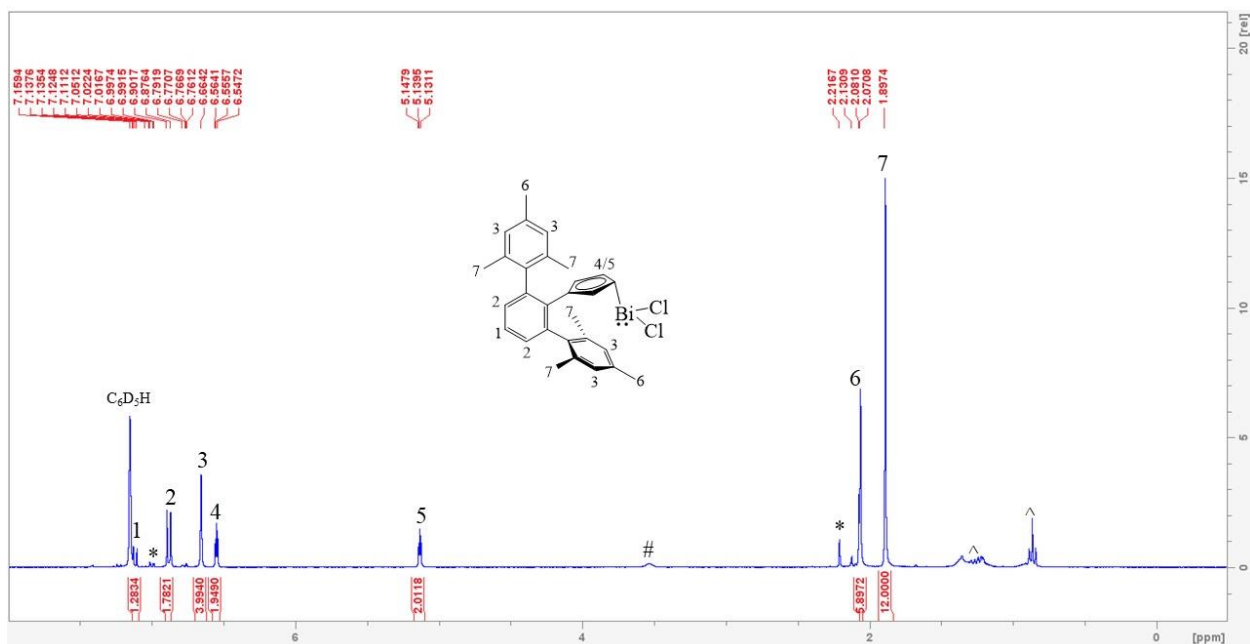


**Figure A6.**  $^1\text{H}$  NMR Spectrum for  $\text{TerMesCpBiCl}_2$ . \* Denotes signals from  $\text{TerMesH}$  impurities, ^ denotes pentane, # denotes THF.

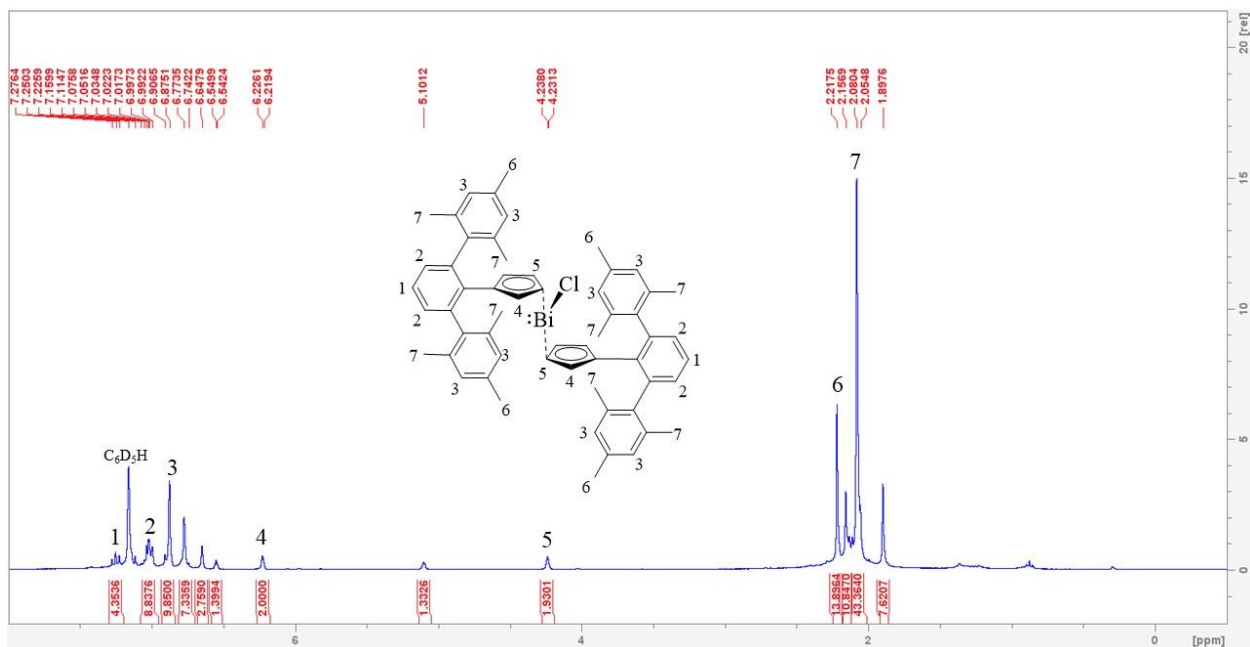


**Figure A7.**  $^1\text{H}$  NMR Spectrum for  $(\text{TerMesCp})_2\text{BiCl}$  contaminated with  $\text{TerMesCpBiCl}_2$ .

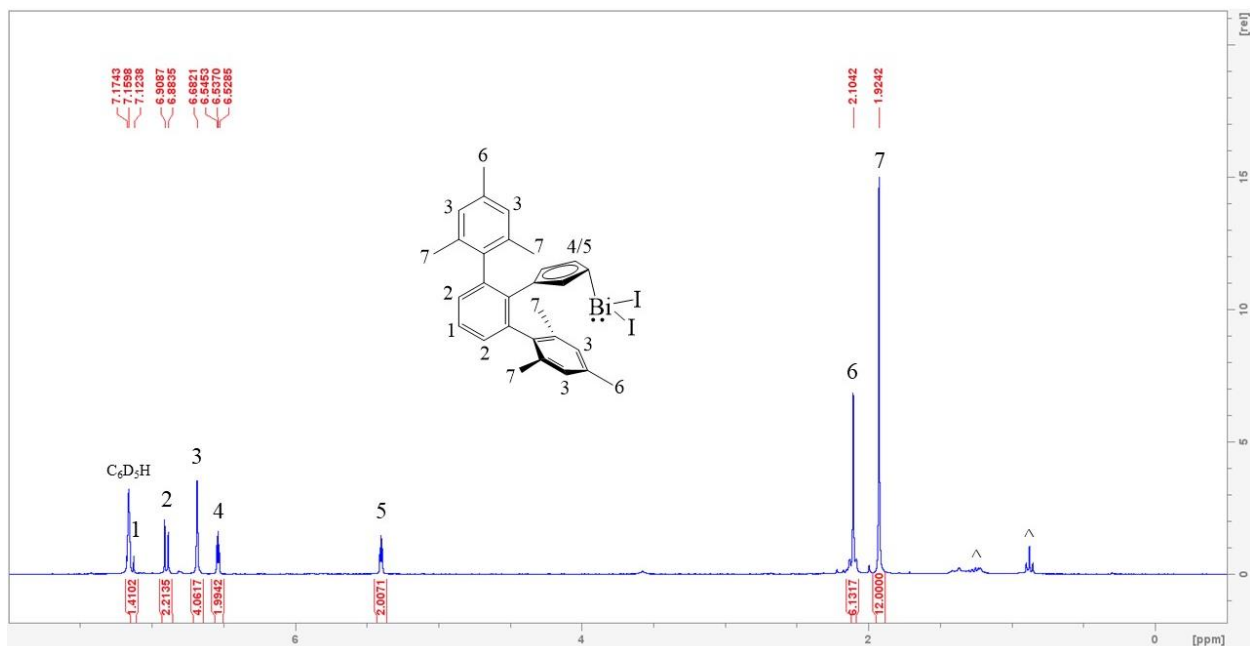


**Figure A8.**  $^1\text{H}$  NMR Spectrum for  $\text{TerMesCpBiI}_2$ . ^ Denotes pentane.

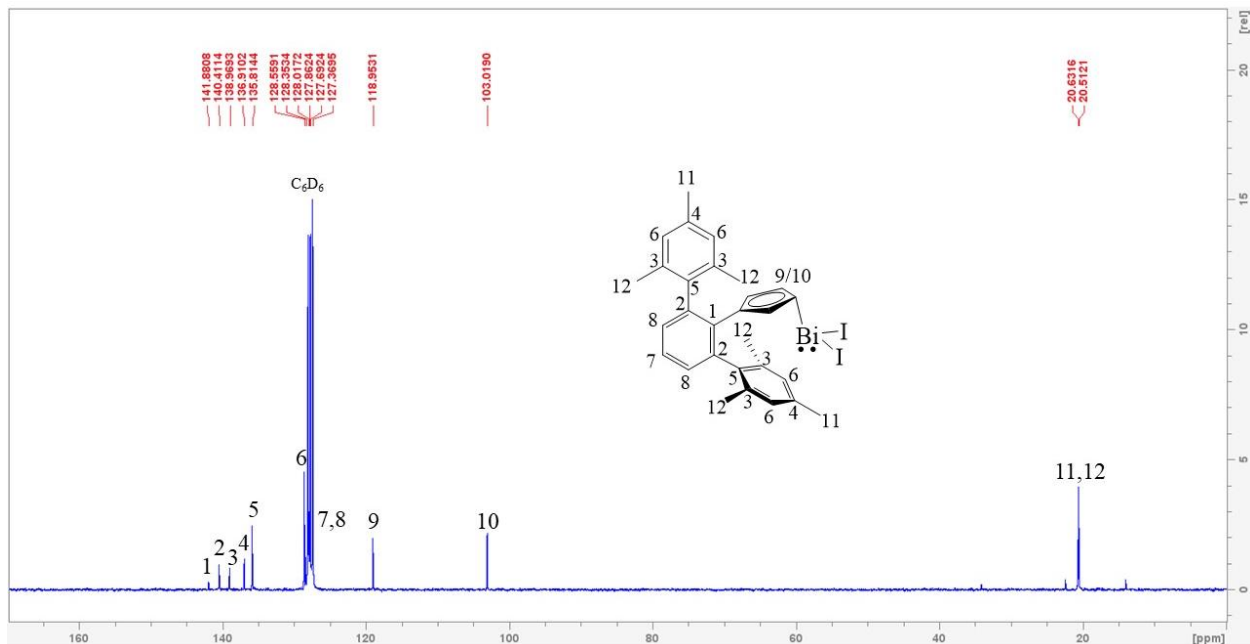


**Figure A9.** <sup>13</sup>C NMR Spectrum for <sup>TerMes</sup>CpBiI<sub>2</sub>.

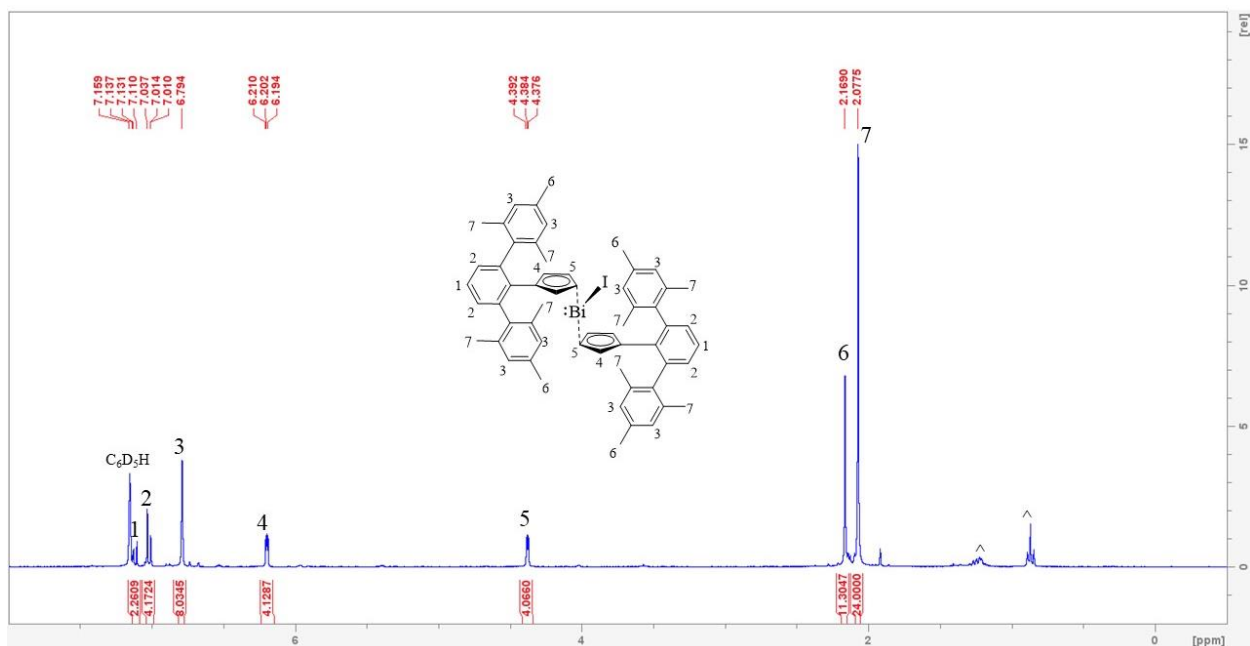


**Figure A10.** <sup>1</sup>H NMR Spectrum for (<sup>TerMes</sup>Cp)<sub>2</sub>BiI. ^ denotes pentane.

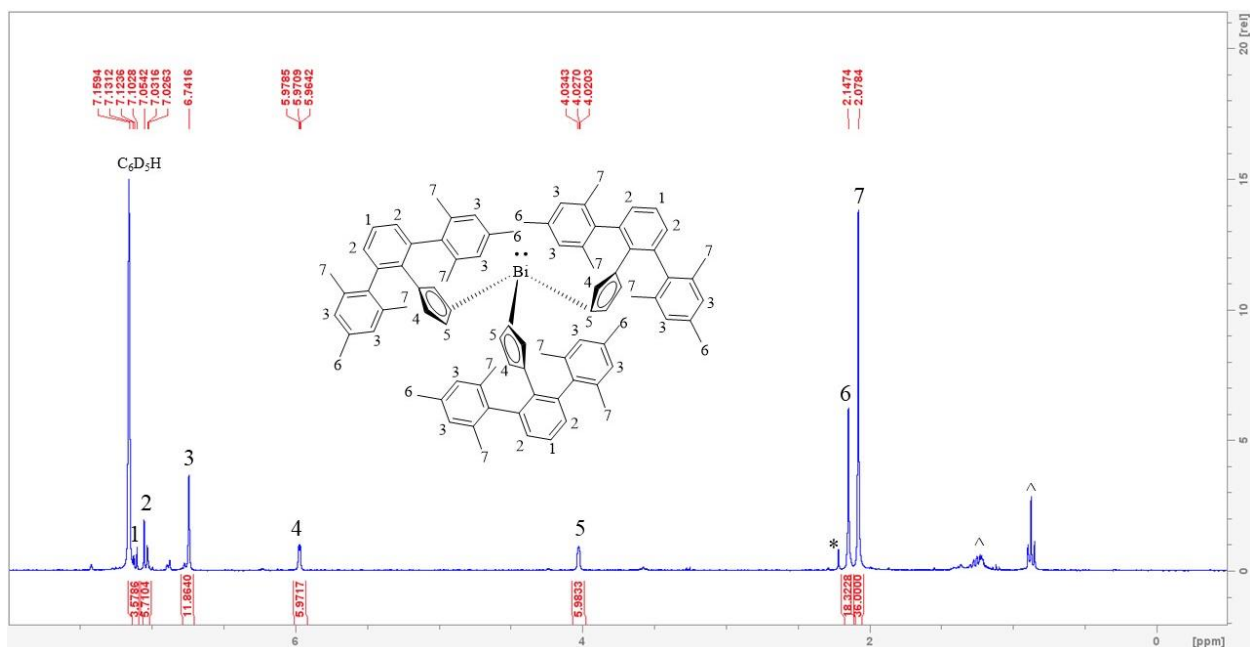


**Figure A11.**  $^1\text{H}$  NMR Spectrum for  $(\text{TerMesCp})_3\text{Bi}$ . ^ Denotes pentane, \* denotes signals from - TerMesH impurities

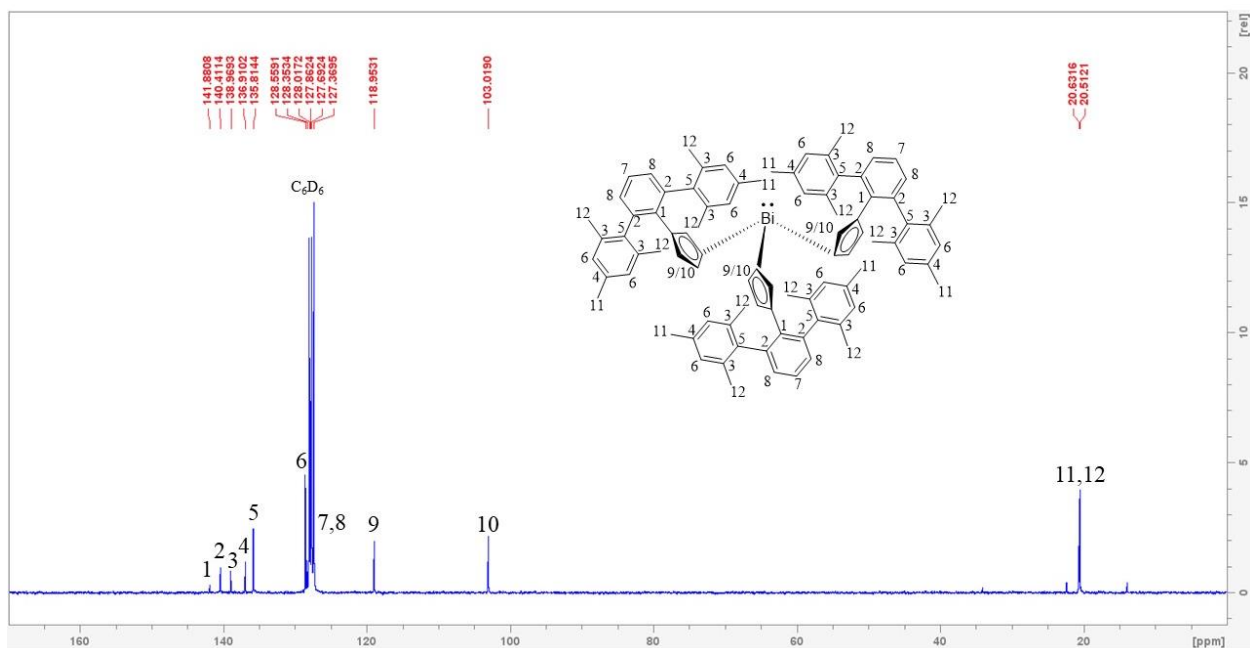


**Figure A12.**  $^{13}\text{C}$  NMR Spectrum for  $(\text{TerMesCp})_3\text{Bi}$ .

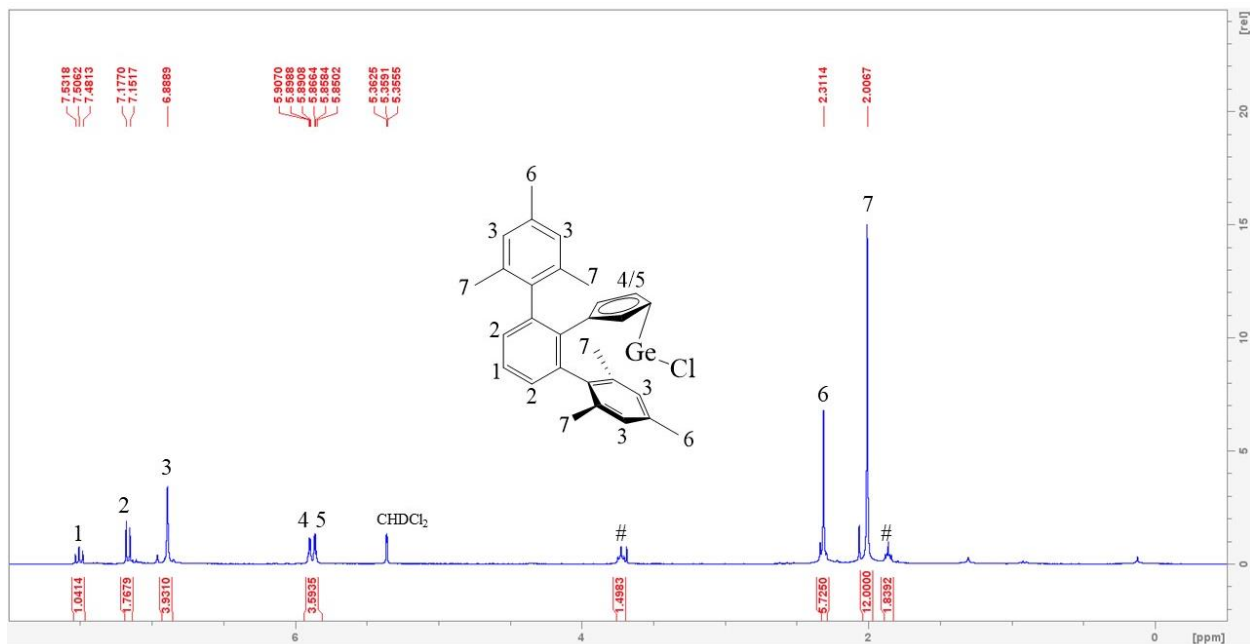


**Figure A13.**  $^1\text{H}$  NMR Spectrum for  $\text{TerMesCpGeCl}$ . # Denotes THF.

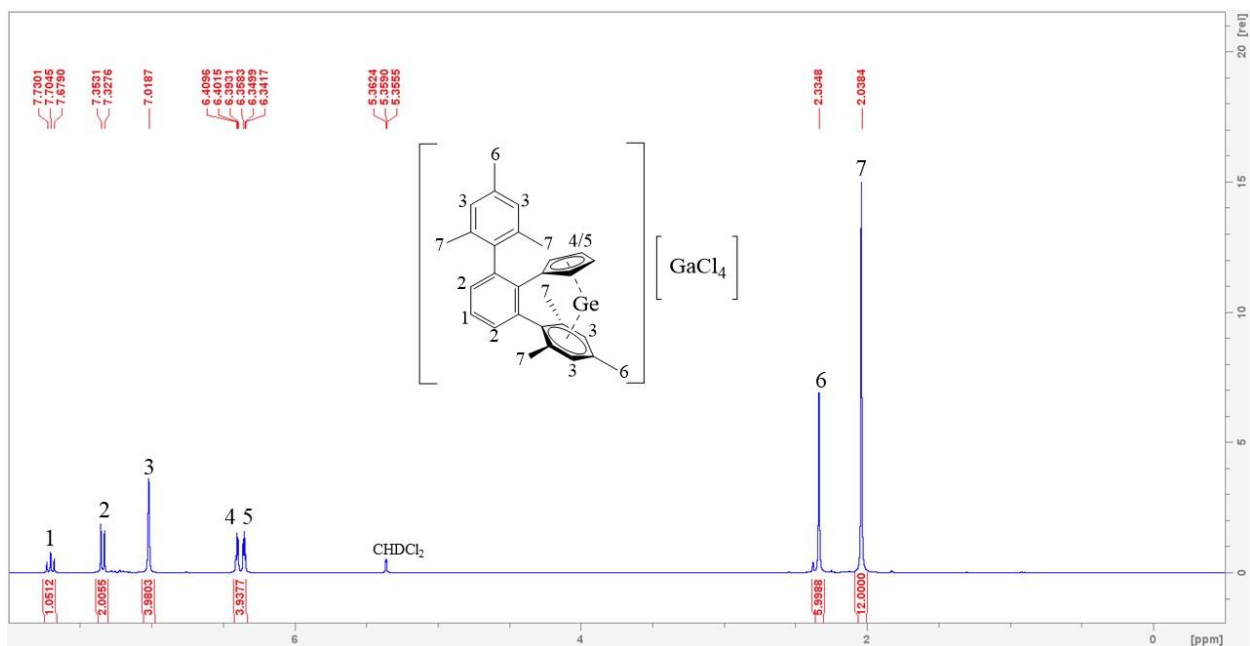


**Figure A14.**  $^1\text{H}$  NMR Spectrum for  $[\text{TerMesCpGe}][\text{GaCl}_4]$ .

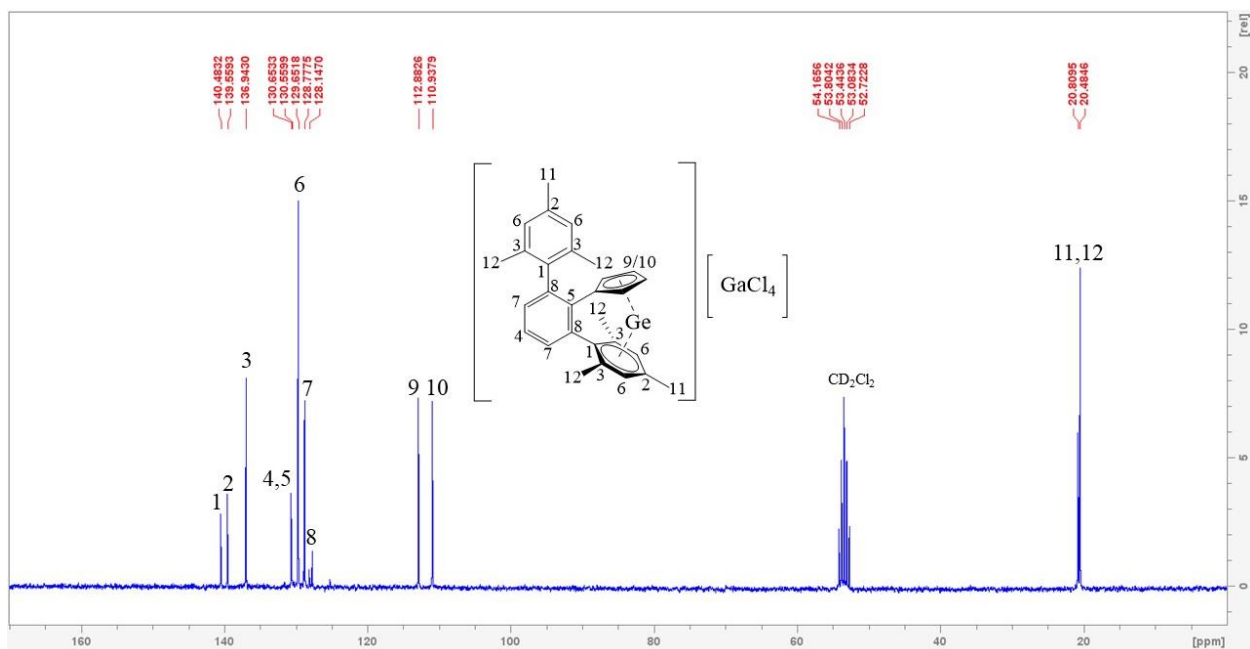


**Figure A15.**  $^{13}\text{C}$  NMR Spectrum for  $[\text{TerMesCpGe}][\text{GaCl}_4]$ .

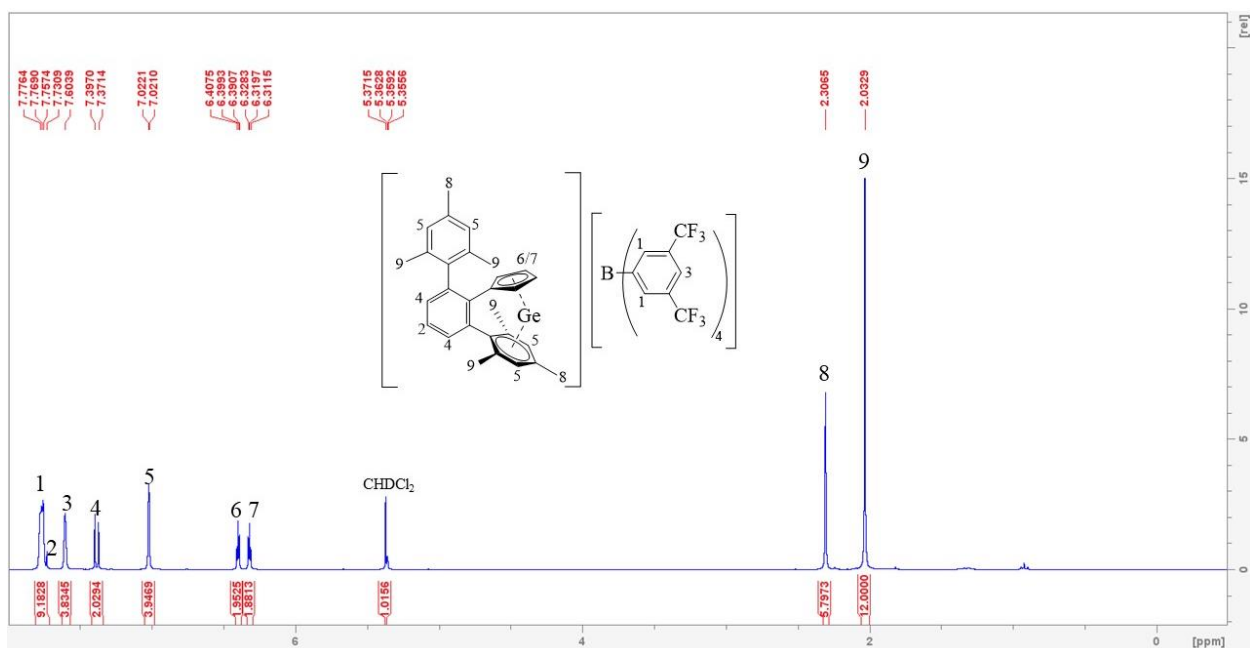


**Figure A16.**  $^1\text{H}$  NMR Spectrum for  $[\text{TerMesCpGe}][\text{BARF}_{24}]$ .

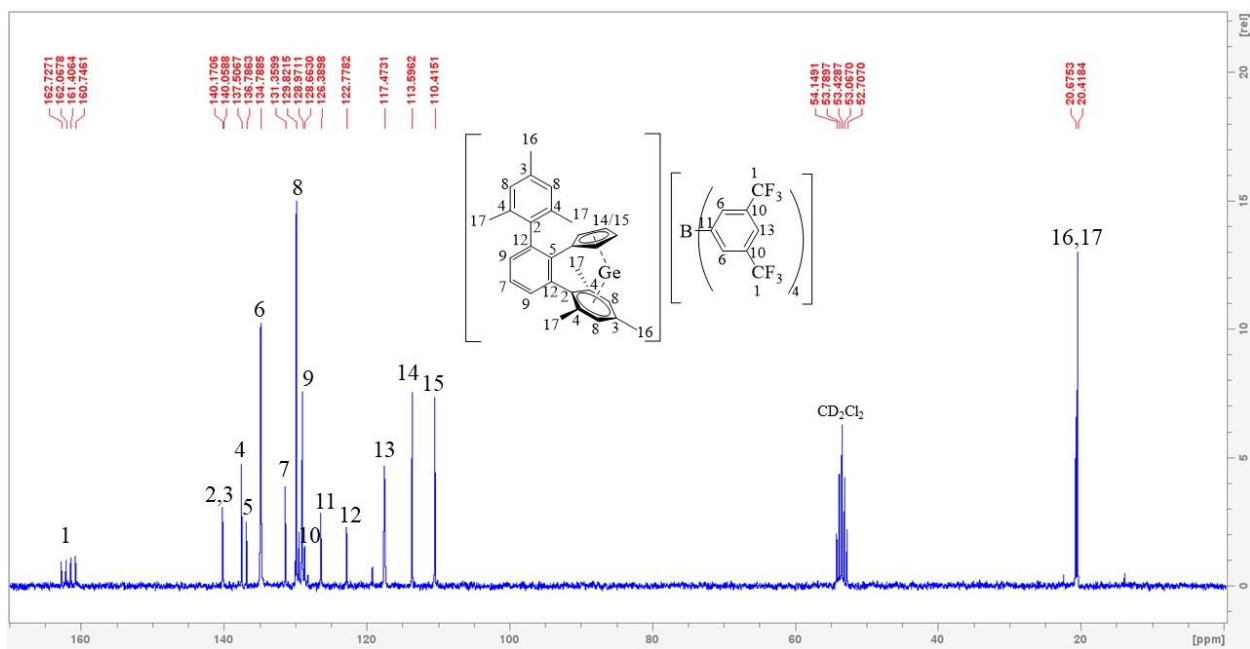


**Figure A17.**  $^{13}\text{C}$  NMR Spectrum for  $[\text{Ter}^{\text{Mes}}\text{CpGe}][\text{BArF}_{24}]$ .

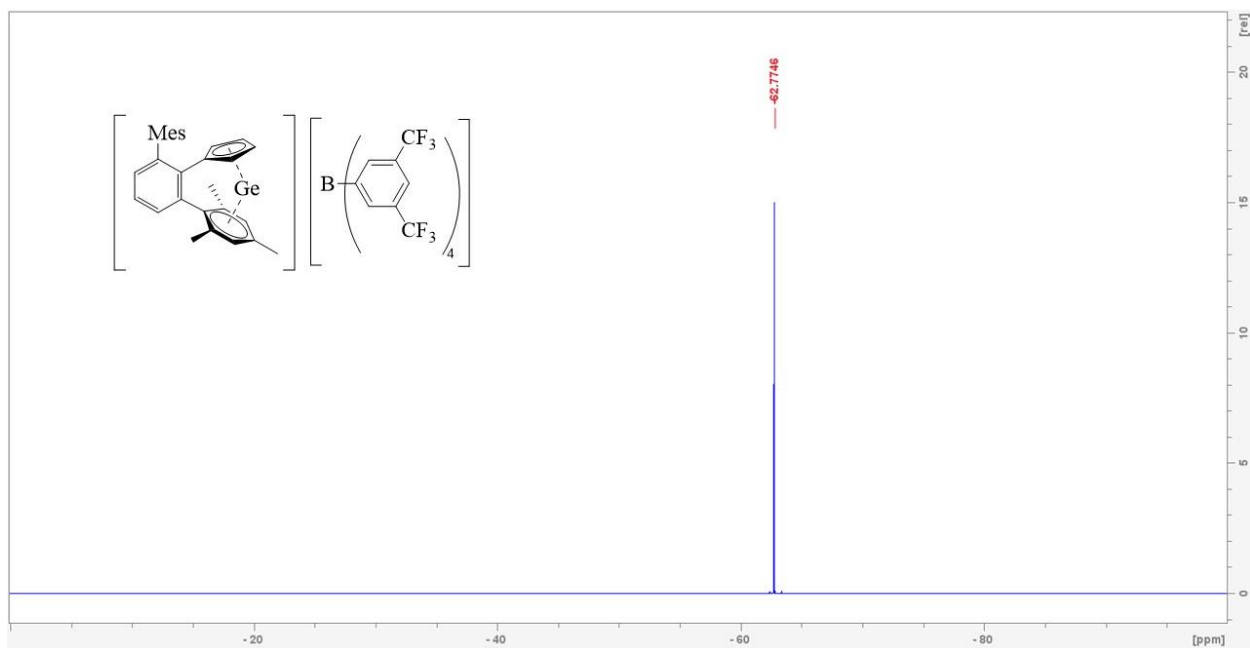


**Figure A18.**  $^{19}\text{F}$  NMR Spectrum for  $[\text{Ter}^{\text{Mes}}\text{CpGe}][\text{BArF}_{24}]$ .

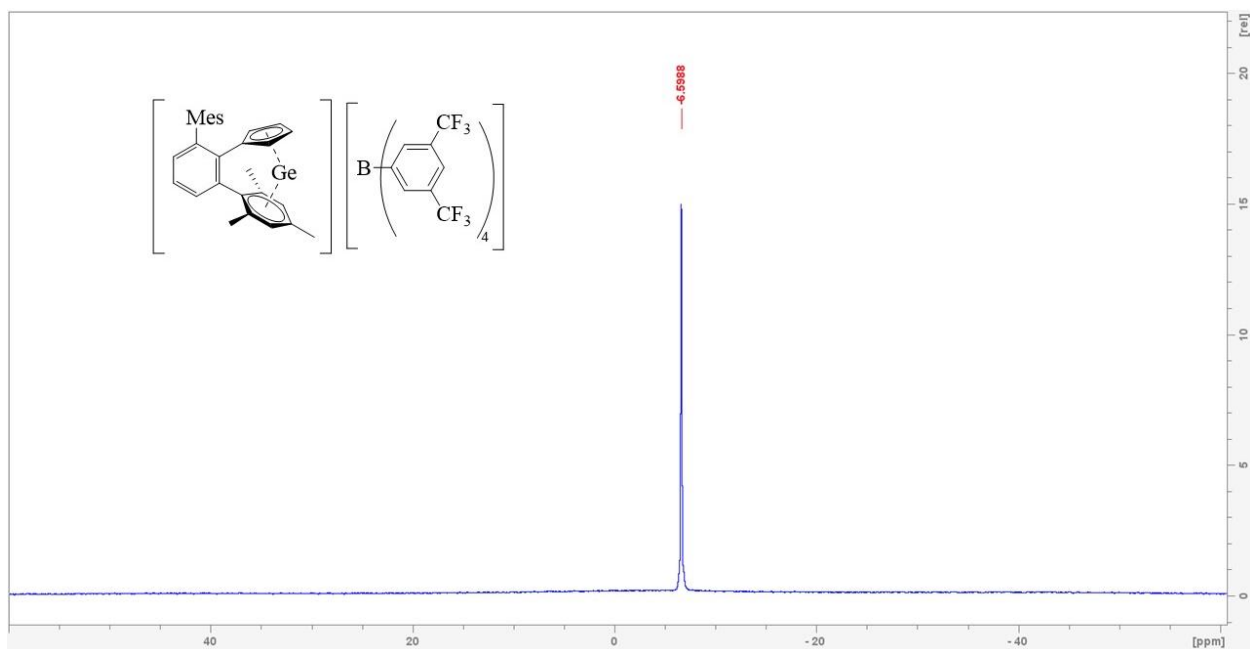


**Figure A19.**  $^{11}\text{B}$  NMR Spectrum for  $[\text{Ter}^{\text{Mes}}\text{CpGe}][\text{BArF}_24]$ .

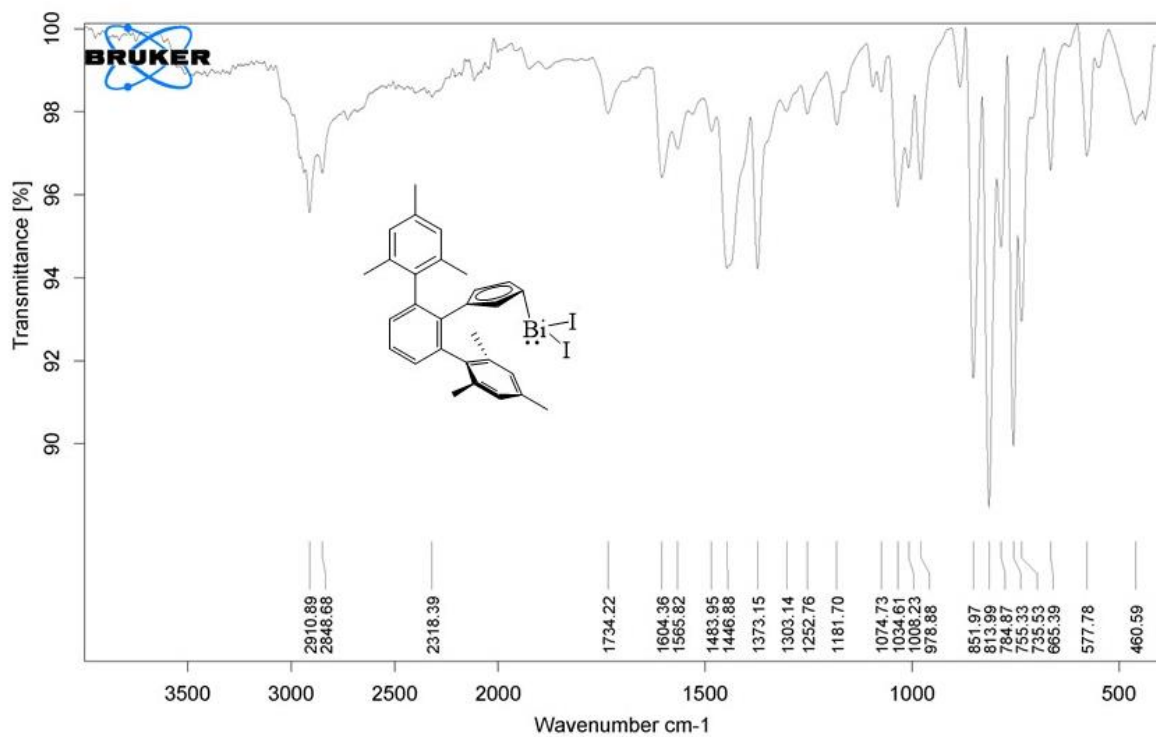


**Figure A20.** FT-IR Spectrum for  $\text{Ter}^{\text{Mes}}\text{CpBiI}_2$ .

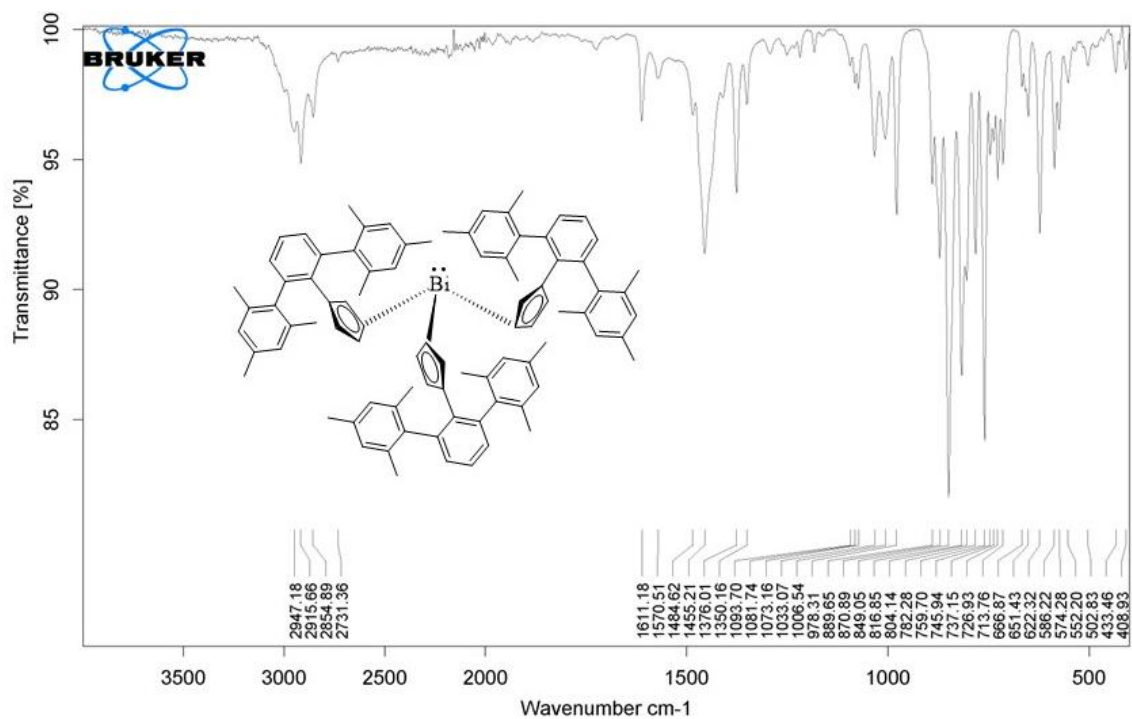


Figure A21. FT-IR Spectrum for  $(\text{Ter}^{\text{Mes}}\text{Cp})_3\text{Bi}$ .

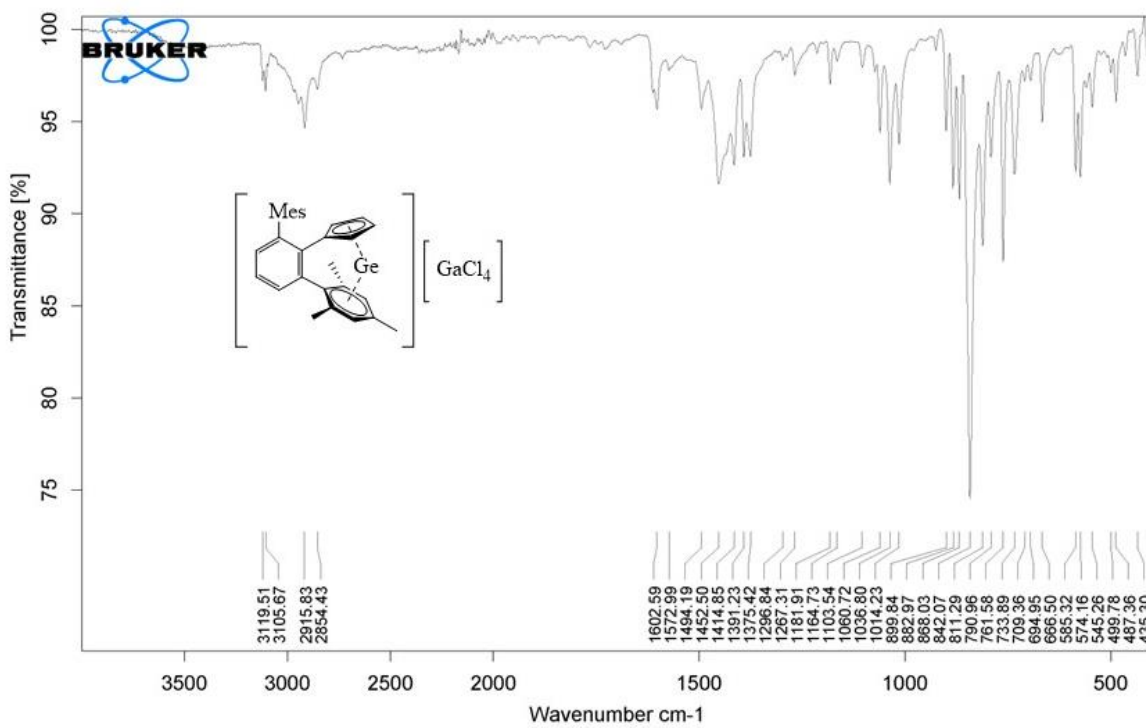


Figure A22. FT-IR Spectrum for  $[\text{Ter}^{\text{Mes}}\text{CpGe}][\text{GaCl}_4]$ .

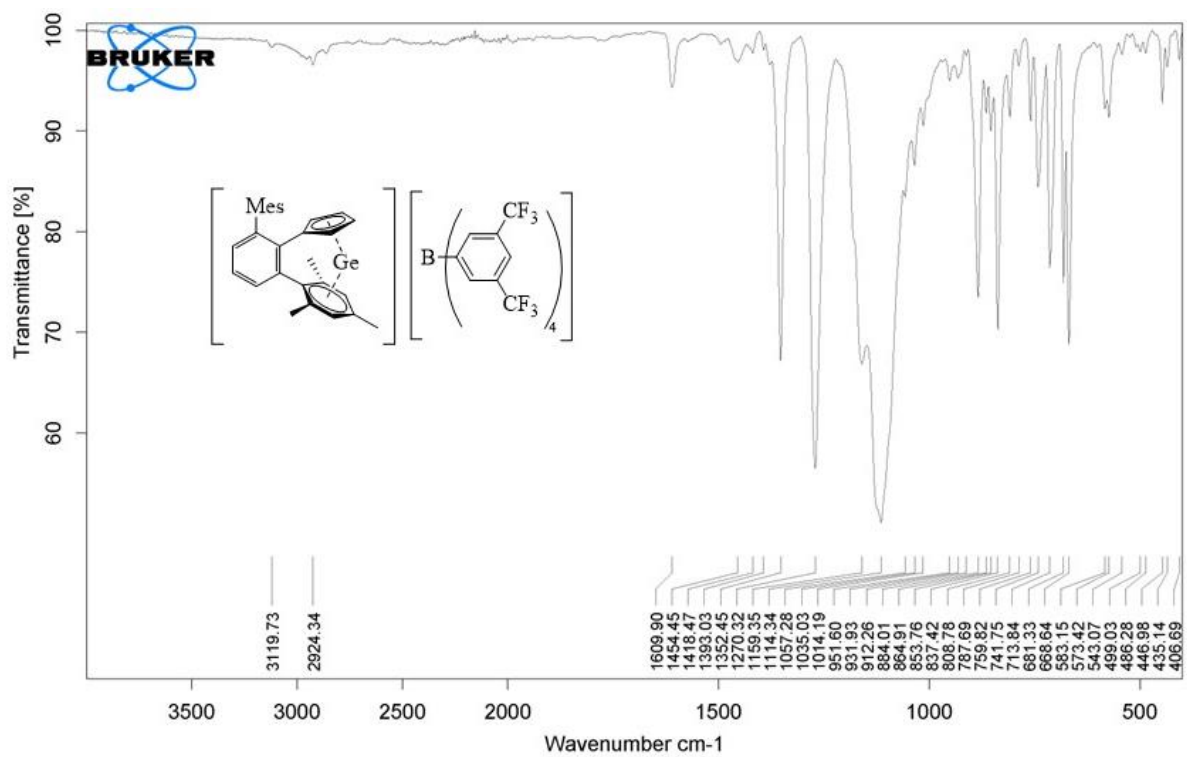


Figure A23. FT-IR Spectrum for [Ter<sup>Mes</sup>CpGe][BArF<sub>24</sub>].